CARDIOTOXIC EFFECTS OF POLYCYCLIC AROMATIC HYDROCARBONS AND ABIOTIC STRESSORS IN EARLY LIFE STAGE ESTUARINE TELEOSTS

by

Elizabeth B. Allmon

A Dissertation

Submitted to the Faculty of Purdue University

In Partial Fulfillment of the Requirements for the degree of

Doctor of Philosophy

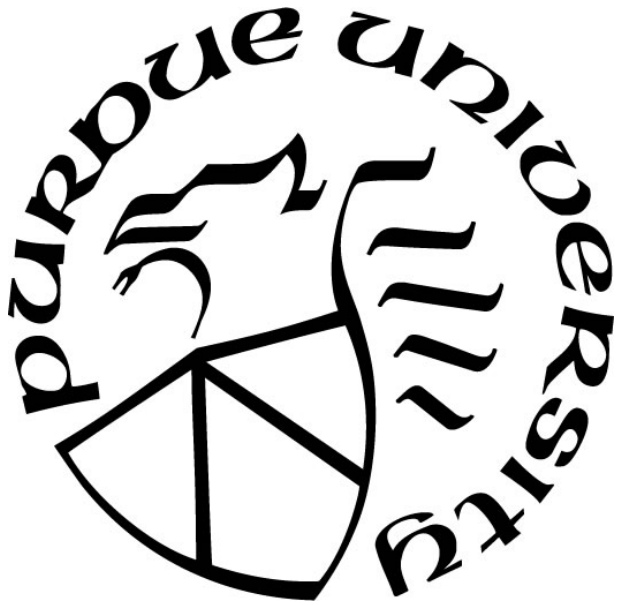

Department of Forestry and Natural Resources

West Lafayette, Indiana

May 2021

THE PURDUE UNIVERSITY GRADUATE SCHOOL
STATEMENT OF COMMITTEE APPROVAL

Dr. Maria S. Sepúlveda, Chair

Department of Forestry and Natural Resources, Purdue University

Dr. Robert J. Griffitt

School of Ocean Science and Technology, University of Southern Mississippi

Dr. Mark R. Christie

Department of Biological Sciences, Purdue University

Dr. Jennifer L. Freeman

School of Health Sciences, Purdue University

Approved by:

Dr. Robert G. Wagner

Dr. Linda S. Lee

Dedicated to my husband, my family, & my dogs.

ACKNOWLEDGMENTS

I would like to first and foremost thank my incredible husband Tommy for his patience, love, and never-ending encouragement over the past few years. I would also like to thank my parents: Ann, Bob, Jackie, Cyndy, and Steve as well as my siblings: Alex, Kevin, Jack, Ashli, and Jeremy; I would not have been able to complete my graduate career without their support.

This dissertation would not have been possible without the tremendous support that I received from my advisor, Dr. Maria S. Sepúlveda. The members of the Sepúlveda lab have been invaluable in their assistance throughout this experience, I would particularly like to thank Dr. Ty Hoskins, Dr. Shuai Chen, Dr. Wes Flynn, Dr. Gary Hoover, Dr. Rui Zhang, Matt Hamilton, Grace Coogan, Mike Iachetta, Sam Guffey, Jennifer Serafin, Maggie Wigren, Alli Scott, Evelyn Barragan, Grace Walker, Lucy Burcham, Samantha Weiss, Savanna Harrison, and Sini Machery. I would also like to thank my network of friends, colleagues, and mentors throughout Purdue and within FNR and ESE including: Dr. Robert Wagner, Dr. Mark Christie, Dr. Jennifer Freeman, Dr. Reuben Goforth, Dr. Linda Lee, Dr. Pavlos Vlachos, Dr. Brandon Quinby, Dr. Rebecca Nixon, Christal Musser, Dierdre Carmichael, Megan Gunn, Jackie Getson, Cortney Mycroft, Tom Bradt, Kevin McCombs, Patricia Nease, Jake Hawes, and Sreyashi Chakraborty.

Dr. Robert Griffitt and his lab at the University of Southern Mississippi are deserving of an incredible amount of credit for their collaborative efforts in helping me complete my research, especially Dr. Maria L. Rodgers, Dr. Elizabeth Jones, and Danielle Simning. Additionally, I would like to thank Dr. Andrew Esbaugh and Dr. Alexis Khursigara for their mentorship, friendship, and willingness to share their skills and expertise with me throughout my graduate career.

Finally, I would like to thank my funding sources and data repositories, without which my research would not have been possible: the Purdue College of Agriculture and the Department of Forestry and Natural Resources for providing me with the Andrews Fellowship, The Gulf of Mexico Research Initiative (award numbers SA 13-01/GoMRI-009 and G-231806), and the Gulf of Mexico Research Initiative Information and Data Cooperative & the Purdue University Research Repository for data archival.

TABLE OF CONTENTS

LIST OF TABLES

LIST OF FIGURES

ABSTRACT

Following the 2010 *Deepwater Horizon* oil spill, extensive research has been conducted on the toxicity of oil and polycyclic aromatic hydrocarbons (PAHs) in the aquatic environment. The location and timing of the Deepwater Horizon surface slick coincided with the spawning seasons of many important pelagic and estuarine fish species. As such, there has been particular emphasis placed on the effects of PAHs on sensitive life history stages in fish, such as the embryonic and larval periods. Additionally, the spill occurred throughout the spring and summer months which, in estuaries, are marked by regular fluctuations in abiotic environmental factors such as dissolved oxygen, salinity, and temperature. Until recently, there has been little work done to elucidate the combined effects that PAHs from oil spills and adverse environmental conditions (hypoxia, increased salinity, and elevated temperatures).

Work presented in this dissertation uses next generation sequencing technology (RNA Seq) to determine differential gene expression in larval estuarine teleosts following exposure to adverse environmental conditions and PAHs. Downstream canonical pathway and toxicological function analysis were then applied to the identified differentially expressed genes (DEGs) to predict cardiotoxic responses at the organismal level. To verify the predicted responses, a phenotypic anchoring study was conducted and identified a cardiotoxic phenotype (pericardial edema) and reduced cardiac output in embryos exposed to oil. Finally, the mechano-genetic interplay governing the morphological development of the teleost heart was investigated and correlations between developmental gene expression and blood flow forces within the cardiovascular system were identified.

CHAPTER 1. INTRODUCTION

1.1 Deepwater Horizon oil spill & PAHs

The Deepwater horizon oil spill in April 2010 was the worst in US history and released an estimated 4.9 million barrels of oil into the northern Gulf of Mexico over the course of 87 days (Beyer et al., 2016; Camilli et al., 2012; Crone and Tolstoy, 2010; McNutt et al., 2012; Norse and Amos, 2010). The plume of crude oil extended to the surface and created a slick that covered more than an estimated 67,000 square kilometers (Norse and Amos, 2010; Sammarco et al., 2013). The slick extended across the northern Gulf of Mexico and impacted approximately 2100 kilometers of shoreline from Louisiana to Florida, with tar-balls later found as far as the Texas coast (Nixon et al., 2016). Following the spill, an abundance of research has been conducted to elucidate the impact of the released oil on the surrounding biota. Many studies have focused on polycyclic aromatic hydrocarbons (PAHs), the primary constituents of crude oil, and their impacts on the fauna of the region (Beyer et al., 2016; Murphy et al., 2016).

PAHs have been identified as the primary driver of oil toxicity (Murphy et al., 2016) and are some of them are extremely persistent in the environment (Carls et al., 2008; Peterson et al., 2003; Short et al., 2003; Wang et al., 2014). PAHs are categorized by the length of their carbon chains (Figure 1.1), with lighter PAHs having shorter carbon chains than their heavier counterparts (Forth et al., 2017). Source oil (oil that was captured directly from the wellhead) has proportionately more volatile, 2 ring PAHs than slick oil collected from the surface - which has been weathered and is comprised largely of 3 and 4 ring PAHs (phenanthrene and chrysene isoforms respectively). These structural and chemical differences play important roles in defining the volatility and toxicity of each PAH. In general, the volatility of PAHs decreases with size while toxicity increases (Esbaugh et al., 2016; Incardona et al., 2014, 2009, 2004;

Mager et al., 2014). This leads to abundant toxic 3 and 4 ring PAHs persisting in the environment (Heintz et al., 1999). PAH degradation rates are dependent on many factors such as weathering processes (evaporation, photooxidation, dissolution, and biodegradation) and the physical, chemical, and biological structure of the molecule (Abdel-Shafy and Mansour, 2016; Collier et al., 2013). For example, the structurally stable, 3 ring PAH phenanthrene can remain in the environment years after a spill has been contained and clean-up has ended (Abdel-Shafy and Mansour, 2016).

1.2 Abiotic stressors in Gulf of Mexico estuaries

The timing of the Deepwater Horizon oil spill, during the spring and summer of 2010 (Crone and Tolstoy, 2010; Norse and Amos, 2010), coincided with the seasonal formation of the "dead zone" in the northern Gulf of Mexico (Beyer et al., 2016; Rabalais et al., 2002; Figure 1.2). Annually, the dead zone begins to intensify in the spring when nutrient rich waters from the Mississippi River watershed enter the Gulf of Mexico and often persists until the end of the summer when storms enhance mixing within the water column. During this time, thermal stratification allows for high oxygen consumption in the upper water column and development of hypoxic waters in the lower water column (Rabalais et al., 2002). Northern Gulf of Mexico estuarine surface waters regularly go through seasonal temperature fluctuations with average ranges from 10°C in the winter months to greater than 30°C during the summer (Caffrey et al., 2014). These seasonal periods of elevated water temperatures trigger thermally driven hypoxic events in nearshore environments, similar to those observed in the dead zone.

Additionally, the biogeochemical aspects of bays along the northern Gulf of Mexico coast contribute to salinity changes in estuaries. Shallow, protected bays with high water residence times, little freshwater input, and high evaporation in the warmer months can result in

hypersaline environments (Laguna Madre, TX estuary system often maintains salinities >40 ppt (Wilson and Dunton, 2012; NOAA, 2021)) while pulses of freshwater inputs from storm events or upstream reservoir discharges may result in reduced salinities as low as 0 ppt in bays and estuaries (Orlando et al., 1993; Schroeder and Wiseman, 1986; Wilson et al., 2015). The dynamic biogeochemical processes that regularly occur within estuaries – such as fluctuations in dissolved oxygen, salinity, and temperatures (Bianchi et al., 1999; NOAA, 2021) - may impart a level of resiliency to the species that reside there as they must be capable of physiologically compensating to maintain homeostasis under a wide range of environmental conditions (Bennett and Beitinger, 1997; Borowiec et al., 2015; Haney and Nordlie, 1997). Strategies employed by inshore marine species to cope with prolonged hypoxia include transitioning to anaerobic metabolism, migration from sub-sediment burrows to the sediment surface, and changes in predation/ foraging behaviors (Gray et al., 2002; Pelster, 1999; Rabalais et al., 2002; Wu, 2002). In particular, inshore fish species have exhibited changes in ventilatory rates, reduced growth rates, and transitions to surface breathing when confined to hypoxic environments (Burggren et al., 2017; Ern and Esbaugh, 2018; Gray et al., 2002; Rabalais et al., 2002; D. J. Randall and Smith, 1967; Stierhoff et al., 2006; Zhang et al., 2009). Fish embryos exposed to increased temperatures, elevated salinities, and/ or low dissolved oxygen levels often exhibit functional and morphological cardiac impairments such as changes in heart rate, blood pressure, vasodilation, and cardiac remodeling (Claireaux et al., 1995; Farrell, 2007; Keen et al., 2017; Klaiman et al., 2011; Lin et al., 1994; A. D. J. Randall and Smith, 1967).

1.3 PAH toxicity in early development

The location and timing of the Deepwater Horizon spill made it particularly relevant in fisheries research as the surface slick formed during the spawning season for many fishes (Block

et al., 2005; Esbaugh et al., 2016; Muhling et al., 2012; Rooker et al., 2013, 2012). The slick occurred both in the pelagic spawning grounds for many marine species and extended into the estuary habitats critical for the life cycle of many nearshore and estuarine fish (Mendelssohn et al., 2012). Previous work has shown that PAHs can have adverse impacts on specific organs and systems (such as the cardiovascular system or the immune system), developmental stages, or act as potential mutagens or carcinogens (Carls et al., 2008; Carvalho et al., 2008; Collier et al., 2013; Edmunds et al., 2015; Esbaugh et al., 2016; Incardona et al., 2014, 2011; Jayasundara et al., 2015; Mager et al., 2014; Magnuson et al., 2018; Pan et al., 2018; Xu et al., 2017, 2016). Additional studies have shown that PAH toxicity in fish is variable depending on the life stage at the time of the exposure (Barron et al., 2004; Collier et al., 2013; Hose et al., 1996; Incardona et al., 2014, 2011). Perhaps the most susceptible life stages for a fish to be exposed to PAHs is during the embryonic/larval stages (Barron et al., 2004; Collier et al., 2013; Hose et al., 1996; Incardona et al., 2014, 2011). These stages represent periods of considerable physiological and morphological changes as well as functional challenges such as transitioning from endogenous nutrition to exogenous feeding. PAH toxicity that manifests in a range of developmental or morphological deformities or toxicity can hinder an organism's ability to function (i.e. through sensory disruptions) and may produce lethal outcomes (Beyer et al., 2016; Collier et al., 2013).

Recent studies have shown that PAH exposure can drive toxicity through cardiovascular dysfunction (Barron et al., 2004; Carls et al., 2008; Collier et al., 2013; Hose et al., 1996; Incardona et al., 2009; Jayasundara et al., 2015; Mendelssohn et al., 2012; Rooker et al., 2013). Specifically, instances of cardiac edema (Carls et al., 2008; Incardona et al., 2014, 2009; Khursigara et al., 2017), decreased contractility, and changes in heart rates (Edmunds et al., 2015; Incardona et al., 2011) have been observed in embryonic pelagic species exposed to

Deepwater Horizon oil. However, relative to large pelagic fish, there has been little work on the cardiac impacts in estuarine fishes exposed to PAHs. When compared to many pelagic species, the embryonic stage of many coastal and estuarine species is relatively prolonged. Pelagic species are often rapidly developing – for example bluefin tuna (*Thunnus thynnus*) and mahi-mahi (*Coryphaena hippurus*) hatch within 36 hours post-fertilization (Mager et al., 2017; Miyashita et al., 2000) - while many estuarine species undergo extended embryonic periods ranging from approximately 6 days post fertilization (dpf) in the sheepshead minnow (*Cyprinodon variegatus*) to up to 30 dpf in the inland silverside (*Menidia beryllina*) (Bosker et al., 2017; Kuntz, 1916; Middaugh and Hemmer, 1992). This prolonged development in the embryonic stage may leave estuarine species more vulnerable to PAH induced cardiotoxicity than more broadly studied pelagic species.

The sheepshead minnow, *Cyprinodon variegatus*, and the Gulf killifish, *Fundulus grandis*, are estuarine species native to the Gulf of Mexico that have been used as models for toxicity testing in a number of PAH studies (Bosker et al., 2017; Magnuson et al., 2018; Oleksiak et al., 2011; Powell et al., 2004; Reid et al., 2016; Simning et al., 2019; Whitehead et al., 2011). Both species inhabit nearshore environments that undergo daily and seasonal fluctuations in temperature, salinity, and dissolved oxygen. They are also widely dispersed in estuaries directly impacted by the Deepwater Horizon oil spill and their spawning seasons directly coincided with the timing of the spill, February through October for *C. variegatus* and March through October for *F. grandis* (Greeley and MacGregor, 1983; Kuntz, 1916), making them ideal candidates for the study of the effects of oil and abiotic factors on transcriptional and morphological responses in the developing cardiac system. Generally, it is assumed that species occupying the same ecological niche will exhibit similar responses to environmental perturbations (Jones et al.,

2020). However, recent studies into the effects of oil on *C. variegatus* and *F. grandis* larval mortality and transcriptional responses suggest that there may be subtle differences in molecular responses that impart differential sensitivities between species (Jones et al., 2020; Serafin et al., 2019; Simning et al., 2019).

1.4 Cardiovascular assessment

Methods of transcriptomic analysis and bioinformatics techniques have become important tools widely used by ecotoxicologists. Next generation sequencing, especially through RNA-Seq, has enabled ecotoxicologists to quantify the transcriptomes of non-model species following exposures to environmental perturbations and better interpret changes to functional aspects of the transcriptome (Garcia et al., 2012; Huang et al., 2014; Martyniuk and Simmons, 2016; Wang et al., 2009; Whitehead et al., 2012; Xu et al., 2017, 2016). This allows for more increased knowledge of cellular functions, development, and disease progression across taxa. Ecotoxicologists are now able to use differential gene expression and measurable changes in the transcriptome of an organism to predict and test changes to in the physiology of the organism following environmental exposures (Wang et al., 2009). These techniques have proven to be particularly relevant in defining the impacts of large environmental disasters, such as the Deepwater Horizon oil spill. Transcriptomic assessments of fish exposed to oil from the Deepwater Horizon oil spill are becoming more prevalent in the literature (Murphy et al., 2016). However, simply identifying differentially expressed genes in an organism does not necessarily confer a change at the functional or organismal level. As such, phenotypic anchoring studies should be conducted in tandem with next generation sequencing studies in order to verify predicted downstream impacts with observed responses.

Cardiovascular morphogenesis during embryonic development is influenced by the interplay between mechanical forces – particularly wall shear stress and blood flow velocities – and initiation of genetic cues (Boselli et al., 2015). A perturbation to this mechano-genetic interplay could lead to cardiovascular malformations. The early structural abnormalities induced by cardiotoxic agents in the heart can be traced to the hemodynamic changes and the corresponding genetic regulation (Boselli et al., 2015). High resolution imaging techniques, such as micro-particle image velocimetry, allows for non-intrusive, in vivo measurements of flow metrics by tracing red blood cell patterns through the developing cardiovascular system (Bark et al., 2017; Nakano et al., 2003; Sugii et al., 2002). Relationships between genetic cues and hemodynamic responses can be defined by combining measurements from advanced imaging techniques with gene expression analysis. Understanding and identifying the framework of these interactions may lead to better understanding of mechanisms of cardiotoxicity in early development.

1.5 Aims and objectives

Research presented in this dissertation aims to define the transcriptomic, morphologic, and functional changes in the developing cardiac system of estuarine species following exposure to sub-optimal abiotic stressors and PAHs. Transcriptomic interrogation revealed that exposure to hypoxia elicits distinct differential gene expression between *C. variegatus* and *F. grandis* larvae. However, predicted impacts on downstream functional responses – reduced cardiac hypertrophy, blood pressure modulation, and increased cardiac apoptosis – appear to be conserved between the species. Combined exposures to oil and sub-optimal environmental conditions in larval *F. grandis* resulted in transcriptomic alterations suggestive of reduced development of systemic vasculature, altered blood pressure maintenance, and inhibited cardiac

function resulting from increased cardiac proliferation. Cardiac morphology and function analysis revealed significant pericardial edema and reduced cardiac output in embryonic *C. variegatus* exposed to oil. Finally, the interplay between mechanical and genetic forces within the developing fish cardiovascular system were assessed and mechano-genetic events critical to cardiac remodeling were defined.

1.6 References

Abdel-Shafy, H.I., Mansour, M.S.M., 2016. A review on polycyclic aromatic hydrocarbons: Source, environmental impact, effect on human health and remediation. Egypt. J. Pet. 25, 107–123. https://doi.org/10.1016/j.ejpe.2015.03.011

Bark, D.L., Johnson, B., Garrity, D., Dasi, L.P., 2017. Valveless pumping mechanics of the embryonic heart during cardiac looping: Pressure and flow through micro-PIV. J. Biomech. 50, 50–55. https://doi.org/10.1016/j.jbiomech.2016.11.036

Barron, M.G., Carls, M.G., Heintz, R., Rice, S.D., 2004. Evaluation of fish early life-stage toxicity models of chronic embryonic exposures to complex polycyclic aromatic hydrocarbon mixtures. Toxicol. Sci. 78, 60–67. https://doi.org/10.1093/toxsci/kfh051

Bennett, W.A., Beitinger, T.L., 1997. Temperature tolerance of the sheepshead minnow , *Cyprinodon variegatus.* American Society of Ichthyologists and Herpetologists. Stable URL : http://www.jstor.org/stable/1447842. Copeia 1997, 77–87.

Beyer, J., Trannum, H.C., Bakke, T., Hodson, P. V., Collier, T.K., 2016. Environmental effects of the Deepwater Horizon oil spill: A review. Mar. Pollut. Bull. 110, 28–51. https://doi.org/10.1016/j.marpolbul.2016.06.027

Bianchi, T.S., Pennock, J.R., Twilley, R.R. (Eds.), 1999. Biogeochemistry of Gulf of Mexico estuaries. John Wiley & Sons, Inc., New York.

Block, B.A., Teo, S.L.H., Walli, A., Boustany, A., Stokesbury, M.J.W., Farwell, C.J., Weng, K.C., Dewar, H., Williams, T.D., 2005. Electronic tagging and population structure of Atlantic bluefin tuna. Lett. to Nat. 434, 1121–1127. https://doi.org/10.1038/nature03463

Borowiec, B.G., Darcy, K.L., Gillette, D.M., Scott, G.R., 2015. Distinct physiological strategies are used to cope with constant hypoxia and intermittent hypoxia in killifish (*Fundulus heteroclitus*). J. Exp. Biol. 218, 1198–1211. https://doi.org/10.1242/jeb.114579

Boselli, F., Freund, J.B., Vermot, J., 2015. Blood flow mechanics in cardiovascular development. Cell. Mol. Life Sci. 72, 2545–2559. https://doi.org/10.1007/s00018-015-1885-3

Bosker, T., van Balen, L., Walsh, B., Sepúlveda, M.S., DeGuise, S., Perkins, C., Griffitt, R.J., 2017. The combined effect of Macondo oil and corexit on sheepshead minnow (*Cyprinodon variegatus*) during early development. J. Toxicol. Environ. Heal. - Part A Curr. Issues 80, 477–484. https://doi.org/10.1080/15287394.2017.1340208

Burggren, W.W., Dubansky, B., Bautista, N.M., 2017. Cardiovascular development in embryonic and larval fishes, 1st ed, Fish Physiology. Elsevier Inc. https://doi.org/10.1016/bs.fp.2017.09.002

Caffrey, J.M., Murrell, M.C., Amacker, K.S., Harper, J.W., Phipps, S., Woodrey, M.S., 2014. Seasonal and inter-annual patterns in primary production, respiration, and net ecosystem metabolism in three estuaries in the northeast Gulf of Mexico. Estuaries and Coasts 37, 222–241. https://doi.org/10.1007/s12237-013-9701-5

Camilli, R., Di Iorio, D., Bowen, A., Reddy, C.M., Techet, A.H., Yoerger, D.R., Whitcomb, L.L., Seewald, J.S., Sylva, S.P., Fenwick, J., 2012. Acoustic measurement of the Deepwater Horizon Macondo well flow rate. Proc. Natl. Acad. Sci. 109, 20235–20239. https://doi.org/10.1073/pnas.1100385108

Carls, M.G., Holland, L., Larsen, M., Collier, T.K., Scholz, N.L., Incardona, J.P., 2008. Fish embryos are damaged by dissolved PAHs, not oil particles. Aquat. Toxicol. 88, 121–127. https://doi.org/10.1016/j.aquatox.2008.03.014

Carvalho, P.S.M., Kalil, D. da C.B., Novelli, G.A.A., Bainy, A.C.D., Fraga, A.P.M., 2008. Effects of naphthalene and phenanthrene on visual and prey capture endpoints during early stages of the dourado *Salminus Brasiliensis*. Mar. Environ. Res. 66, 205–207. https://doi.org/10.1016/j.marenvres.2008.02.059

Claireaux, G., Webber, D.M., Kerr, S.R., Boutilier, R.G., 1995. Physiology and behaviour of free-swimming Atlantic cod (*Gadus morhua*) facing fluctuating temperature conditions. J. Exp. Biol. 198, 49–60.

Collier, T.K., Anulacion, B.F., Arkoosh, M.R., Dietrich, J.P., Incardona, J.P., Johnson, L.L., Ylitalo, G.M., Myers, M.S., 2013. Effects on fish of polycyclic aromatic hydrocarbons (PAHS) and naphthenic acid exposures, First Edit. ed, Fish Physiology. Elsevier Inc. https://doi.org/10.1016/B978-0-12-398254-4.00004-2

Crone, T.J., Tolstoy, M., 2010. Magnitude of the 2010 Gulf of Mexico oil leak. Science (80-.). 330, 634–634. https://doi.org/10.1126/science.1195840

Edmunds, R.C., Gill, J.A., Baldwin, D.H., Linbo, T.L., French, B.L., Brown, T.L., Esbaugh, A.J., Mager, E.M., Stieglitz, J., Hoenig, R., Benetti, D., Grosell, M., Scholz, N.L., Incardona, J.P., 2015. Corresponding morphological and molecular indicators of crude oil toxicity to the developing hearts of mahi mahi. Sci. Rep. 5, 1–18. https://doi.org/10.1038/srep17326

Ern, R., Esbaugh, A.J., 2018. Effects of salinity and hypoxia-induced hyperventilation on oxygen consumption and cost of osmoregulation in the estuarine red drum (*Sciaenops ocellatus*). Comp. Biochem. Physiol. -Part A Mol. Integr. Physiol. 222, 52–59. https://doi.org/10.1016/j.cbpa.2018.04.013

Esbaugh, A.J., Mager, E.M., Stieglitz, J.D., Hoenig, R., Brown, T.L., French, B.L., Linbo, T.L., Lay, C., Forth, H., Scholz, N.L., Incardona, J.P., Morris, J.M., Benetti, D.D., Grosell, M., 2016. The effects of weathering and chemical dispersion on Deepwater Horizon crude oil toxicity to mahi-mahi (*Coryphaena hippurus*) early life stages. Sci. Total Environ. 543, 644–651. https://doi.org/10.1016/j.scitotenv.2015.11.068

Farrell, A.P., 2007. Tribute to P. L. Lutz: A message from the heart - Why hypoxic bradycardia in fishes? J. Exp. Biol. 210, 1715–1725. https://doi.org/10.1242/jeb.02781

Forth, H.P., Mitchelmore, C.L., Morris, J.M., Lay, C.R., Lipton, J., 2017. Characterization of dissolved and particulate phases of water accommodated fractions used to conduct aquatic toxicity testing in support of the Deepwater Horizon natural resource damage assessment. Environ. Toxicol. Chem. 36, 1460–1472. https://doi.org/10.1002/etc.3803

Garcia, T.I., Shen, Y., Crawford, D., Oleksiak, M.F., Whitehead, A., Walter, R.B., 2012. RNA-Seq reveals complex genetic response to deepwater horizon oil release in *Fundulus grandis*. BMC Genomics 13, 1–9. https://doi.org/10.1186/1471-2164-13-474

Gray, J.S., Wu, R.S.S., Ying, Y.O., 2002. Effects of hypoxia and organic enrichment on the coastal marine environment. Mar. Ecol. Prog. Ser. 238, 249–279. https://doi.org/10.3354/meps238249

Greeley, M.S., MacGregor, R., 1983. Annual and semilunar reproductive cycles of the Gulf killifish, *Fundulus grandis*, on the Alabama Gulf coast. Copeia 1983, 711–718. https://doi.org/10.2307/1444337

Haney, D.C., Nordlie, F.G., 1997. Influence of environmental salinity on routine metabolic rate and critical oxygen tension of *Cyprinodon variegatus*. Physiol. Zool. 70, 511–518. https://doi.org/10.1086/515867

Heintz, R.A., Short, J.W., Rice, S.D., 1999. Sensitivity of fish embryos to weathered crude oil: Part II. Increased mortality of pink salmon (*Oncorhynchus gorbuscha*) embryos incubating downstream from weathered Exxon Valdez crude oil. Environ. Toxicol. Chem. 18, 494–503. https://doi.org/10.1897/1551-5028(1999)018<0494:SOFETW>2.3.CO;2

Hose, J.E., McGurk, M.D., Marty, G.D., Hinton, D.E., Brown, E.D., Baker, T.T., 1996. Sublethal effects of the (Exxon Valdez) oil spill on herring embryos and larvae: morphological, cytogenetic, and histopathological assessments, 1989–-1991. Can. J. Fish. Aquat. Sci. 53, 2355–2365. https://doi.org/10.1139/f96-174

Huang, L., Zuo, Z., Zhang, Y., Wu, M., Lin, J.J., Wang, C., 2014. Use of toxicogenomics to predict the potential toxic effect of Benzo(a)pyrene on zebrafish embryos: ocular developmental toxicity. Chemosphere 108, 55–61. https://doi.org/10.1016/j.chemosphere.2014.02.078

Incardona, J.P., Carls, M.G., Day, H.L., Sloan, C.A., Bolton, J.L., Collier, T.K., Schoiz, N.L., 2009. Cardiac arrhythmia is the primary response of embryonic pacific herring (*Clupea pallasi*) exposed to crude oil during weathering. Environ. Sci. Technol. 43, 201–207. https://doi.org/10.1021/es802270t

Incardona, J.P., Collier, T.K., Scholz, N.L., 2011. Oil spills and fish health: Exposing the heart of the matter. J. Expo. Sci. Environ. Epidemiol. 21, 3–4. https://doi.org/10.1038/jes.2010.51

Incardona, J.P., Collier, T.K., Scholz, N.L., 2004. Defects in cardiac function precede morphological abnormalities in fish embryos exposed to polycyclic aromatic hydrocarbons. Toxicol. Appl. Pharmacol. 196, 191–205. https://doi.org/10.1016/j.taap.2003.11.026

Incardona, J.P., Gardner, L.D., Linbo, T.L., Brown, T.L., Esbaugh, A.J., Mager, E.M., Stieglitz, J.D., French, B.L., Labenia, J.S., Laetz, C.A., Tagal, M., Sloan, C.A., Elizur, A., Benetti, D.D., Grosell, M., Block, B.A., Scholz, N.L., 2014. Deepwater Horizon crude oil impacts the developing hearts of large predatory pelagic fish. Proc. Natl. Acad. Sci. 111, E1510–E1518. https://doi.org/10.1073/pnas.1320950111

Jayasundara, N., Van Tiem Garner, L., Meyer, J.N., Erwin, K.N., Di Giulio, R.T., 2015. AHR2-mediated transcriptomic responses underlying the synergistic cardiac developmental toxicity of PAHs. Toxicol. Sci. 143, 469–481. https://doi.org/10.1093/toxsci/kfu245

Jones, E.R., Simning, D., Serafin, J., Sepúlveda, M.S., Griffitt, R.J., 2020. Acute exposure to oil induces age and species-specific transcriptional responses in embryo-larval estuarine fish. Environ. Pollut. 263, 1–10. https://doi.org/10.1016/j.envpol.2020.114325

Keen, A.N., Klaiman, J.M., Shiels, H.A., Gillis, T.E., 2017. Temperature-induced cardiac remodelling in fish. J. Exp. Biol. 220, 147–160. https://doi.org/10.1242/jeb.128496

Khursigara, A.J., Perrichon, P., Martinez Bautista, N., Burggren, W.W., Esbaugh, A.J., 2017. Cardiac function and survival are affected by crude oil in larval red drum, *Sciaenops ocellatus*. Sci. Total Environ. 579, 797–804. https://doi.org/10.1016/j.scitotenv.2016.11.026

Klaiman, J.M., Fenna, A.J., Shiels, H.A., Macri, J., Gillis, T.E., 2011. Cardiac remodeling in fish: Strategies to maintain heart function during temperature change. PLoS One 6. https://doi.org/10.1371/journal.pone.0024464

Kuntz, A., 1916. Notes on the embryology and larval development of five species of teleostean fishes. Bull. Bur. Fish. 34, 409–429.

Lin, H., Pfeiffer, D., Vogl, A., Pan, J., Randall, D., 1994. Immunolocalization of H+-ATPase in the gill epithelia of rainbow trout. J. Exp. Biol. 195, 169–83.

Mager, E.M., Esbaugh, A.J., Stieglitz, J.D., Hoenig, R., Bodinier, C., Incardona, J.P., Scholz, N.L., Benetti, D.D., Grosell, M., 2014. Acute embryonic or juvenile exposure to deepwater horizon crude oil impairs the swimming performance of mahi-mahi (*Coryphaena hippurus*). Environ. Sci. Technol. 48, 7053–7061. https://doi.org/10.1021/es501628k

Mager, E.M., Pasparakis, C., Schlenker, L.S., Yao, Z., Bodinier, C., Stieglitz, J.D., Hoenig, R., Morris, J.M., Benetti, D.D., Grosell, M., 2017. Assessment of early life stage mahi-mahi windows of sensitivity during acute exposures to Deepwater Horizon crude oil. Environ. Toxicol. Chem. 36, 1887–1895. https://doi.org/10.1002/etc.3713

Magnuson, J.T., Khursigara, A.J., Allmon, E.B., Esbaugh, A.J., Roberts, A.P., 2018. Effects of Deepwater Horizon crude oil on ocular development in two estuarine fish species, red drum (*Sciaenops ocellatus*) and sheepshead minnow (*Cyprinodon variegatus*). Ecotoxicol. Environ. Saf. 166, 186–191. https://doi.org/10.1016/j.ecoenv.2018.09.087

Martyniuk, C.J., Simmons, D.B., 2016. Spotlight on environmental omics and toxicology: a long way in a short time. Comp. Biochem. Physiol. - Part D Genomics Proteomics 19, 97–101. https://doi.org/10.1016/j.cbd.2016.06.010

McNutt, M.K., Camilli, R., Crone, T.J., Guthrie, G.D., Hsieh, P.A., Ryerson, T.B., Savas, O., Shaffer, F., 2012. Review of flow rate estimates of the Deepwater Horizon oil spill. Proc. Natl. Acad. Sci. 109, 20260–20267. https://doi.org/10.1073/pnas.1112139108

Mendelssohn, I.A., Andersen, G.L., Baltz, D.M., Caffey, R.H., Carman, K.R., Fleeger, J.W., Joye, S.B., Lin, Q., Maltby, E., Overton, E.B., Rozas, L.P., 2012. Oil impacts on coastal wetlands: Implications for the Mississippi River delta ecosystem after the Deepwater Horizon oil spill. Bioscience 62, 562–574. https://doi.org/10.1525/bio.2012.62.6.7

Middaugh, D.P., Hemmer, M.J., 1992. Reproductive ecology of the inland silverside, *Menidia beryllina*, (Pisces: Atherinidae) from Blackwater Bay, Florida. Copeia 1992, 53. https://doi.org/10.2307/1446535

Miyashita, S., Tanaka, Y., Sawada, Y., Takii, K., Mukai, Y., Kumai, H., 2000. Embryonic development and effects of water temperature on hatching of the bluefin tuna, *Thunnus thynnus*. Fish. Breed. 48, 199–207. https://doi.org/https://doi.org/10.11233/aquaculturesci1953.48.199

Muhling, B.A., Roffer, M.A., Lamkin, J.T., Ingram, G.W., Upton, M.A., Gawlikowski, G., Muller-Karger, F., Habtes, S., Richards, W.J., 2012. Overlap between Atlantic bluefin tuna spawning grounds and observed Deepwater Horizon surface oil in the northern Gulf of Mexico. Mar. Pollut. Bull. 64, 679–687. https://doi.org/10.1016/j.marpolbul.2012.01.034

Murphy, D., Gemmell, B., Vaccari, L., Li, C., Bacosa, H., Evans, M., Gemmell, C., Harvey, T., Jalali, M., Niepa, T.H.R., 2016. An in-depth survey of the oil spill literature since 1968: Long term trends and changes since Deepwater Horizon. Mar. Pollut. Bull. 113, 371–379. https://doi.org/10.1016/j.marpolbul.2016.10.028

Nakano, A., Sugii, Y., Minamiyama, M., Niimi, H., 2003. Measurement of red cell velocity in microvessels using particle image velocimetry (PIV). Clin. Hemorheol. Microcirc. 29, 445–455.

Nixon, Z., Zengel, S., Baker, M., Steinhoff, M., Fricano, G., Rouhani, S., Michel, J., 2016. Shoreline oiling from the Deepwater Horizon oil spill. Mar. Pollut. Bull. 107, 170–178. https://doi.org/10.1016/j.marpolbul.2016.04.003

NOAA National Estuarine Research Reserve System (NERRS). 2021. System-wide Monitoring Program. Data accessed from the NOAA NERRS Centralized Data Management Office website: http://www.nerrsdata.org; accessed 12 February 2021.

Norse, E.A., Amos, J., 2010. Impacts, perception, and policy implications of the Deepwater Horizon oil and gas disaster. Environ. Law Report. 40, 11058–11073. https://doi.org/10.1038/nn.2937

Oleksiak, M.F., Karchner, S.I., Jenny, M.J., Franks, D.G., Mark Welch, D.B., Hahn, M.E., 2011. Transcriptomic assessment of resistance to effects of an aryl hydrocarbon receptor (AHR) agonist in embryos of Atlantic killifish (*Fundulus heteroclitus*) from a marine Superfund site. BMC Genomics 12, 1–18. https://doi.org/10.1186/1471-2164-12-263

Orlando, S.P.J., Rozas, L.P., Ward, G.H., Klein, C.J., 1993. Salinity characteristics of Gulf of Mexico estuaries. Natl. Ocean. Atmos. Adm. Off. Ocean Resour. Conserv. Assess. 209. https://doi.org/10.1016/0004-6981(75)90067-0

Pan, Y.K., Khursigara, A.J., Johansen, J.L., Esbaugh, A.J., 2018. The effects of oil induced respiratory impairment on two indices of hypoxia tolerance in Atlantic croaker (*Micropogonias undulatus*). Chemosphere 200, 143–150. https://doi.org/10.1016/j.chemosphere.2018.02.028

Pelster, B., 1999. Environmental influences on the development of the cardiac system in fish and amphibians. Comp. Biochem. Physiol. - A Mol. Integr. Physiol. 124, 407–412. https://doi.org/10.1016/S1095-6433(99)00132-4

Peterson, C.H., Rice, S.D., Short, J.W., Esler, D., Bodkin, J.L., Ballachey, B.E., Irons, D.B., 2003. Long-term ecosystem response to the Exxon Valdez oil spill. Science. 302, 2082–6. https://doi.org/10.1126/science.1084282

Powell, W.H., Morrison, H.G., Weil, E.J., Karchner, S.I., Sogin, M.L., Stegeman, J.J., Hahn, M.E., 2004. Cloning and analysis of the CYP1A promoter from the Atlantic killifish (*Fundulus heteroclitus*). Mar. Environ. Res. 58, 119–124. https://doi.org/10.1016/j.marenvres.2004.03.005

Rabalais, N.N., Turner, R.E., Wiseman, W.J., 2002. Gulf of Mexico hypoxia, A.K.A. "The dead zone." Annu. Rev. Ecol. Syst. 33, 235–263. https://doi.org/10.1146/annurev.ecolsys.33.010802.150513

Randall, D.J., Smith, J.C., 1967. The regulation of cardiac activity in fish in a hypoxic environment. Physiol. Zool. 40, 104–113. https://doi.org/10.1086/physzool.40.2.30152445

Reid, N.M., Proestou, D.A., Clark, B.W., Warren, W.C., Colbourne, J.K., Shaw, J.R., Karchner, S.I., Hahn, M.E., Nacci, D., Oleksiak, M.F., Crawford, D.L., Whitehead, A., 2016. The genomic landscape of rapid repeated evolutionary adaptation to toxic pollution in wild fish. Science. 354, 1305–1308. https://doi.org/10.1126/science.aah4993

Rooker, J.R., Kitchens, L.L., Dance, M.A., Wells, R.J.D., Falterman, B., Cornic, M., 2013. Spatial, temporal, and habitat-related variation in abundance of pelagic fishes in the Gulf of Mexico: Potential implications of the Deepwater Horizon oil spill. PLoS One 8, 1–10. https://doi.org/10.1371/journal.pone.0076080

Rooker, J.R., Simms, J.R., David Wells, R.J., Holt, S.A., Holt, G.J., Graves, J.E., Furey, N.B., 2012. Distribution and habitat associations of billfish and swordfish larvae across mesoscale features in the Gulf of Mexico. PLoS One 7. https://doi.org/10.1371/journal.pone.0034180

Sammarco, P.W., Kolian, S.R., Warby, R.A.F., Bouldin, J.L., Subra, W.A., Porter, S.A., 2013. Distribution and concentrations of petroleum hydrocarbons associated with the BP/Deepwater Horizon oil spill, Gulf of Mexico. Mar. Pollut. Bull. 73, 129–143. https://doi.org/10.1016/j.marpolbul.2013.05.029

Schroeder, W.W., Wiseman, W.J., 1986. Low-frequency shelf-estuarine exchange processes in Mobile Bay and other estuarine systems on the northern Gulf of Mexico, estuarine variability. Academic Press, Inc. https://doi.org/10.1016/B978-0-12-761890-6.50027-7

Serafin, J., Guffey, S.C., Bosker, T., Griffitt, R.J., De Guise, S., Perkins, C., Szuter, M., Sepúlveda, M.S., 2019. Combined effects of salinity, temperature, hypoxia, and Deepwater Horizon oil on *Fundulus grandis* larvae. Ecotoxicol. Environ. Saf. 181, 106–113. https://doi.org/10.1016/j.ecoenv.2019.05.059

Short, J.W., Rice, S.D., Heintz, R.A., Carls, M.G., Moles, A., 2003. Long-term effects of crude oil on developing fish: Lessons from the Exxon Valdez oil spill. Energy Sources 25, 509–517. https://doi.org/10.1080/00908310390195589

Simning, D., Sepulveda, M., De Guise, S., Bosker, T., Griffitt, R.J., 2019. The combined effects of salinity, hypoxia, and oil exposure on survival and gene expression in developing sheepshead minnows, *Cyprinodon variegatus*. Aquat. Toxicol. 214, 105234. https://doi.org/10.1016/j.aquatox.2019.105234

Stierhoff, K.L., Targett, T.E., Miller, K., 2006. Ecophysiological responses of juvenile summer and winter flounder to hypoxia: Experimental and modeling analyses of effects on estuarine nursery quality. Mar. Ecol. Prog. Ser. 325, 255–266. https://doi.org/10.3354/meps325255

Sugii, Y., Nishio, S., Okamoto, K., 2002. In vivo PIV measurement of red blood cell velocity field in microvessels considering mesentery motion. Physiol. Meas. 23, 403–416. https://doi.org/10.1088/0967-3334/23/2/315

Wang, Z., Gerstein, M., Snyder, M., 2009. RNA-Seq: a revolutionary tool for transcriptomics. Nat. Rev. Genet. 10, 57–63. https://doi.org/10.1038/nrg2484

Wang, Z., Liu, Z., Xu, K., Mayer, L.M., Zhang, Z., Kolker, A.S., Wu, W., 2014. Concentrations & sources of polycyclic aromatic hydrocarbons in surface coastal sediments of the northern Gulf of Mexico. Geochem. Trans. 15, 1–12. https://doi.org/10.1186/1467-4866-15-2

Whitehead, A., Dubansky, B., Bodinier, C., Garcia, T.I., Miles, S., Pilley, C., Raghunathan, V., Roach, J.L., Walker, N., Walter, R.B., Rice, C.D., Galvez, F., 2012. Genomic and physiological footprint of the Deepwater Horizon oil spill on resident marsh fishes. Proc. Natl. Acad. Sci. 109, 20298–20302. https://doi.org/10.1073/pnas.1109545108

Whitehead, A., Roach, J.L., Zhang, S., Galvez, F., 2011. Genomic mechanisms of evolved physiological plasticity in killifish distributed along an environmental salinity gradient. Proc. Natl. Acad. Sci. U. S. A. 108, 6193–6198. https://doi.org/10.1073/pnas.1017542108

Wilson, B.J., Mortazavi, B., Kiene, R.P., 2015. Spatial and temporal variability in carbon dioxide and methane exchange at three coastal marshes along a salinity gradient in a northern Gulf of Mexico estuary. Biogeochemistry 123, 329–347. https://doi.org/10.1007/s10533-015-0085-4

Wilson, C.J., Dunton, K.H., 2012. Assessment of seagrass habitat quality and plant physiological conditions in south Texas waters.

Wu, R.S.S., 2002. Hypoxia: From molecular responses to ecosystem responses. Mar. Pollut. Bull. 45, 35–45. https://doi.org/10.1016/S0025-326X(02)00061-9

Xu, E.G., Khursigara, A.J., Magnuson, J., Hazard, E.S., Hardiman, G., Esbaugh, A.J., Roberts, A.P., Schlenk, D., 2017. Larval red drum (*Sciaenops ocellatus*) sublethal exposure to weathered Deepwater Horizon crude oil: Developmental and transcriptomic consequences. Environ. Sci. Technol. 51, 10162–10172. https://doi.org/10.1021/acs.est.7b02037

Xu, E.G., Mager, E.M., Grosell, M., Pasparakis, C., Schlenker, L.S., Stieglitz, J.D., Benetti, D., Hazard, E.S., Courtney, S.M., Diamante, G., Freitas, J., Hardiman, G., Schlenk, D., 2016. Time- and oil-dependent transcriptomic and physiological responses to Deepwater Horizon oil in Mahi-Mahi (*Coryphaena hippurus*) embryos and larvae. Environ. Sci. Technol. 50, 7842–7851. https://doi.org/10.1021/acs.est.6b02205

Zhang, H., Ludsin, S.A., Mason, D.M., Adamack, A.T., Brandt, S.B., Zhang, X., Kimmel, D.G., Roman, M.R., Boicourt, W.C., 2009. Hypoxia-driven changes in the behavior and spatial distribution of pelagic fish and mesozooplankton in the northern Gulf of Mexico. J. Exp. Mar. Bio. Ecol. 381, S80–S91. https://doi.org/10.1016/j.jembe.2009.07.014

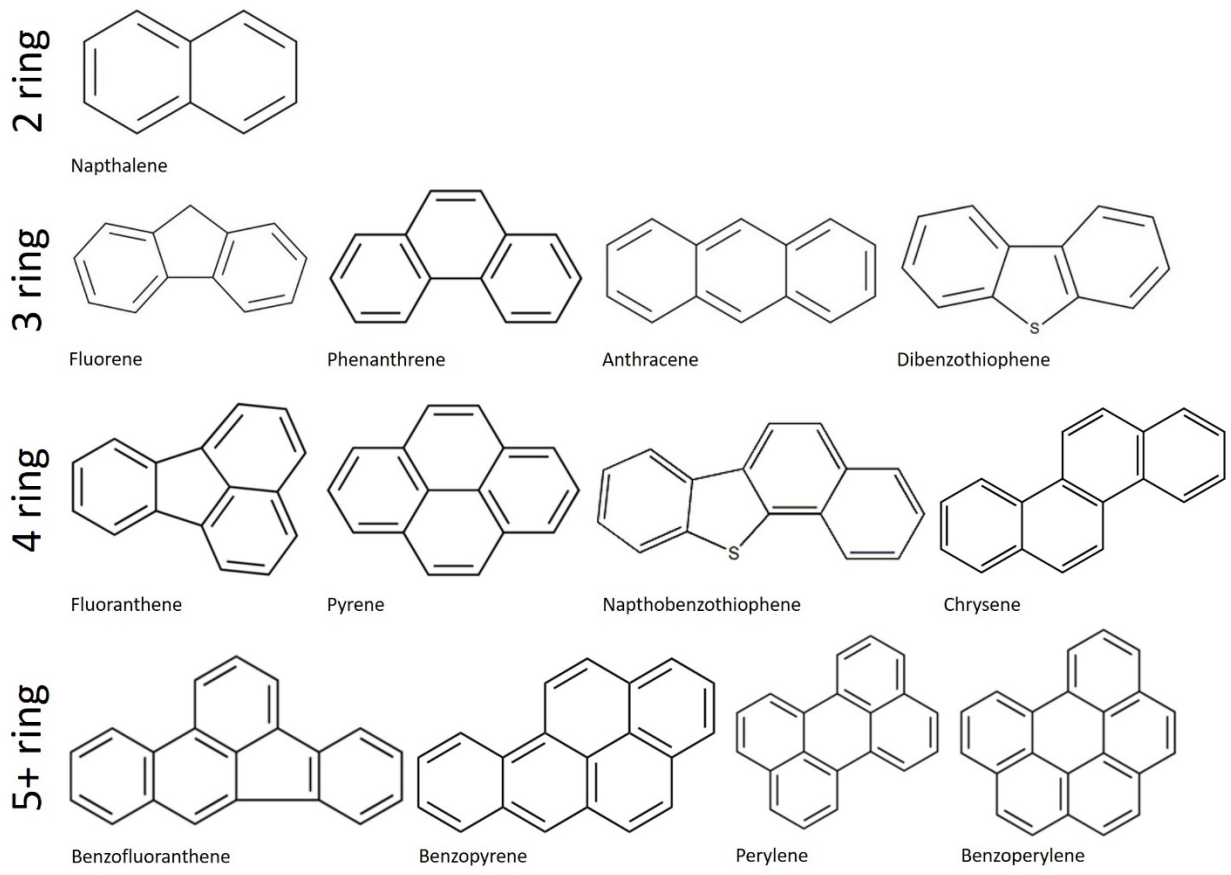

Figure 1.1. Chemical structures of common polycyclic aromatic hydrocarbons present in weathered oil from the Deepwater Horizon oil spill.

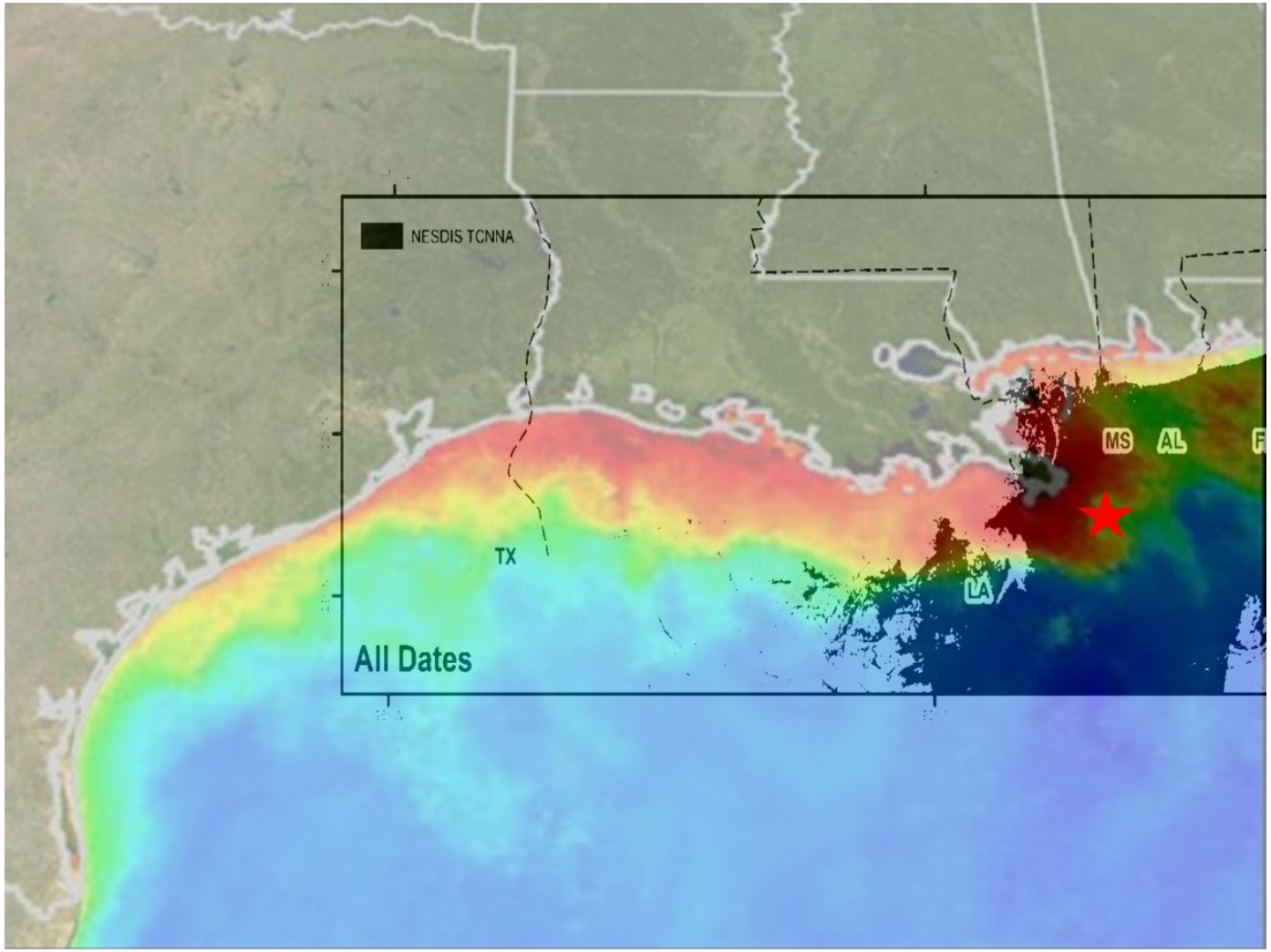

Figure 1.2. Map depicting the spatial coincidence of the 2010 northern Gulf of Mexico hypoxic "dead zone" (NOAA) and the surface slick of the Deepwater Horizon oil spill (Nixon et al., 2016). Heat map indicates severity of hypoxia with warmer colors representing lower dissolved oxygen levels (hypoxia/anoxia) and cooler colors representing higher dissolved oxygen levels within the water column (normoxia). Shaded areas within the black box represent location of the surface slick between April and September 2010. Red star indicates location of the Deepwater Horizon wellhead.

CHAPTER 2. THE INFLUENCE OF HYPOXIA ON THE CARDIAC TRANSCRIPTOMES OF TWO ESTUARINE SPECIES - *C. VARIEGATUS* AND *F. GRANDIS*

A version of this chapter has been previously published; reproduced from:
Allmon, E., Serafin, J., Chen, S., Simning, D., Griffitt, R., Bosker, T., De Guise, S., Sepúlveda, M.S. 2021. The influence of hypoxia on the cardiac transcriptomes of two estuarine species – *C. variegatus* and *F. grandis*. Comp. Biochem. Physiol. D. 39, 100837.
https://doi.org/10.1016/j.cbd.2021.100837

2.1 Abstract

Increased nutrient loading has led to eutrophication of coastal shelf waters which has resulted in increased prevalence of persistent hypoxic zones – areas in which the dissolved oxygen content of the water drops below 2 mg/L. The northern Gulf of Mexico, fed primarily by the Mississippi River watershed, undergoes annual establishment of one of the largest hypoxic zones in the world. Exposure to hypoxia can induce physiological impacts in fish cardiac systems that include bradycardia, changes in stroke volume, and altered cardiovascular vessel development. While these impacts have been addressed at the functional level, there is little information regarding the molecular basis for these changes. This study used transcriptomic analysis techniques to interrogate the effects of hypoxia exposure on the developing cardiovascular system in newly hatched larvae of two estuarine species that occupy the same ecological niche – the sheepshead minnow (*Cyprinodon variegatus*) and the Gulf killifish (*Fundulus grandis*). Results suggest that while differential gene expression is largely distinct between the two species, downstream impacts on pathways and functional responses such as reduced cardiac hypertrophy, modulation of blood pressure, and increased incidence of apoptosis appear to be conserved. Further, differences in the magnitude of these conserved responses may suggest that

the length of embryonic development could impart a level of resiliency to hypoxic perturbation in early life stage fish.

2.2 Introduction

The presence of hypoxic zones (waters in which dissolved oxygen (DO) levels fall below 2 mg/L) in coastal waters have steadily increased on a global scale since the mid-1900's (Diaz and Rosenberg, 2008; Rabalais et al., 2010). While some hypoxic zones occur naturally in areas of coastal upwelling (Grantham et al., 2004; Helly and Levin, 2004; Rabalais et al., 2010), many are attributed to increased nutrient loading (Conley et al., 2009; Rabalais et al., 2010, 2002) - particularly due to excess nitrogen runoff from coastal watersheds (Rabalais et al., 2010, 2007, 2002; Rabalais and Turner, 2019; Turner and Rabalais, 1991). The associated eutrophication of surface waters often leads to algal blooms, which ultimately die and sink to the sea floor - leading to increased microbial respiration and decreased water oxygen levels (Rabalais et al., 2010, 2002; Rabalais and Turner, 2019). One of the largest hypoxic zones in the world is in the Northern Gulf of Mexico. Fed by the Mississippi and Atchafalaya Rivers and extending to the mid-continental shelf along the Texas and Louisiana coasts, the Gulf of Mexico "Dead Zone" forms annually and covers an average of 15,000 km^2 (Rabalais et al., 2007; Turner and Rabalais, 2018). The duration of hypoxic conditions varies from year to year and is driven by seasonal stratification of the water column (Rabalais and Turner, 2019; Turner and Rabalais, 2018). Annual establishment of the Dead Zone generally begins in late spring and persists until strong cold fronts and tropical storms/hurricanes drive mixing of the water column and reoxygenation of subsurface waters in the late summer to early fall (Rabalais et al., 2010; Turner and Rabalais, 2018).

The coast of the Northern Gulf of Mexico is defined in many areas by shallow estuaries, protected bays, and seagrass beds that play important roles in the life cycles of many marine species (Nordlie, 2003). For example, estuaries act as spawning grounds and nursery habitats for many fish species, providing settlement habitat for juveniles, shelter, and protection from predators (Boehlert and Mundy, 1988; Morrell and Gobler, 2020; Rooker and Holt, 1997; Stierhoff et al., 2006). The complex biogeochemical processes within estuaries are driven by inland influences (e.g. from adjacent watersheds) as well as tidally driven pelagic influences, which requires that species inhabiting these inshore environments need to be capable of compensating for changing environments – including persistent hypoxic events (Conley et al., 2009). In addition to hypoxic influences of the Dead Zone, these estuaries are susceptible to thermally driven hypoxic events during which water temperatures throughout the water column rise, resulting in decreased water oxygen saturation. Exposure to hypoxia has a multitude of impacts on organisms and ecosystem processes including reduced survival, diminished reproductive capacity, reduced local biodiversity, and changes in trophic structures and interactions (Cheek et al., 2009; Craig, 2012; Eby and Crowder, 2002; Gray et al., 2002; Jeppesen et al., 2018; LaBone et al., 2019; Landry et al., 2007; Morrell and Gobler, 2020; Rabalais et al., 2002; Shang and Wu, 2004; Thomas et al., 2007; Vaquer-Sunyer and Duarte, 2008; Wu, 2002; Wu et al., 2003; Zhang et al., 2009). Organism's responses to hypoxia are varied and range from behavioral changes to metabolic adaptation across species (Gray et al., 2002; Limburg et al., 2015; Rabalais et al., 2002; Wu, 2002; Zhang et al., 2009). For example, mobile, pelagic species such as Atlantic croaker (*Micropogonias undulatus*), may vertically migrate out of hypoxic bottom waters or fully migrate out of the hypoxic zone until the waters become reoxygenated (Hazen et al., 2009; Wannamaker and Rice, 2000). Inshore or sessile

species, however, may not be able to physically escape hypoxic waters and therefore must employ strategies to physiologically compensate for low oxygen levels.

Strategies employed by inshore marine species to cope with prolonged hypoxia include transitioning to anaerobic metabolism, migration from sub-sediment burrows to the sediment surface, and changes in predation/ foraging behaviors (Gray et al., 2002; Pelster, 1999; Rabalais et al., 2002; Wu, 2002). In particular, inshore fish species have exhibited changes in ventilatory rates, reduced growth rates, and transitions to surface breathing when confined to hypoxic environments (Burggren et al., 2017; Ern and Esbaugh, 2018; Gray et al., 2002; Rabalais et al., 2002; Randall and Smith, 1967; Stierhoff et al., 2006; Zhang et al., 2009). In addition, the cardiac system of fish has been proven to be sensitive to exposure to hypoxia and studies on the impacts of hypoxia on the cardiac systems of fish have revealed rapid onset of bradycardia, changes in stroke volume, altered cardiovascular vessel development, and changes in cardiac metabolism pathways (Bagatto, 2005; Burggren et al., 2017; Everett et al., 2012; Farrell, 2007; Gamperl and Farrell, 2004; Johnston et al., 2013; Pelster, 1999; Randall and Smith, 1967). Although there have been numerous studies on the impact of hypoxia on the cardiac system at the organismal level, the number of studies that have investigated the transcriptomic effects of hypoxia during early life history on the developing cardiac system of fish are relatively low in comparison. These studies have shown that early life stage exposure to hypoxia, especially in the embryonic stages, induces gene expression changes that can impact physiological function in later life history (Johnston et al., 2013; Robertson et al., 2014; Ton et al., 2003).

This study aims to elucidate the effects of hypoxia on the cardiac transcriptome of newly hatched juveniles in two estuarine species – the sheepshead minnow (*Cyprinodon variegatus*) and the Gulf killifish (*Fundulus grandis*). Generally, it is assumed that species occupying the

same ecological niche will exhibit similar responses to environmental perturbations, such as hypoxia (Jones et al., 2020). Recently, studies into the effects of oil on *C. variegatus* and *F. grandis* larval mortality and transcriptional responses suggest that there may be subtle differences in molecular responses that impart differential sensitivities between species (Jones et al., 2020; Serafin et al., 2019; Simning et al., 2019). *C. variegatus* and *F. grandis* are both widely distributed species within Gulf of Mexico estuaries and are commonly used in laboratory studies. Estuaries in the northern Gulf of Mexico regularly undergo thermally driven hypoxic events during the summer months during which water temperatures rise and often exceed 30°C. These periods of elevated water temperatures coincide with the spawning seasons of both species – February through October for *C. variegatus* and March through October for *F. grandis*. However, the embryonic period is longer in *F. grandis* (14 days; Greeley and MacGregor, 1983) than *C. variegatus* (6 days; Kuntz, 1916) resulting in a more complete development of the cardiovascular system at hatch in *F. grandis* (Armstrong and Child, 1965). We predict that transcriptomic and downstream functional cardiac responses to hypoxia exposure will be similar between species. Due to its shorter development time in the embryonic stage and less developed cardiovascular system at hatch, we hypothesize that post-hatch *C. variegatus* will be more susceptible to hypoxic perturbation and exhibit increased transcriptomic responses to hypoxia exposure than post-hatch *F. grandis*.

2.3 Materials and Methods

2.3.1 Broodstock collection and spawning

All animals were treated humanely in accordance with approved IACUC protocols from Purdue University. Adult broodstock and embryos were maintained at species-specific optimal

spawning and rearing conditions (for optimal *F. grandis* conditions see Green, 2013; for optimal *C. variegatus* conditions see USEPA, 2002) until initiation of exposures post-hatch.

C. variegatus embryos were collected from adult broodstock maintained at the University of Southern Mississippi's Gulf Coast Research Lab (Ocean Springs, MS, USA) during natural spawning events. Adult broodstock were housed in 12, 300 L recirculating raceways supplied with 15 ppt artificial seawater (prepared with local well water, Fritz SuperSalt Concentrate (Fritz Industries, Mesquite, TX, USA), and Tru-Soft water softener pellets (United Salt Corporation, Houston, TX, USA)) maintained at 6 mg/L DO and 25°C on a 16L:8D photoperiod (Simning et al., 2019; USEPA, 2002). Adults were fed commercial flake food to satiation twice daily. Benthic breeding mats were introduced into each raceway for 24 hours, after which breeding mats were removed and embryos were pooled into a single collection and washed in fresh water to remove parasites and/or pathogens. Cleaned embryos were gently rolled on fine nylon mesh to remove embryonic microvilli to prevent embryos from adhering to each other (USEPA, 2002) and were then examined for fertilization. Fertilized embryos were transferred into 4 L holding tanks supplied with 30 ppt artificial seawater (prepared as described above) maintained at 30 °C until hatch, at which time larvae were immediately moved into exposure chambers.

Adult *F. grandis* were sampled from wild populations in Gulf of Mexico estuaries along the Mississippi coast in March 2015 and were subsequently shipped to the Purdue Aquatic Research Lab at Purdue University (West Lafayette, IN, USA). Adults were housed in 12, 130 L aquaria connected as a recirculation aquaculture system maintained at ideal spawning conditions - 10 ppt artificial seawater (prepared with Fritz SuperSalt concentrate), 6 mg/L DO and 25°C on a 16L:8D photoperiod (Green, 2013). Fish were fed a mixed diet of frozen chironomids and

frozen brine shrimp twice daily to satiation. Breeding was initialized through the introduction of polyester filter mats (Pentair, Minneapolis, MN, USA) following methodologies described in Green, 2013. Following spawning, fertilized embryos were collected and maintained in mesh hatching chambers within the spawning tanks (see Serafin et al., 2019 for full methodology). At hatch, larvae were immediately moved into exposure chambers.

2.3.2 Exposure design

C. variegatus larvae (< 10 h post-hatch) were randomly selected and placed in 150 mL crystalizing beakers supplied with 100 mL artificial seawater (30 ppt) prepared as described above (n = 30 larvae/beaker). Normoxic conditions (DO > 5 mg/L; n = 3) were maintained in a temperature controlled environmental chamber at 30°C with a 16L:8D photoperiod, exposure chambers were placed in the environmental chamber 4 h prior to initiation of the experiment to allow water temperature to reach 30°C. Hypoxic conditions (DO ≤ 2 mg/L; n = 3) were maintained by introducing nitrogen gas into a Biospherix I-Glove incubator glovebox equipped with a PROOX model 360 oxygen control module (See Simning et al., 2019 for full description of methodology). Exposures lasted for 48 h with water quality monitored daily in all exposure chambers. *C. variegatus* larvae remained reliant on endogenous feeding from yolk sac reserves and were not fed during the course of the exposures.

F. grandis larvae (<24 h post-hatch) were randomly chosen and placed in individual 125 mL glass jars sealed with Teflon lined caps. Exposure chambers [n = 9 normoxia (DO = 6 mg/L); n = 9 hypoxia (DO ≤ 2 mg/L)] were maintained within temperature controlled environmental chambers at 30°C with a 16L:8D photoperiod and salinity was maintained using reconstituted saltwater at 30 ppt as described above. Hypoxia was established through aeration of exposure solution with nitrogen gas. Exposures lasted 48 h with water quality monitored

daily. Larvae were not fed during the course of the exposure as they were still reliant on yolk sac.

2.3.3 Water chemistry

Temperature, DO, and salinity were recorded at the onset of exposures and every 24 h throughout the experiment. Temperature and DO were measured using a YSI PRO 1020 multi-parameter meter (YSI Inc., Yellow Springs, Ohio, USA). Salinity was measured using a Pentair Vital Sine SR6 handheld refractometer (Pentair AES, Cary, NC, USA). See Simning et al., 2019 (*C. variegatus*) and Serafin et al., 2019 (*F. grandis*) for full water quality methodologies.

2.3.4 RNA isolation/ RNA Seq

Immediately following conclusion of 48 h exposures, whole larvae were collected for RNA analysis. To ensure sufficient RNA for library generation, 10 larvae were randomly sampled from each *C. variegatus* exposure chamber and pooled to constitute one replicate. Similarly, three *F. grandis* larvae were pooled to constitute one replicate, resulting in 3 normoxic and 3 hypoxic replicates per species. Larvae were flash frozen and stored at -80°C until RNA extraction. RNA was isolated with RNeasy Mini Kits (Qiagen, Valencia, CA, USA) following manufacturer's protocols. Extracted *C. variegatus* RNA was shipped from The University of Southern Mississippi to Purdue University overnight on dry ice. RNA concentrations were quantified on a NanoDrop 2000 spectrophotometer with associated software (Thermo Fisher, Waltham, MA, USA). All library preparation and RNA sequencing (RNA Seq) was performed by the Purdue University Genomics Core Facility (West Lafayette, IN, USA) using Illumina TruSeq Stranded mRNA Sample Preparations Guide (Illumina, San Diego, CA, USA) to construct polyA+ libraries. Libraries were sequenced on an Illumina HiSeq 2500 (Illumina, San

Diego, CA, USA) to a minimum of 30 million 2 x 100 bp sequencing reads for *C. variegatus* and 15 million 2 x 100 bp sequencing reads for *F. grandis*.

2.3.5 Bioinformatic analysis

All sequencing data have been submitted and archived through the Gulf of Mexico Research Initiative Information & Data Cooperative (GRIIDC) and are publicly available through NCBI's Gene Expression Omnibus (GEO) database (*C. variegatus*: GSE123469; *F. grandis*: GSE129998). Quality checks of sequenced reads were conducted using the FastQC toolkit (Andrews, 2010), Trimmomatic (Bolger et al., 2014) was used to remove adapter and low-quality reads, and additional quality checks were run post-cleaning using FastQC. Filtered sequences were loaded into CLC Genomics Workbench (Qiagen, Hilden, Germany) where *C. variegatus* paired-end reads were merged and mapped to the *C. variegatus* reference genome (RefSeq: GCF_000732505.1) and *F. grandis* paired-end reads were merged and mapped to the *F. heteroclitus* reference genome (RefSeq: GCF_000826765.1). Gene expression values were calculated as transcripts per million (TPM) and differential expression was calculated in the CLC Genomics Workbench. Differentially expressed genes (DEGs) were defined as those with a fold change absolute value ≥ 2 and an FDR p-value of $p \leq 0.05$ when compared to the normoxia control group within the same species. A full list of all mapped genes from each *C. variegatus* and *F. grandis* library can be found in Supplemental Table 2.1 (https://doi.org/10.1016/j.cbd.2021.100837). Heat maps of all mapped genes and DEGs across both species using Euclidean distance hierarchical clustering and complete linkages were created in R using pheatmap package (Kolde, 2012). Venny 2.1 was used to generate Venn diagrams of shared and unique DEGs between species. DEGs were converted to their human orthologs and analyzed to predict impacted downstream pathways and functions through the use of Ingenuity

Pathway Analysis (IPA; Qiagen, Hilden, Germany) software with a FDR p-value cut-off at 0.05. While zebrafish orthologs would be taxonomically similar to the species in this analysis, IPA's extensive database of human and mammalian gene-association findings facilitate a more in depth analysis of gene interactions and associated downstream pathways and functions than data currently available for teleost models alone (Jones et al., 2020; Xu et al., 2017a, 2017b). In order to maintain the cardiac related scope of this analysis, only canonical pathways and toxicological functions related to cardiac effects were included (Jones et al., 2020; Rodgers et al., 2018; Serafin et al., 2019). Gene networks for cardiac apoptosis were generated for each species in IPA with an FDR p-value cutoff of ≤ 0.01 in order to include only the most significantly impacted genes involved in each network.

2.4 Results

2.4.1 Water quality

Nominal exposure conditions as well as associated measurements of water quality parameters are listed in Table 2.1. For all experiments across both species, temperature and salinities were maintained at ± 1°C and ± 1 ppt of the nominal concentrations, respectively. For *C. variegatus* experiments, DO was maintained at nominal concentrations throughout the course of the 48 h exposure period. *F. grandis* exposures were conducted in sealed chambers without active maintenance of DO levels and thus DO levels decreased by an average of 1.45 ± 0.73 mg/L in normoxic conditions and 0.75 ± 0.47 mg/L under hypoxic conditions over the course of the 48 h exposures. There were no measurable changes in pH or ammonia levels for either species over the course of the exposures.

2.4.2 Read mapping

Reads generated from the *C. variegatus* libraries mapped to the *C. variegatus* reference genome with > 98% success and reads from the *F. grandis* libraries were mapped to the *F. heteroclitus* reference genome with > 94% mapping success (Table 2.2). In total, 11580 annotated genes were identified across all samples from both species and used for hierarchical clustering, differential expression, and downstream analysis. The hierarchical clustering of all genes from both species (Figure 2.1) indicates that species differences in gene expression play a stronger role in clustering than hypoxia exposure.

2.4.3 Differential expression

Differential expression analysis revealed a total of 4908 DEGs across both species following hypoxia exposure (Supplemental Table 2.2; https://doi.org/10.1016/j.cbd.2021.100837). *C. variegatus* larvae exposed to hypoxia expressed a total of 3123 DEGs, of which 2173 were uniquely expressed. *F. grandis* accounted for a total of 2735 DEGs with 1785 unique DEGs; 950 DEGs were expressed by both species (Figure 2.2A). Hierarchical clustering of all DEGs (Figure 2.2B) revealed patterns similar to those seen in the clustering of all genes – where species differences appear to be the strongest influence followed by hypoxia exposure. Hypoxia elicited differential expression in 254 cardiac related genes (as identified by IPA) across both species, 160 of which were uniquely expressed in *C. variegatus*, 23 unique to *F. grandis*, and 71 expressed in both species (Figure 2.3A). Comparable to previous analysis, hypoxia was not the primary factor when cardiac-specific DEGs were hierarchically clustered (Figure 2.3B).

2.4.4 Canonical pathway analysis

Analyses conducted through IPA included only those predicted pathways and functions that showed both a significant response ($p < 0.05$) and directional response (activation z-score $\neq 0$) in at least one species. Canonical pathway analysis revealed 11 cardiac-related pathways that exhibited transcriptional responses in at least one species (Figure 2.4A). These pathways strongly impact several cardiac processes that include hypertrophy, inflammation, angiogenesis, apoptosis, blood pressure maintenance. To a lesser extent, processes such as contractility, vasodilation, cardiac fibrosis, and blood clotting are also impacted. Activation (positive z-scores, orange tones) and inhibition (negative z-scores, blue tones) of signaling pathways are consistent between both *C. variegatus* and *F. grandis*. However, the strength of activation/ inhibition is almost universally greater in *C. variegatus* than *F. grandis* – the one exception being *F. grandis* exhibiting a stronger response in "Factors Promoting Cardiogenesis in Vertebrates".

2.4.5 Toxicological function analysis

Continued analysis into the toxicological functions impacted by hypoxia exposure revealed 14 cardiac-related functions (Figure 2.4B). An important point to note is that IPA analyses are conducted on human orthologs of DEGs and therefore careful interpretation is needed when evaluating results. The list of predicted cardiovascular functions impacted by hypoxia includes several variations of cardiac apoptosis and heart dysfunction. When these repetitive functions are grouped together, the list of impacted functions can be reduced to four primary functions – congenital heart disease, heart dysfunction, cardiac apoptosis, and tachycardia. As with predicted trends in impacted canonical pathways, activation and inhibition responses between *C.*

variegatus and *F. grandis* are similar with *C. variegatus* exhibiting stronger responses to hypoxia exposure.

To explore the mechanisms driving the strong apoptotic response observed in both species, gene networks were created for "Apoptosis of heart cells" – the apoptotic function with the strongest response in the toxicological function analysis (Figure 2.5). IPA generated gene networks include expression patterns for all DEGs in the apoptotic pathway for both species. In total, 50 DEGs were found within the pathway with 14 DEGs shared between the species, 19 DEGs unique to *C. variegatus*, and 17 DEGs unique to *F. grandis* (Table 2.3). Gene expression patterns within the shared DEGs were similar between the two species with the exception of *casp9* and *gapdh* which were both significantly increased in *C. variegatus* but significantly decreased in *F. grandis*.

2.5 Discussion

This study aimed to investigate the impacts of hypoxia on the developing cardiac transcriptomes of two estuarine fish species. Other studies have described the impacts of hypoxia on the development and physiological function of the cardiac system in developing fish – including bradycardia, changes in stroke volume, differing cardiac metabolism, and altered cardiovascular development (Jacob et al., 2002; Johnston et al., 2013; Pelster, 2002, 1999; Shang and Wu, 2004) as well as genotypically plastic responses (Robertson et al., 2014; Ton et al., 2003). To our knowledge this study is one of the first to go beyond targeted gene expression analysis and analyze transcriptomic effects in order to predict cardiovascular pathways and functions impacted by hypoxia exposure in newly hatched fish. Further, this study expanded the analysis to include two ecologically similar species, *C. variegatus* and *F. grandis*, to determine if

exposure to hypoxia elicits similar responses across taxa that inhabit similar ecological niches. Embryological descriptions of development suggest that the cardiovascular system is less developed in *C. variegatus* than *F. grandis* at hatch (Greeley and MacGregor, 1983; Kuntz, 1916) which was hypothesized to impart an increased sensitivity to hypoxia in *C. variegatus* larvae. Similar to many rapidly developing teleost species, *C. variegatus* appears to continue angiogenesis post-hatch (Kuntz, 1916) and likely relies on cutaneous exchange of respiratory gasses and ions until complete branchial transition has occurred (see Burggren et al., 2017 for full review of cardiovascular development in embryonic and larval fishes). Results presented here confirm that responses to hypoxia are generally similar but differ in magnitude between both species and appear to support the hypothesis that newly hatched *F. grandis* are more robust to hypoxia exposure than newly hatched *C. variegatus*.

Analysis into the differential gene expression data revealed distinct differences in expression in *C. variegatus* larvae exposed to hypoxia compared to *F. grandis* larvae, as evidenced by the hierarchical clustering driven by species and not exposure conditions (Figures 2.1, 2.2B, 2.3B). It is important to note that while not controlled for in this study, the wild-caught *F. grandis* broodstock may have previously been exposed to hypoxia resulting in potential epigenetic impacts on differential gene expression not present in the laboratory reared *C. variegatus* broodstock population. Although *C. variegatus* exhibited nearly 2.5 times the number of cardiac related DEGs than *F. grandis* and hierarchical clustering suggests distinct differences between the species, predicted impacts on canonical pathways showed some similarities in both species (Figure 2.4A). An important caveat to note is that DEG analysis was completed on whole larvae extracts and while many genes addressed in this analysis are primarily expressed in cardiac tissues, potential expression influences from outside the

cardiovascular system cannot be definitively excluded. Nevertheless, trends in canonical pathway analysis suggest that hypoxia exposure results in reduced cardiac hypertrophy through inhibition of NFAT, as well as through Apelin and Endothelin-1 signaling pathways. Similar interactions between these signaling pathways and hypertrophic responses have been observed in mammalian cardiomyocyte models (Pu et al., 2003; Xie et al., 2015). Additionally, modulation of blood pressure was impacted in both species through inhibition of Adrenomedullin, Aldosterone, Renin-Angiotensin and P2Y purinergic receptor signaling pathways. This data corroborates results from studies done on mammalian cardiomyocytes that have shown that these pathways all have roles in blood pressure maintenance and can be induced by exposure to hypoxic conditions (Burnstock, 1987; Cormier-Regard et al., 1998; Foster et al., 2010).

Further downstream analysis into toxicological functions, or pathological endpoints, predicted to be impacted by hypoxia exposure aligned well with the DEG analysis and canonical pathway analysis. Generally, activation/inhibition responses were consistent across both species, however *C. variegatus* tended to respond to a higher degree (larger absolute value z-scores) than *F. grandis*. An important caveat to IPA analysis is that it requires the conversion of DEGs within an RNA Seq dataset to their human orthologs and then runs functional analyses based on their associated human/mammalian functions. As a result, there are a number of repetitious toxicological functions predicted by this analysis – for example several functions listed in Figure 2.4B are specific iterations of cardiac apoptosis (i.e. “Apoptosis of heart cells”, “Apoptosis of cardiomyocytes”, “Cell death of heart ventricle”, etc.). Overwhelmingly, most toxicological functions represented in this analysis in both species are involved in increased incidence of cardiac apoptosis. Consequently, a deeper analysis into the gene networks driving apoptosis in each species were conducted.

"Apoptosis of heart cells" was the apoptotic toxicological function that resulted in the strongest response in the toxicological function analysis and therefore, was chosen as the function for mechanistic analysis. Common trends in both species included reduced expression of genes involved in cellular proliferation and the regulation of cell growth. This data corresponds with previous studies in mammalian models (rat and human cell lines) that have found that protein coding genes such as nicotinamide phosphoribosyltransferase (*nampt*), prohibitin (*phb*), and heat-shock protein B8 (*hspb8*) play important roles in proliferation and the induction of cardiac hypertrophy (Mishra et al., 2010; Pillai et al., 2013; Shemetov et al., 2008). Similarly, both species saw reduced expression in genes that have been shown to be involved in the protection against apoptosis including pleiotropic regulator 1 (*plrg1),* eukaryotic translation termination factor 1 (*raf1),* heat-shock protein B6 (*hspb6),* and *hspb8* (Dreiza et al., 2010; Kleinridders et al., 2009; Shemetov et al., 2008; Yamaguchi et al., 2004). Interestingly, the small heat-shock protein HspB8 has been identified as capable of conferring both pro- and anti-apoptotic properties in human cells, depending on expression levels and the nature and quantity of proteins bound to it (Shemetov et al., 2008). Conversely, the small heat-shock protein HspB6, does not appear to initiate apoptosis but does serve a cardioprotective role in mouse cardiomyocytes by preventing cardiac apoptosis (Dreiza et al., 2010).

Unsurprisingly, a number of genes involved in the induction of apoptosis were significantly upregulated in gene networks for both species. Genes such as cellular communication network factor 1 (*ccn1),* lipocalin 2 (*lcn2),* tumor protein 53 (*tp53),* ubiquitin protein ligase E4B (*ube4b),* and the *e2f1/ tfdp1* transcription factor complex were identified in this analysis and have been shown in murine and *C. elegans* models to promote cellular apoptosis (Antoniou et al., 2020; Hitchens and Robbins, 2003; Hsu et al., 2013; Long et al.,

1997; Xu et al., 2012). Tumor protein 53 (p53), encoded by *tp53*, is responsive to various cellular stressors (Vogelstein and Kinzler, 1992) and plays a critical role in the apoptotic response by regulating the expression of various target genes, activating intracellular signaling pathways (Long et al., 1997), and inducing cell cycle arrest or apoptosis (Chen et al., 1996). Specific to this analysis, genes such as glyceraldehyde-3-phosphate dehydrogenase *(gapdh), plrg1, ube4b,* and the *e2f1/ tfdp1* complex have all been shown to be regulated, at least in part, by the action of p53 (Antoniou et al., 2020; Chen et al., 1999; Hitchens and Robbins, 2003; Kleinridders et al., 2009). p53 has also been shown to inhibit hypoxia inducible factor 1a (HIF1α) activity and induce cardiac dysfunction in mice (Sano et al., 2007). This is consistent with the counterintuitive reduction of *hif1a* in this analysis observed in both *C. variegatus* and *F. grandis* larvae following hypoxia exposure.

Expression trends in DEGs involved in apoptotic pathways common to both species were largely consistent, with the exception of *gapdh* and *casp9*, both of which were expectedly upregulated in *C. variegatus* but downregulated in *F. grandis*. *gapdh* has been shown to induce apoptosis in murine species (Dastoor and Dreyer, 2001), especially following upregulation by p53 (Chen et al., 1999); however, p53 was not upregulated in *F. grandis* which may explain the lack of *gapdh* expression in this species. Caspase 9, encoded by the *casp9* gene, is an essential activator in the caspase cascade that terminates in cellular apoptosis (Kuida et al., 1998). Studies in mammalian models have shown that inhibition of Caspase 9 in cardiomyocytes confers significant protection from apoptosis (Han et al., 2006). An important regulator of caspase activity central to apoptotic pathways is the *e2f1/ tfdp1* complex (Hitchens and Robbins, 2003). This complex, formed by the binding of two transcription factors – E2F and DP1 – promotes apoptosis through p53 dependent and independent pathways, the latter of which results in the

upregulation of several caspases. It is interesting that both aspects of the *e2f1/ tfdp1* complex are upregulated in *F. grandis* while *casp9* is not. Further studies will need to be conducted to elucidate the interplay between expression of *e2f1/ tfdp1* and *casp9* in hypoxia exposed *F. grandis* larvae.

2.6 Conclusions

This study is one of the first to examine the predicted functional effects of hypoxia on the developing cardiovascular system of estuarine fish through transcriptomic analysis. Trends apparent throughout multiple levels of analysis presented here support previous literature regarding the hypoxic influence on the cardiovascular system, including changes in cardiac hypertrophy and blood pressure modulation (Burnstock, 1987; Cormier-Regard et al., 1998; Foster et al., 2010; Pu et al., 2003; Xie et al., 2015). Data presented here expands that knowledge to include potential mechanisms driving hypoxia induced apoptotic pathways in two ecologically similar species. Overall, responses to hypoxia at all levels of analysis appear to be conserved between both species, although the magnitude of response is almost universally greater in *C. variegatus* relative to *F. grandis*. This result lends support to the hypothesis that extended embryonic development prior to hatch results in cardiovascular systems that are more robust to hypoxic perturbation; whereas shortened embryonic development time may result in cardiovascular systems that are more susceptible to environmental disruption. However, results should be interpreted cautiously as transcriptomic alterations do not necessarily confer physiological changes (see Evans, 2015 for full review of transcriptomic limitations). As such, additional studies into hypoxia's impact on associated protein activity and phenotypic anchoring studies should be completed to further verify these conclusions.

2.7 References

Andrews, S., 2010. FastQC: a quality control tool for high throughput sequence data.

Antoniou, N., Lagopati, N., Balourdas, D.I., Nikolaou, M., Papalampros, A., Vasileiou, P.V.S., Myrianthopoulos, V., Kotsinas, A., Shiloh, Y., Liontos, M., Gorgoulis, V.G., 2020. The role of E3, E4 ubiquitin ligase (UBE4B) in human pathologies. Cancers (Basel). 12, 1–15. https://doi.org/10.3390/cancers12010062

Armstrong, P.B., Child, J.S., 1965. Stages in the normal development of *Fundulus heteroclitus*. Biol. Bull. 128, 143–168.

Bagatto, B., 2005. Ontogeny of cardiovascular control in zebrafish (*Danio rerio*): Effects of developmental environment. Comp. Biochem. Physiol. - A Mol. Integr. Physiol. 141, 391–400. https://doi.org/10.1016/j.cbpb.2005.07.002

Boehlert, G.W., Mundy, B.C., 1988. Roles of behavioral and physical factors in larval and juvenile fish recruitment to estuarine nursery areas. Am. Fish. Soc. Symp. 3, 61–67.

Bolger, A.M., Lohse, M., Usadel, B., 2014. Trimmomatic: A flexible trimmer for Illumina sequence data. Bioinformatics 30, 2114–2120. https://doi.org/10.1093/bioinformatics/btu170

Burggren, W.W., Dubansky, B., Bautista, N.M., 2017. Cardiovascular Development in Embryonic and Larval Fishes, 1st ed, Fish Physiology. Elsevier Inc. https://doi.org/10.1016/bs.fp.2017.09.002

Burnstock, G., 1987. Local control of blood pressure by purines. J. Vasc. Res. 24, 156–160. https://doi.org/10.1159/000158691

Cheek, A.O., Landry, C.A., Steele, S.L., Manning, S., 2009. Diel hypoxia in marsh creeks impairs the reproductive capacity of estuarine fish populations. Mar. Ecol. Prog. Ser. 392, 211–221. https://doi.org/10.3354/meps08182

Chen, R.W., Saunders, P.A., Wei, H., Li, Z., Seth, P., Chuang, D.M., 1999. Involvement of glyceraldehyde-3-phosphate dehydrogenase (GAPDH) and p53 in neuronal apoptosis: Evidence that GAPDH is upregulated by p53. J. Neurosci. 19, 9654–9662. https://doi.org/10.1523/jneurosci.19-21-09654.1999

Chen, X., Ko, L.J., Jayaraman, L., Prives, C., 1996. p53 levels, functional domains, and DNA damage determine the extent of the apoptotic response of tumor cells. Genes Dev. 10, 2438–2451. https://doi.org/10.1101/gad.10.19.2438

Conley, D.J., Carstensen, J., Vaquer-Sunyer, R., Duarte, C.M., 2009. Ecosystem thresholds with hypoxia. Hydrobiologia 21–29. https://doi.org/10.1007/s10750-009-9764-2

Cormier-Regard, S., Nguyen, S. V., Claycomb, W.C., 1998. Adrenomedullin gene expression is developmentally regulated and induced by hypoxia in rat ventricular cardiac myocytes. J. Biol. Chem. 273, 17787–17792. https://doi.org/10.1074/jbc.273.28.17787

Craig, J.K., 2012. Aggregation on the edge: Effects of hypoxia avoidance on the spatial distribution of brown shrimp and demersal fishes in the Northern Gulf of Mexico. Mar. Ecol. Prog. Ser. 445, 75–95. https://doi.org/10.3354/meps09437

Dastoor, Z., Dreyer, J.L., 2001. Potential role of nuclear translocation of glyceraldehyde-3-phosphate dehydrogenase in apoptosis and oxidative stress. J. Cell Sci. 114, 1643–1653.

Diaz, R.J., Rosenberg, R., 2008. Spreading dead zones and consequences for marine ecosystems. Science. 321, 926–929. https://doi.org/10.1126/science.1156401

Dreiza, C.M., Komalavilas, P., Furnish, E.J., Flynn, C.R., Sheller, M.R., Smoke, C.C., Lopes, L.B., Brophy, C.M., 2010. The small heat shock protein, HSPB6, in muscle function and disease. Cell Stress Chaperones 15, 1–11. https://doi.org/10.1007/s12192-009-0127-8

Eby, L.A., Crowder, L.B., 2002. Hypoxia-based habitat compression in the Neuse River Estuary: Context-dependent shifts in behavioral avoidance thresholds. Can. J. Fish. Aquat. Sci. 59, 952–965. https://doi.org/10.1139/f02-067

Ern, R., Esbaugh, A.J., 2018. Effects of salinity and hypoxia-induced hyperventilation on oxygen consumption and cost of osmoregulation in the estuarine red drum (*Sciaenops ocellatus*). Comp. Biochem. Physiol. -Part A Mol. Integr. Physiol. 222, 52–59. https://doi.org/10.1016/j.cbpa.2018.04.013

Evans, T.G., 2015. Considerations for the use of transcriptomics in identifying the "genes that matter" for environmental adaptation. J. Exp. Biol. 218, 1925–1935. https://doi.org/10.1242/jeb.114306

Everett, M.V., Antal, C.E., Crawford, D.L., 2012. The effect of short-term hypoxic exposure on metabolic gene expression. J. Exp. Zool. 317, 9-23. https://doi.org/10.1002/jez.717

Farrell, A.P., 2007. Tribute to P. L. Lutz: A message from the heart - Why hypoxic bradycardia in fishes? J. Exp. Biol. 210, 1715–1725. https://doi.org/10.1242/jeb.02781

Foster, G.E., Hanly, P.J., Ahmed, S.B., Beaudin, A.E., Pialoux, V., Poulin, M.J., 2010. Intermittent hypoxia increases arterial blood pressure in humans through a renin-angiotensin system-dependent mechanism. Hypertension 56, 369–377. https://doi.org/10.1161/HYPERTENSIONAHA.110.152108

Gamperl, A.K., Farrell, A.P., 2004. Cardiac plasticity in fishes: Environmental influences and intraspecific differences. J. Exp. Biol. 207, 2539–2550. https://doi.org/10.1242/jeb.01057

Grantham, B.A., Chan, F., Nielsen, K.J., Fox, D.S., Barth, J.A., Huyer, A., Lubchenco, J., Menge, B.A., 2004. Upwelling-driven nearshore hypoxia signals ecosystem and oceanographic changes in the northeast Pacific. Nature 429, 749–754. https://doi.org/10.1038/nature02605

Gray, J.S., Wu, R.S.S., Ying, Y.O., 2002. Effects of hypoxia and organic enrichment on the coastal marine environment. Mar. Ecol. Prog. Ser. 238, 249–279. https://doi.org/10.3354/meps238249

Greeley, M.S., MacGregor, R., 1983. Annual and Semilunar Reproductive Cycles of the Gulf Killifish, *Fundulus grandis*, on the Alabama Gulf Coast. Copeia 1983, 711–718. https://doi.org/10.2307/1444337

Green, C., 2013. Intensive (non-pond) culture of Gulf Killifish. SRAC Publ. no. 2012.

Han, Y., Chen, Y.S., Liu, Z., Bodyak, N., Rigor, D., Bisping, E., Pu, W.T., Kang, P.M., 2006. Overexpression of HAX-1 protects cardiac myocytes from apoptosis through caspase-9 inhibition. Circ. Res. 99, 415–423. https://doi.org/10.1161/01.RES.0000237387.05259.a5

Hazen, E.L., Craig, J.K., Good, C.P., Crowder, L.B., 2009. Vertical distribution of fish biomass in hypoxic waters on the gulf of Mexico shelf. Mar. Ecol. Prog. Ser. 375, 195–207. https://doi.org/10.3354/meps07791

Helly, J.J., Levin, L.A., 2004. Global distribution of naturally occurring marine hypoxia on continental margins. Deep. Res. Part I Oceanogr. Res. Pap. 51, 1159–1168. https://doi.org/10.1016/j.dsr.2004.03.009

Hitchens, M.R., Robbins, P.D., 2003. The role of the transcription factor DP in apoptosis. Apoptosis 8, 461–468. https://doi.org/10.1023/A:1025586207239

Hsu, P.L., Su, B.C., Kuok, Q.Y., Mo, F.E., 2013. Extracellular matrix protein CCN1 regulates cardiomyocyte apoptosis in mice with stress-induced cardiac injury. Cardiovasc. Res. 98, 64–72. https://doi.org/10.1093/cvr/cvt001

Jacob, E., Drexel, M., Schwerte, T., Pelster, B., 2002. Influence of hypoxia and of hypoxemia on the development of cardiac activity in zebrafish larvae. Am. J. Physiol. - Regul. Integr. Comp. Physiol. 283, 911–917. https://doi.org/10.1152/ajpregu.00673.2001

Jeppesen, R., Rodriguez, M., Rinde, J., Haskins, J., Hughes, B., Mehner, L., Wasson, K., 2018. Effects of Hypoxia on Fish Survival and Oyster Growth in a Highly Eutrophic Estuary. Estuaries and Coasts 41, 89–98. https://doi.org/10.1007/s12237-016-0169-y

Johnston, E.F., Alderman, S.L., Gillis, T.E., 2013. Chronic hypoxia exposure of trout embryos alters swimming performance and cardiac gene expression in larvae. Physiol. Biochem. Zool. 86, 567–575. https://doi.org/10.1086/672012

Jones, E.R., Simning, D., Serafin, J., Sepúlveda, M.S., Griffitt, R.J., 2020. Acute exposure to oil induces age and species-specific transcriptional responses in embryo-larval estuarine fish. Environ. Pollut. 263, 1–10. https://doi.org/10.1016/j.envpol.2020.114325

Kleinridders, A., Pogoda, H.-M., Irlenbusch, S., Smyth, N., Koncz, C., Hammerschmidt, M., Brüning, J.C., 2009. PLRG1 is an essential regulator of Ccll proliferation and apoptosis during vertebrate development and tissue homeostasis. Mol. Cell. Biol. 29, 3173–3185. https://doi.org/10.1128/mcb.01807-08

Kolde, R., 2012. Pheatmap: pretty heatmaps.

Kuida, K., Haydar, T.F., Kuan, C.-Y., Gu, Y., Taya, C., Karasuyama, H., S-S Su, M., 1998. Reduced apoptosis and Cytochrome c-mediated Caspase activation in mice lacking Caspase 9. Cell 94, 325–337.

Kuntz, A., 1916. Notes on the embryology and larval development of five species of teleostean fishes. Bull. Bur. Fish. 34, 409–429.

LaBone, E., Justic, D., Rose, K., Wang, L., Huang, H., 2019. Modeling Fish Movement in 3-D in the Gulf of Mexico Hypoxic Zone. Estuaries and Coasts 42, 1662–1685. https://doi.org/10.1007/s12237-019-00601-6

Landry, C.A., Steele, S.L., Manning, S., Cheek, A.O., 2007. Long term hypoxia suppresses reproductive capacity in the estuarine fish, *Fundulus grandis*. Comp. Biochem. Physiol. - A Mol. Integr. Physiol. 148, 317–323. https://doi.org/10.1016/j.cbpa.2007.04.023

Limburg, K.E., Walther, B.D., Lu, Z., Jackman, G., Mohan, J., Walther, Y., Nissling, A., Weber, P.K., Schmitt, A.K., 2015. In search of the dead zone: Use of otoliths for tracking fish exposure to hypoxia. J. Mar. Syst. 141, 167–178. https://doi.org/10.1016/j.jmarsys.2014.02.014

Long, X., Boluyt, M.O., De Lourdes Hipolito, M., Lundberg, M.S., Zheng, J.S., O'Neill, L., Cirielli, C., Lakatta, E.G., Crow, M.T., 1997. P53 and the hypoxia-induced apoptosis of cultured neonatal rat cardiac myocytes. J. Clin. Invest. 99, 2635–2643. https://doi.org/10.1172/JCI119452

Mishra, S., Ande, S.R., Nyomba, B.L.G., 2010. The role of prohibitin in cell signaling. FEBS J. 277, 3937–3946. https://doi.org/10.1111/j.1742-4658.2010.07809.x

Morrell, B.K., Gobler, C.J., 2020. Negative effects of diurnal changes in acidification and hypoxia on early-life stage estuarine fishes. Diversity 12, 1–27. https://doi.org/10.3390/d12010025

Nordlie, F.G., 2003. Fish communities of estuarine salt marshes of eastern North America, and comparisons with temperate estuaries of other continents. Rev. Fish Biol. Fish. 13, 281–325.

Pelster, B., 2002. Developmental plasticity in the cardiovascular system of fish, with special reference to the zebrafish. Comp. Biochem. Physiol. - A Mol. Integr. Physiol. 133, 547–553. https://doi.org/10.1016/S1095-6433(02)00194-0

Pelster, B., 1999. Environmental influences on the development of the cardiac system in fish and amphibians. Comp. Biochem. Physiol. - A Mol. Integr. Physiol. 124, 407–412. https://doi.org/10.1016/S1095-6433(99)00132-4

Pillai, V.B., Sundaresan, N.R., Kim, G., Samant, S., Moreno-Vinasco, L., Garcia, J.G.N., Gupta, M.P., 2013. Nampt secreted from cardiomyocytes promotes development of cardiac hypertrophy and adverse ventricular remodeling. Am. J. Physiol. - Hear. Circ. Physiol. 304, H415–H426. https://doi.org/10.1152/ajpheart.00468.2012

Pu, W.T., Ma, Q., Izumo, S., 2003. NFAT transcription factors are critical survival factors that inhibit cardiomyocyte apoptosis during phenylephrine stimulation in vitro. Circ. Res. 92, 725–731. https://doi.org/10.1161/01.RES.0000069211.82346.46

Rabalais, N.N., Díaz, R.J., Levin, L.A., Turner, R.E., Gilbert, D., Zhang, J., 2010. Dynamics and distribution of natural and human-caused hypoxia. Biogeosciences 7, 585–619. https://doi.org/10.5194/bg-7-585-2010

Rabalais, N.N., Turner, R.E., 2019. Gulf of Mexico Hypoxia: Past, Present, and Future. Limnol. Oceanogr. Bull. 28, 117–124. https://doi.org/10.1002/lob.10351

Rabalais, N.N., Turner, R.E., Sen Gupta, B.K., Boesch, D.F., Chapman, P., Murrell, M.C., 2007. Hypoxia in the northern Gulf of Mexico: Does the science support the plan to reduce, mitigate, and control hypoxia? Estuaries and Coasts 30, 753–772.

Rabalais, N.N., Turner, R.E., Wiseman, W.J., 2002. Gulf of Mexico hypoxia, a.k.a. "The dead zone." Annu. Rev. Ecol. Syst. 33, 235–263. https://doi.org/10.1146/annurev.ecolsys.33.010802.150513

Randall, D.J., Smith, J.C., 1967. The regulation of cardiac activity in fish in a hypoxic environment. Physiol. Zool. 40, 104–113. https://doi.org/10.1086/physzool.40.2.30152445

Robertson, C.E., Wright, P.A., Köblitz, L., Bernier, N.J., 2014. Hypoxia-inducible factor-1 mediates adaptive developmental plasticity of hypoxia tolerance in zebrafish, *Danio rerio*. Proc. R. Soc. B Biol. Sci. 281. https://doi.org/10.1098/rspb.2014.0637

Rodgers, M.L., Jones, E.R., Klinkhamer, C., Mahapatra, C.T., Serafin, J., Bosker, T., Perkins, C., Griffitt, R.J., De Guise, S., Sepúlveda, M.S., 2018. Combined effects of Deepwater Horizon crude oil and environmental stressors on *Fundulus grandis* embryos. Environ. Toxicol. Chem. 37, 1916–1925. https://doi.org/10.1002/etc.4153

Rooker, J., Holt, S., 1997. Utilization of subtropical seagrass meadows by newly settled red drum *Sciaenops ocellatus*: patterns of distribution and growth . Mar. Ecol. Prog. Ser. 158, 139–149. https://doi.org/10.3354/meps158139

Sano, M., Minamino, T., Toko, H., Miyauchi, H., Orimo, M., Qin, Y., Akazawa, H., Tateno, K., Kayama, Y., Harada, M., Shimizu, I., Asahara, T., Hamada, H., Tomita, S., Molkentin, J.D., Zou, Y., Komuro, I., 2007. p53-induced inhibition of Hif-1 causes cardiac dysfunction during pressure overload. Nature 446, 444–448. https://doi.org/10.1038/nature05602

Serafin, J., Guffey, S.C., Bosker, T., Griffitt, R.J., De Guise, S., Perkins, C., Szuter, M., Sepúlveda, M.S., 2019. Combined effects of salinity, temperature, hypoxia, and Deepwater Horizon oil on *Fundulus grandis* larvae. Ecotoxicol. Environ. Saf. 181, 106–113. https://doi.org/10.1016/j.ecoenv.2019.05.059

Shang, E.H.H., Wu, R.S.S., 2004. Aquatic hypoxia is a teratogen and affects fish embryonic development. Environ. Sci. Technol. 38, 4763–4767. https://doi.org/10.1021/es0496423

Shemetov, A.A., Seit-Nebi, A.S., Gusev, N.B., 2008. Structure, properties, and functions of the human small heat-shock protein HSP22 (HspB8, H11, E2IG1): A critical review. J. Neurosci. Res. 86, 264–269. https://doi.org/10.1002/jnr.21441

Simning, D., Sepulveda, M., De Guise, S., Bosker, T., Griffitt, R.J., 2019. The combined effects of salinity, hypoxia, and oil exposure on survival and gene expression in developing sheepshead minnows, *Cyprinodon variegatus*. Aquat. Toxicol. 214, 105234. https://doi.org/10.1016/j.aquatox.2019.105234

Stierhoff, K.L., Targett, T.E., Miller, K., 2006. Ecophysiological responses of juvenile summer and winter flounder to hypoxia: Experimental and modeling analyses of effects on estuarine nursery quality. Mar. Ecol. Prog. Ser. 325, 255–266. https://doi.org/10.3354/meps325255

Thomas, P., Rahman, M.S., Khan, I.A., Kummer, J.A., 2007. Widespread endocrine disruption and reproductive impairment in an estuarine fish population exposed to seasonal hypoxia. Proc. R. Soc. B Biol. Sci. 274, 2693–2701. https://doi.org/10.1098/rspb.2007.0921

Ton, C., Stamatiou, D., Liew, C.C., 2003. Gene expression profile of zebrafish exposed to hypoxia during development. Physiol. Genomics 13, 97–106. https://doi.org/10.1152/physiolgenomics.00128.2002

Turner, R.E., Rabalais, N.N., 2018. 2017 Forecast : Summer Hypoxic Zone Size , Northern Gulf of Mexico.

Turner, R.E., Rabalais, N.N., 1991. Changes in Mississippi River Water Quality This Century. Bioscience 41, 140–147. https://doi.org/10.2307/1311453

USEPA, 2002. Method 1004.0: Sheepshead Minnow, *Cyprinodon variegatus*, Embryo-Larval Survival and Teratogenicity Test; Chronic Toxicity, United States Environmental Protection Agency. https://doi.org/EPA-821-R-02-014

Vaquer-Sunyer, R., Duarte, C.M., 2008. Thresholds of hypoxia for marine biodiversity. Proc. Natl. Acad. Sci. U. S. A. 105, 15452–15457. https://doi.org/10.1073/pnas.0803833105

Vogelstein, B., Kinzler, K.W., 1992. P53 Function and Dysfunction. Cell 70, 523–526. https://doi.org/10.1016/0092-8674(92)90421-8

Wannamaker, C.M., Rice, J.A., 2000. Effects of hypoxia on movements and behavior of selected estuarine organisms from the southeastern United States. J. Exp. Mar. Bio. Ecol. 249, 145–163. https://doi.org/10.1016/S0022-0981(00)00160-X

Wu, R.S.S., 2002. Hypoxia: From molecular responses to ecosystem responses. Mar. Pollut. Bull. 45, 35–45. https://doi.org/10.1016/S0025-326X(02)00061-9

Wu, R.S.S., Zhou, B.S., Randall, D.J., Woo, N.Y.S., Lam, P.K.S., 2003. Aquatic hypoxia is an endocrine disruptor and impairs fish reproduction. Environ. Sci. Technol. 37, 1137–1141. https://doi.org/10.1021/es0258327

Xie, F., Liu, W., Feng, F., Li, X., He, L., Lv, D., Qin, X., Li, Lifang, Li, Lanfang, Chen, L., 2015. Apelin-13 promotes cardiomyocyte hypertrophy via PI3K-Akt-ERK1/2-p70S6K and PI3K-induced autophagy. Acta Biochim. Biophys. Sin. (Shanghai). 47, 969–980. https://doi.org/10.1093/abbs/gmv111

Xu, E.G., Khursigara, A.J., Magnuson, J., Hazard, E.S., Hardiman, G., Esbaugh, A.J., Roberts, A.P., Schlenk, D., 2017a. Larval Red Drum (*Sciaenops ocellatus*) Sublethal Exposure to Weathered Deepwater Horizon Crude Oil: Developmental and Transcriptomic Consequences. Environ. Sci. Technol. 51, 10162–10172. https://doi.org/10.1021/acs.est.7b02037

Xu, E.G., Mager, E.M., Grosell, M., Hazard, E.S., Hardiman, G., Schlenk, D., 2017b. Novel transcriptome assembly and comparative toxicity pathway analysis in mahi-mahi (*Coryphaena hippurus*) embryos and larvae exposed to Deepwater Horizon oil. Sci. Rep. 7, 1–13. https://doi.org/10.1038/srep44546

Xu, G., Ahn, J.H., Chang, S.Y., Eguchi, M., Ogier, A., Han, S.J., Park, Y.S., Shim, C.Y., Jang, Y.S., Yang, B., Xu, A., Wang, Y., Sweeney, G., 2012. Lipocalin-2 induces cardiomyocyte apoptosis by increasing intracellular iron accumulation. J. Biol. Chem. 287, 4808–4817. https://doi.org/10.1074/jbc.M111.275719

Yamaguchi, O., Watanabe, T., Nishida, K., Kashiwase, K., Higuchi, Y., Takeda, T., Hikoso, S., Hirotani, S., Asahi, M., Taniike, M., Nakai, A., Tsujimoto, I., Matsumura, Y., Miyazaki, J., Chien, K.R., Matsuzawa, A., Sadamitsu, C., Ichijo, H., Baccarini, M., Hori, M., Otsu, K., 2004. Cardiac-specific disruption of the c-raf-1 gene induces cardiac dysfunction and apoptosis. J. Clin. Invest. 114, 937–943. https://doi.org/10.1172/JCI200420317

Zhang, H., Ludsin, S.A., Mason, D.M., Adamack, A.T., Brandt, S.B., Zhang, X., Kimmel, D.G., Roman, M.R., Boicourt, W.C., 2009. Hypoxia-driven changes in the behavior and spatial distribution of pelagic fish and mesozooplankton in the northern Gulf of Mexico. J. Exp. Mar. Bio. Ecol. 381, S80–S91. https://doi.org/10.1016/j.jembe.2009.07.014

Table 2.1. Nominal and measured water quality parameters over the course of the 48 h control and hypoxia experiments with *C. variegatus* and *F. grandis*. Values represented as mean ± S.D.

Species	Condition	Variable	Nominal Value	0h Value	24h Value	48h Value
C. variegatus	Normoxia	DO	5 mg/L	5.33 ± 0.09 mg/L	5.33 ± 0.09 mg/L	5.33 ± 0.09 mg/L
		Temperature	30°C	29.29 ± 0.08°C	29.29 ± 0.08°C	29.29 ± 0.08°C
		Salinity	30 ppt	30 ± 0 ppt	30 ± 0 ppt	30 ± 0 ppt
	Hypoxia	DO	2 mg/L	2.52 ± 0.05 mg/L	2.52 ± 0.05 mg/L	2.52 ± 0.05 mg/L
		Temperature	30°C	28.74 ± 0.1°C	28.74 ± 0.1°C	28.74 ± 0.1°C
		Salinity	30 ppt	31.73 ± 0.17 ppt	31.73 ± 0.17 ppt	31.73 ± 0.17 ppt
F. grandis	Normoxia	DO	6 mg/L	5.87 ± 0.15 mg/L	4.98 ± 0.39 mg/L	4.41 ± 0.88 mg/L
		Temperature	30°C	30 ± 1°C	30 ± 1°C	30 ± 1°C
		Salinity	30 ppt	30 ± 0.5 ppt	30 ± 0.5 ppt	30 ± 0.5 ppt
	Hypoxia	DO	2 mg/L	2.39 ± 1.04 mg/L	1.13 ± 0.86 mg/L	1.35 ± 0.63 mg/L
		Temperature	30°C	30 ± 1°C	30 ± 1°C	30 ± 1°C
		Salinity	30 ppt	30 ± 0.5 ppt	30 ± 0.5 ppt	30 ± 0.5 ppt

Table 2.2. Summary statistics for each RNA Seq library generated from *C. variegatus* and *F. grandis* larvae following 48 h exposure to normoxia or hypoxia.

RNASeq Library	Total Reads	Mapped Reads	Reads Mapped	Annotated Genes
C. variegatus Normoxia 1	63,052,636	62,253,364	98.73%	9,999
C. variegatus Normoxia 2	70,755,822	69,866,371	98.74%	9,991
C. variegatus Normoxia 3	62,964,228	62,168,903	98.74%	9,999
C. variegatus Hypoxia 1	71,102,886	70,096,035	98.58%	9,994
C. variegatus Hypoxia 2	56,100,342	55,263,288	98.51%	9,990
C. variegatus Hypoxia 3	72,171,170	71,176,683	98.62%	9,996
F. grandis Normoxia 1	18,922,036	18,602,458	98.31%	9,614
F. grandis Normoxia 2	16,997,452	16,721,628	98.38%	9,574
F. grandis Normoxia 3	28,684,164	28,212,819	98.36%	9,660
F. grandis Hypoxia 1	15,008,146	14,716,725	98.06%	9,644
F. grandis Hypoxia 2	18,634,622	18,278,967	98.09%	9,675
F. grandis Hypoxia 3	17,484,322	17,160,229	98.15%	9,661

Table 2.3. DEGs identified by IPA in "apoptosis of heart cells" pathway with FDR $p \leq 0.01$. All values presented as log(TPM).

Species	***C. variegatus***						***F. grandis***					
Treatment	**Normoxia**			**Hypoxia**			**Normoxia**			**Hypoxia**		
ID	**1**	**2**	**3**	**1**	**2**	**3**	**1**	**2**	**3**	**1**	**2**	**3**
agt	2.002	2.074	2.024	1.851	1.862	1.913	1.633	1.392	1.570	1.570	1.346	1.454
atg16l1	1.403	1.386	1.410	1.217	1.146	1.171	1.309	1.272	1.257	1.178	1.176	1.085
bach1	0.910	0.929	0.958	0.777	0.804	0.642						
bnip3	2.151	2.189	2.183	2.015	2.039	1.925	2.108	2.119	2.149	1.818	1.650	1.982
calcrl	0.447	0.691	0.720	0.386	0.346	0.276	0.158	0.292	0.307	0.493	0.508	0.360
camk2n2	1.436	1.446	1.425	1.217	1.311	1.117						
casp9	0.948	0.951	0.925	1.062	1.019	0.997	1.050	1.185	1.211	1.045	0.989	1.093
cat	2.075	2.052	2.082	2.032	2.046	1.981	2.474	2.428	2.465	2.275	2.168	2.389
cdk2	0.528	0.512	0.412	0.713	0.555	0.693	0.090	-0.244	0.072	0.572	0.730	0.481
cdk9	1.385	1.388	1.381	1.298	1.208	1.253	1.336	1.345	1.357	1.236	1.261	1.225
cdkn1b	1.630	1.620	1.668	1.501	1.453	1.388						
crem							0.727	0.744	0.785	0.509	0.617	0.626
csk	0.813	0.831	0.885	0.952	0.958	0.886						
ccn1	1.599	1.626	1.547	1.647	1.714	1.711	1.667	1.572	1.609	1.717	1.604	1.645
e2f1	-0.569	-0.367	-0.301	-0.229	-0.337	-0.167	-1.097		-0.658	-0.119	0.064	-0.456
fadd							1.292	1.293	1.372	1.268	1.288	1.193
fasn	0.722	0.757	0.700	0.193	0.274	0.104	0.876	0.796	0.770	0.956	0.943	0.779
foxo3	1.608	1.594	1.587	1.354	1.388	1.323	1.469	1.488	1.483	1.423	1.356	1.412
fstl1	2.001	2.058	2.048	2.211	2.149	2.086	1.658	1.663	1.679	1.801	1.897	1.789
fstl3	1.724	1.844	1.814	1.578	1.611	1.498	0.827	0.861	0.900	0.633	0.744	0.821
gapdh	3.711	3.675	3.724	3.808	3.809	3.811	3.421	3.466	3.448	3.409	3.356	3.413
gsk3a	1.087	1.131	1.116	1.059	1.002	1.033	0.453	0.637	0.498	0.857	0.881	0.857
gsk3b	1.216	1.205	1.117	1.117	1.096	1.061	0.391	0.241	0.446	0.760	0.899	0.750
hif1a	1.625	1.574	1.581	1.450	1.407	1.398	1.448	1.393	1.442	1.273	1.309	1.335
hspb6	1.673	1.606	1.497	1.357	1.609	1.605	1.322	1.249	1.334	1.228	1.208	0.868
hspb8	1.390	1.392	1.473	1.153	1.008	1.243	1.475	1.501	1.341	1.192	1.224	1.151

Table 2.3 continued

il6st	**1.484**	**1.537**	**1.533**	**1.381**	**1.361**	**1.204**						
irak4	0.838	0.831	0.824	0.825	0.784	0.832	0.934	0.943	0.862	0.667	0.850	0.770
kras	1.567	1.541	1.581	1.616	1.645	1.629	0.980	0.953	0.972	1.367	1.334	1.304
lcn2	1.606	1.688	1.702	1.773	1.817	1.806						
lepr	1.393	1.431	1.466	1.321	1.370	1.291	1.089	1.069	1.111	0.694	0.633	0.949
map2k4	1.823	1.836	1.824	1.628	1.668	1.612	1.663	1.701	1.673	1.541	1.531	1.627
map2k5	0.158	0.220	0.201	0.389	0.398	0.253	0.580	0.509	0.486	0.746	0.714	0.761
mapk1	1.604	1.594	1.556	1.381	1.400	1.347	1.567	1.590	1.487	1.677	1.696	1.646
mmp2	1.657	1.698	1.673	1.850	1.801	1.756	0.943	0.840	1.005	1.326	1.336	1.340
mtpn	2.033	2.011	1.988	2.133	2.143	2.110	1.516	1.508	1.584	1.722	1.763	1.725
nampt	1.389	1.360	1.331	1.227	1.225	1.120	0.825	0.774	0.712	1.002	1.080	0.881
ndufa13	2.355	2.344	2.365	2.259	2.260	2.299	2.342	2.398	2.340	2.262	2.267	2.266
nppa	1.235	1.226	1.318	1.459	1.437	1.376						
nub1	1.693	1.656	1.723	1.595	1.501	1.522	1.368	1.455	1.474	1.026	0.985	1.117
phb	2.209	2.211	2.230	2.197	2.166	2.207	2.199	2.310	2.289	2.105	2.098	2.104
plrg1	1.397	1.483	1.460	1.440	1.399	1.308	1.327	1.375	1.360	1.309	1.277	1.338
prkaa2	0.763	0.845	0.795	0.657	0.601	0.428	0.655	0.715	0.846	0.595	0.810	0.752
prkcd	1.102	1.141	1.154	1.210	1.212	1.099	1.111	1.061	1.127	1.286	1.373	1.298
raf1	1.345	1.324	1.340	1.207	1.251	1.152	1.335	1.269	1.354	1.258	1.255	1.317
sfrp2	1.671	1.726	1.642	1.798	1.757	1.752	0.550	0.250	0.666	1.101	1.337	0.967
tfdp1	0.959	1.038	1.011	1.108	1.084	0.950	0.450	0.380	0.601	0.884	0.865	0.804
tp53	1.601	1.605	1.625	1.667	1.687	1.601						
txnip	2.358	2.382	2.382	2.481	2.420	2.440						
ube4b	1.422	1.462	1.421	1.201	1.208	1.148	1.446	1.475	1.472	1.386	1.362	1.412

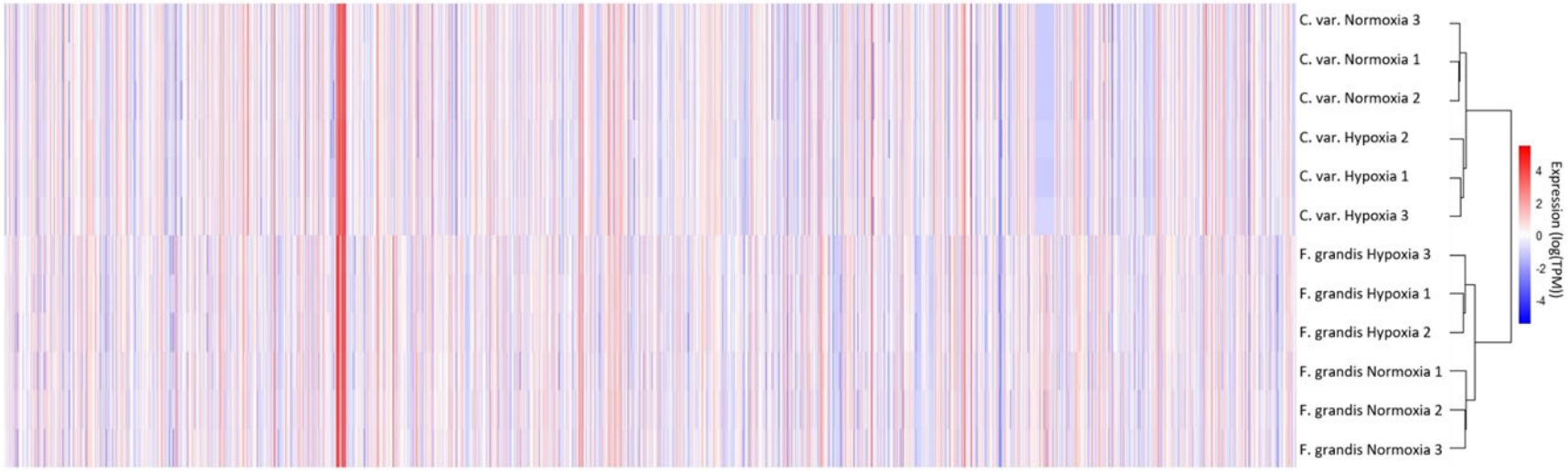

Figure 2.1. Heatmap with hierarchical clustering of all mapped genes in *C. variegatus* and *F. grandis* larvae following 48 h exposure to either hypoxia or normoxia. Expression values represented as log(TPM).

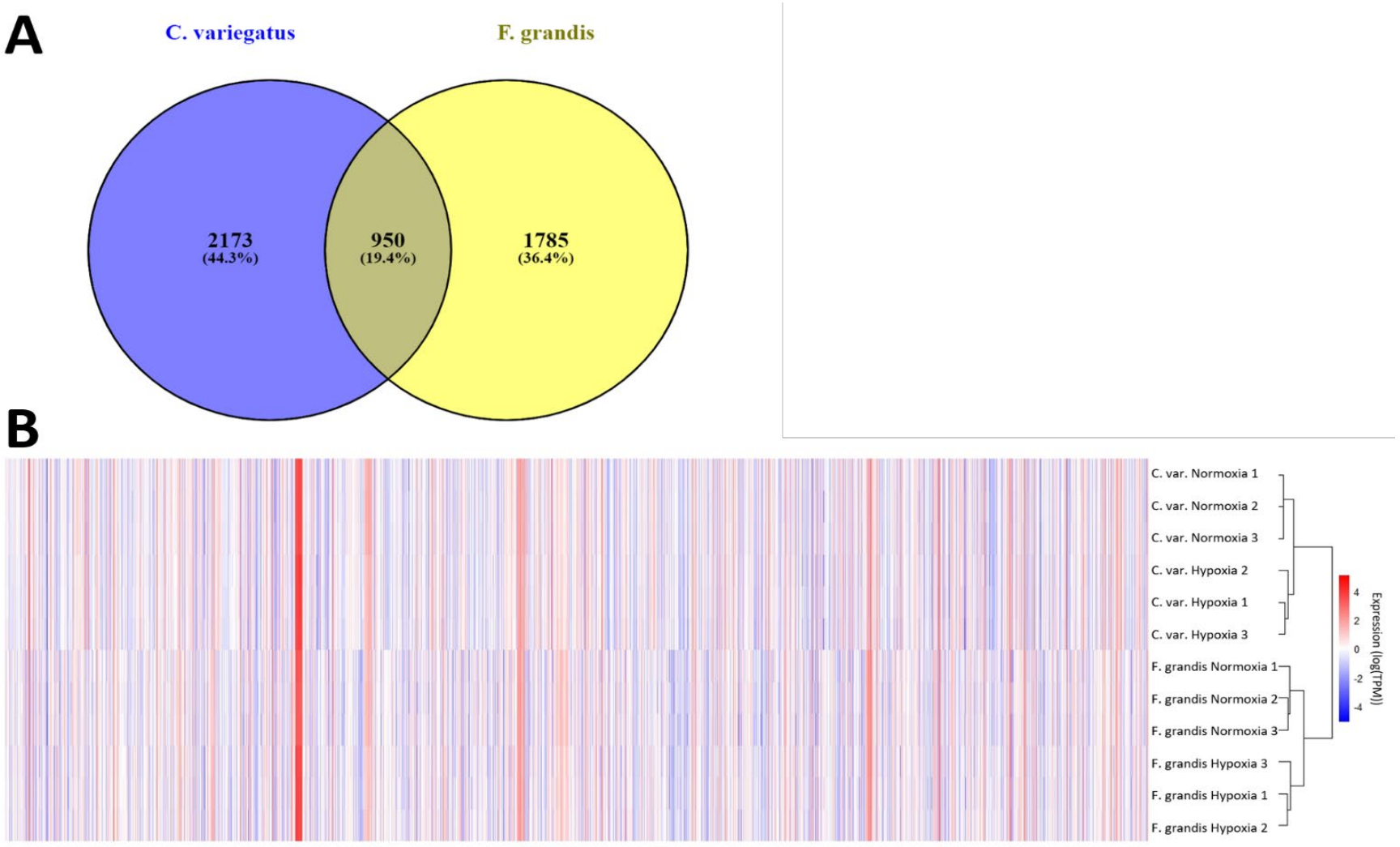

Figure 2.2. **(A)** Comparison of 4908 shared and unique DEGs present in *C. variegatus* (blue) and *F. grandis* (yellow) following 48 h exposure to hypoxia. **(B)** Heatmap with hierarchical clustering of all DEGs in *C. variegatus* and *F. grandis* larvae following 48 h exposure to either hypoxia or normoxia. Expression values represented as log(TPM).

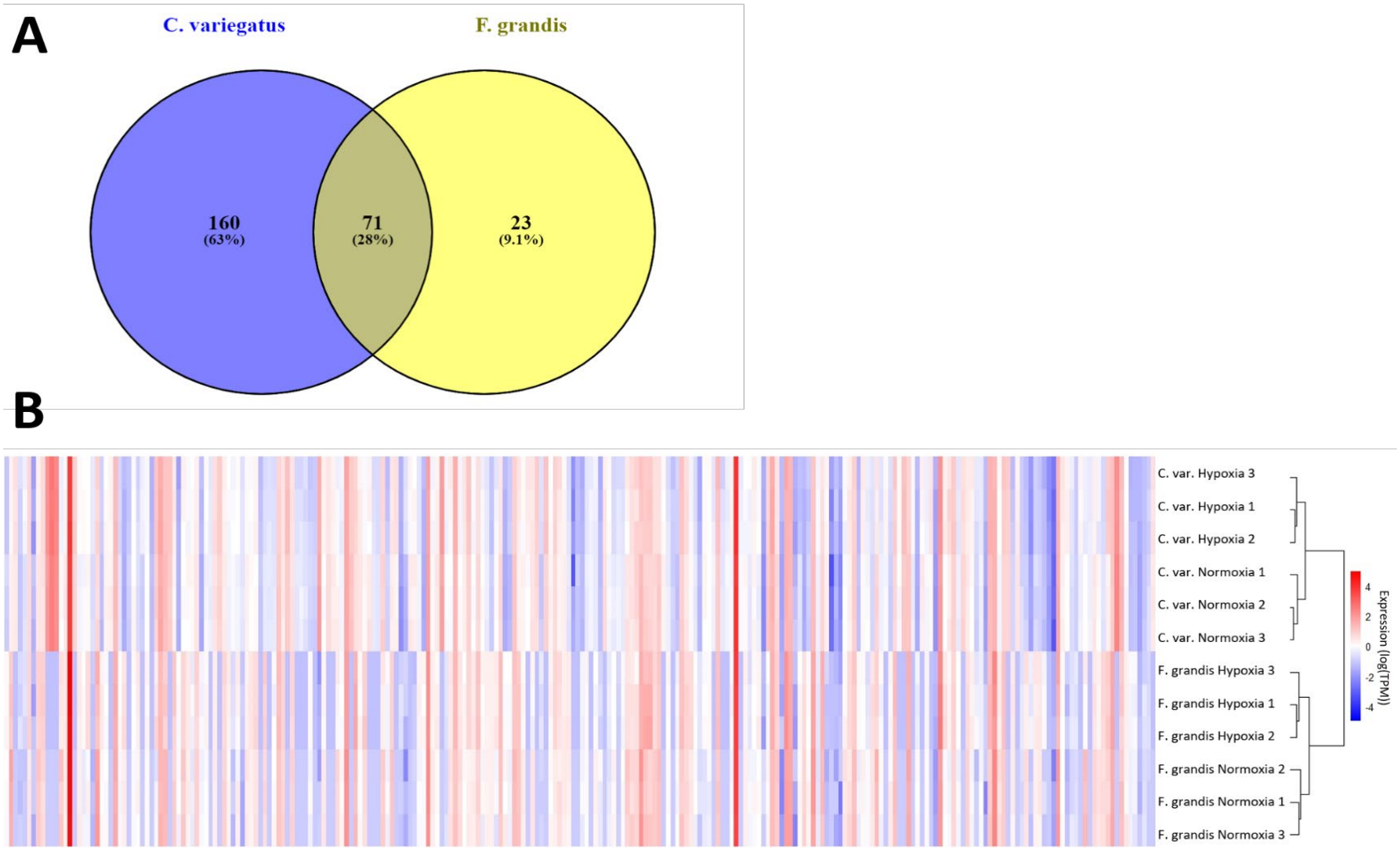

Figure 2.3. **(A)** Comparison of 254 shared and unique cardiac specific DEGs present in *C. variegatus* (blue) and *F. grandis* (yellow) following 48 h exposure to hypoxia. **(B)** Heatmap with hierarchical clustering of cardiac specific DEGs in *C. variegatus* and *F. grandis* larvae following 48 h exposure to either hypoxia or normoxia. Expression values represented as log(TPM).

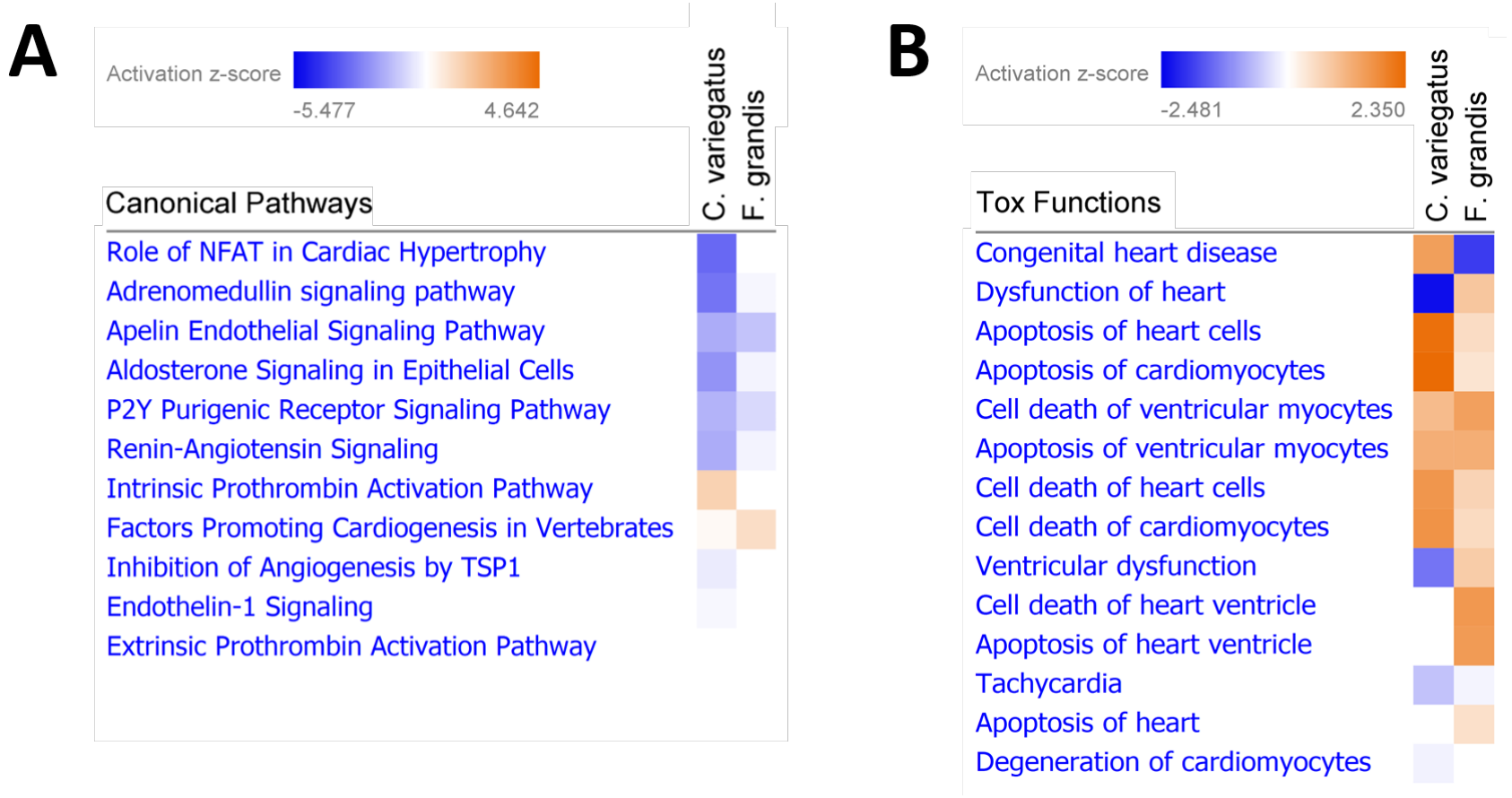

Figure 2.4. IPA analysis of cardiac canonical pathways **(A)** and cardiac toxicological functions **(B)** following hypoxia exposure in *C. variegatus* and *F. grandis* that were both significantly impacted ($p \leq 0.05$) and showed directionality (activation z-score $\neq 0$). Warm shades indicate pathway/function activation, cool shades indicate pathway/function inhibition.

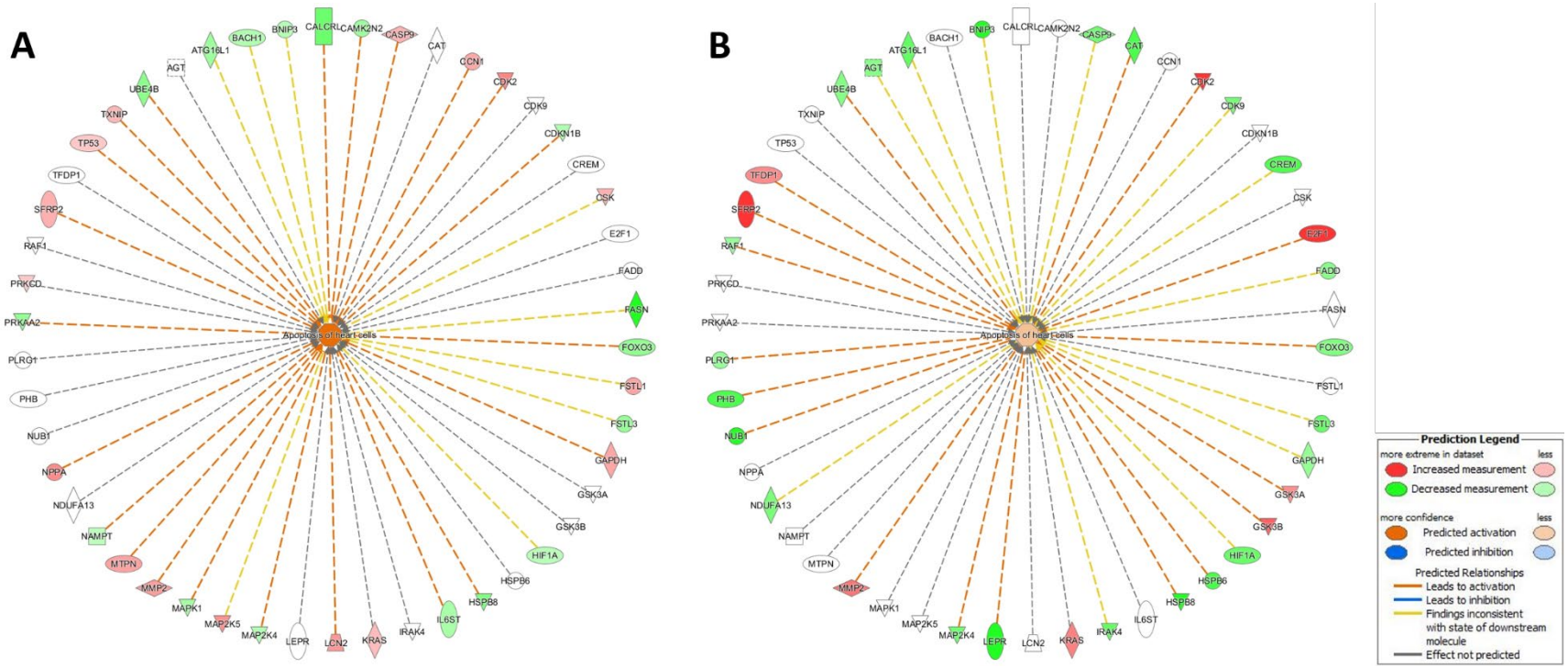

Figure 2.5. Changes in DEG expression and their predicted roles in the activation of "apoptosis of heart cells" pathway as predicted by IPA following 48 h hypoxia exposure in newly hatched *C. variegatus* **(A)** and *F. grandis* **(B)** larvae. DEGs shaded in red represent measured increased expression, DEGs shaded in greens represent measured decreased expression relative to normoxia controls.

CHAPTER 3. EFFECTS OF POLYCYCLIC AROMATIC HYDROCARBONS AND ABIOTIC STRESSORS ON *FUNDULUS GRANDIS* CARDIAC TRANSCRIPTOMICS

A version of this chapter has been previously published; reproduced from:
Allmon, E., Serafin, J., Chen, S., Rodgers, M.L., Griffitt, R., Bosker, T., De Guise, S., Sepúlveda, M.S., 2021. Effects of polycyclic aromatic hydrocarbons and abiotic stressors on *Fundulus grandis* cardiac transcriptomics. Sci. Total Environ. 752, p.142156. https://doi.org/10.1016/j.scitotenv.2020.142156

3.1 Abstract

Following the 2010 *Deepwater Horizon* oil spill, extensive research has been conducted on the toxicity of oil and polycyclic aromatic hydrocarbons (PAHs) in the aquatic environment. Many studies have identified the toxicological effects of PAHs in estuarine and marine fishes, however, only recently has work begun to identify the combinatorial effect of PAHs and abiotic environmental factors such as hypoxia, salinity, and temperature. This study aims to characterize the combined effects of abiotic stressors and PAH exposure on the cardiac transcriptomes of developing *Fundulus grandis* larvae. In this study, *F. grandis* larvae were exposed to varying environmental conditions (dissolved oxygen (DO) 2, 6 ppm; temperature 20, 30°C; and salinity 3, 30 ppt) as well as a to a single concentration of high energy water accommodated fraction (HEWAF) (∑PAHs 15 ppb). Whole larvae were sampled for RNA and transcriptional changes were quantified using RNA-Seq followed by qPCR for a set of target genes. Analysis revealed that exposure to oil and abiotic stressors impacts signaling pathways associated with cardiovascular function. Specifically, combined exposures appear to reduce development of the systemic vasculature as well as strongly impact the cardiac musculature through cardiomyocyte proliferation resulting in inhibited cardiac function and modulated blood pressure maintenance. Results of this study provide a holistic view of impacts of PAHs and common environmental

stressors on the cardiac system in early life stage estuarine species. To our knowledge, this study is one of the first to simultaneously manipulate oil exposure with abiotic factors (DO, salinity, temperature) and the first to analyze cardiac transcriptional responses under these co-exposures.

3.2 Introduction

Coastal estuaries are dynamic environments that play an important role in the life cycle of many marine species. These inshore environments are subject to influences from adjacent inland watersheds as well as tidal influences from pelagic waters. This interplay creates complex biogeochemical profiles wherein fluctuating abiotic factors such as dissolved oxygen (DO), salinity, and water temperatures interact and influence organisms living within estuaries (Orlando et al., 1993; Schroeder and Wiseman, 1986). The Northern Gulf of Mexico annually undergoes seasonal intensification of the dead zone – a regional hypoxia event that forms at the mouth of the Mississippi River – in the late spring and summer months. During this time, DO levels within the water column drop to less than 2 parts per million (ppm) presenting oxic challenges to organisms residing in the dead zone (Rabalais et al., 2002). In addition to oxic challenges from the dead zone, estuaries in the Northern Gulf of Mexico undergo regular salinity fluctuations driven by changes in freshwater inputs from river discharge, precipitation, and tidally driven marine inputs. These fluctuations create brackish environments within estuaries with salinities that can range from fully fresh water (0 ppt) to hypersaline environments (> 35 ppt) (Orlando et al., 1993). Next, estuarine habitats are often very shallow and are therefore susceptible to changes in thermal regimes driven by ambient air temperatures, warm freshwater inputs from watersheds, and cooler marine waters driven in by tides (Schroeder and Wiseman, 1986). These dynamic interactions require the organisms that reside in these estuaries be capable

of physiologically compensating for the changing environments (Bennett and Beitinger, 1997; Borowiec et al., 2015; Haney and Nordlie, 1997).

In addition to adapting to fluctuating abiotic factors, estuarine species are often faced with anthropogenic stressors. An important example is the *Deepwater Horizon* oil spill that occurred in the Northern Gulf of Mexico from April to September 2010 and released an estimated 4.9 million barrels of crude oil into the environment (Beyer et al., 2016; Camilli et al., 2012; McNutt et al., 2012; Norse and Amos, 2010). The plume from the wellhead reached the surface and created a slick that reached shorelines from Louisiana to Florida and was estimated to cover > 26,000 square miles (Beyer et al., 2016; Norse and Amos, 2010; Sammarco et al., 2013). The location and timing of the spill coincided with the annual development of the dead zone as well as the spawning periods for many pelagic and estuarine fish species (Esbaugh et al., 2016; Muhling et al., 2012; Rooker et al., 2013). Following the spill there has been a breadth of research on the effects of oil (see Murphy et al., 2016 for a literature review), particularly its primary constituents – polycyclic aromatic hydrocarbons (PAHs) – on the early life stages of fishes. Importantly, previous work with PAHs has shown that PAH toxicity in fish is variable and depends on the life stage at the time of the exposure. PAHs can have adverse impacts on specific organ and systems (such as the cardiovascular system or the immune system), developmental stages, or act as potential mutagens or carcinogens (Carls et al., 2008; Carvalho et al., 2008; Collier et al., 2013; Edmunds et al., 2015; Esbaugh et al., 2016; Incardona et al., 2014, 2011; Jayasundara et al., 2015; Mager et al., 2014; Magnuson et al., 2018; Pan et al., 2018; Xu et al., 2017a, 2016).

While many studies have identified the toxicological effects of oil in estuarine and marine fishes (for a review, see Murphy et al., 2016), only recently has work begun to identify the

combined effects of oil and abiotic environmental factors such as hypoxia, salinity, and temperature (Hedgpeth and Griffitt, 2016; Jasperse et al., 2019; Mauduit et al., 2018; Milinkovitch et al., 2020; Serafin et al., 2019; Simning et al., 2019). Specifically, a number of studies have found impacts of abiotic stressors on the developing cardiac system in fish. Cardiac impairments such as changes in heart rate, blood pressure, vasodilation, and cardiac remodeling are common when embryos are exposed to increased temperatures, elevated salinities, and/ or low DO levels (Claireaux et al., 1995; Farrell, 2007; Keen et al., 2017; Klaiman et al., 2011; Lin et al., 1994; Randall and Smith, 1967). Similarly, exposure to PAHs under otherwise optimal environmental conditions have repeatedly shown cardiac effects including heart malformations, reductions in cardiac output, and increases in pericardial edema in both estuarine and pelagic fishes(Carls et al., 2008; Incardona et al., 2014, 2011, 2009; Jayasundara et al., 2015; Khursigara et al., 2017).

Currently, the combined effects of abiotic factors and PAH exposure on the developing cardiac system are largely unknown. This study aims to characterize these effects in developing Gulf killifish (*Fundulus grandis*). *F. grandis* is an estuarine species native to the Gulf of Mexico and alongside a closely related species (*Fundulus heteroclitus*) has been used as a model for toxicity testing in a number of PAH studies (Oleksiak et al., 2011; Powell et al., 2004; Reid et al., 2016; Whitehead et al., 2011). *F. grandis* inhabit nearshore environments that undergo daily and seasonal fluctuations in temperature, salinity, and DO. They are also widely dispersed in estuaries directly impacted by the *Deepwater Horizon* oil spill and their spawning seasons directly coincided with the timing of the spill (Greeley and MacGregor, 1983), making them ideal candidates for the study of the combined effects of oil and abiotic factors on transcriptional responses in the developing cardiac system. We hypothesize that exposure to PAHs or

environmentally relevant abiotic factors (hypoxia, salinity, temperature) will result in changes to cardiac related transcriptional responses. Additionally, we expect that the combination of PAHs with an abiotic factor will result in altered transcriptional responses relative to independent exposure to PAHs or abiotic factors alone.

3.3 Materials and Methods

3.3.1 Broodstock collection and spawning

Wild caught adult *F. grandis* broodstock were collected from Mississippi estuaries in Gautier, Ocean Springs, Deer Island, and Bay St. Louis in March 2015. Fish underwent a 14-day quarantine period upon arrival to Purdue Aquaculture Research Lab at Purdue University, West Lafayette, Indiana, USA. Fish were maintained in 130 L aquaria at 25±1°C, 6 mg/L DO, 10 ppt salinity (reconstituted saltwater prepared with Fritz SuperSalt Concentrate, Fritz Industries, Mesquite, TX, USA), and 16L:8D photoperiod. Fish were fed to satiation twice daily with frozen chironomids (morning) and frozen brine shrimp (JEHM Co., Lambertville, NJ, USA) (evening). A single mating pair of *F. grandis* was bred 2-3 times per week and embryos were collected on Pentair polyester filter mats (Minneapolis, MN, USA) using techniques described by Green 2013. Embryos were then transferred to floating mesh cylinders (15 cm x 5 cm) in the adult tanks from which they were collected and were monitored daily until hatch.

3.3.2 Exposure design

F. grandis larvae (<24h post hatch) were randomly chosen and placed in individual 125 mL glass jars sealed with Teflon lined caps. A fully factorial design was used to combine PAH exposure (0, 15 µg/L), DO (2, 6 ppm), salinity (3, 30 ppt), and temperature (20, 30°C); n = 9 larvae per treatment. Exposure chambers were maintained within temperature controlled environmental

chambers with a 16L:8D photoperiod. Hypoxic conditions (DO ≤ 2 ppm) were established through aeration with nitrogen gas. Salinity was maintained using reconstituted saltwater at the appropriate salinity as described above. Exposures lasted 48 h with water quality monitored daily. Fish were not fed during the course of the exposure as they were still reliant on yolk sac. There were 9 replicates (one larvae per replicate) per treatment.

3.3.3 High energy water accommodated fraction (HEWAF) preparation

1 g/L of Macondo crude oil was blended with seawater using a stainless steel blender (Waring, Stamford, CT, USA) at low speed for 30 s, utilizing previously established methods (Forth et al., 2017b, 2017a). HEWAF was allowed to settle for 1 hour in a glass separatory funnel before 450 mL was drained and used immediately for exposures.

3.3.4 PAH analysis

Gas chromatography coupled with tandem mass spectrometry (GC/MS/MS) was used to quantify concentrations of 29 parent PAHs, alkyl PAHs, and alkyl PAH homologs from stock solutions at the University of Connecticut Center for Environmental Sciences and Engineering (Storrs, CT, USA). PAH concentrations from HEWAF dilutions and test solutions over time were calculated using fluorescence methodology by measuring fluorescence between 270 and 380 nm (Greer et al., 2012). See Serafin et al. (2019), Table S2 for total PAH concentrations and the 29 analytes quantified (tPAH29).

3.3.5 Water chemistry

Temperature, DO, salinity, and PAH content were measured at the onset of exposures and throughout the 48h exposure. Temperature and DO were measured using a YSI PRO 1020

multi-parameter meter. Salinity was measured using a Pentair Vital Sine SR6 handheld refractometer. PAH concentrations were indirectly quantified through fluorometry (Greer et al., 2012) using a Turner Designs AU-10 fluorometer (Turner Designs, San Jose, CA, USA). For full water chemistry methodology see Serafin et al. (2019).

3.3.6 RNA isolation/ RNA Seq

Following 48h exposures, individuals were collected for RNA analysis. To ensure sufficient RNA, three larvae were pooled to constitute one replicate, resulting in three replicates per treatment. RNA isolation was completed using RNeasy Mini Kits (Qiagen, Valencia, CA, USA) according to manufacturer's protocols. RNA quantification was measured using a NanoDrop 2000 spectrophotometer and associated software (Thermo Fisher, Waltham, MA, USA). RNA sequencing (RNAseq) was performed at the Purdue University Genomics Core Facility (West Lafayette, IN, USA) with an Illumina HiSeq 2500 (Illumina, San Diego, CA, USA) to sequence a minimum of 15 million 2 x 100 bp sequencing reads; average sequencing depth was 23 million reads/sample.

3.3.7 Bioinformatic analysis

All gene expression data have been submitted and archived through the Gulf of Mexico Research Initiative Information & Data Cooperative (GRIIDC). Sequenced reads were quality checked using the FastQC toolkit (Andrews, 2010), adapter sequences and low-quality reads were trimmed using Trimmomatic (Bolger et al., 2014), and a post-cleaning quality check was run again using FastQC. Filtered sequences were loaded into CLC Genomics Workbench (Qiagen, Hilden, Germany) where paired-end reads were merged and mapped to the *F. heteroclitus* reference genome (NCBI genome: 743) with >94% mapping success. Gene expression values

were calculated as transcripts per million and differential expression was calculated in the CLC Genomics Workbench. Differentially expressed genes (DEGs) were defined as those with an FDR p-value ≤ 0.05 when compared to expression under control conditions. Heat maps for DEGs using Euclidean distance hierarchical clustering and complete linkages were created in R using pheatmap package (Kolde, 2012). DEGs were converted to their human orthologs and analyzed using Ingenuity Pathway Analysis (IPA) (Qiagen, Hilden, Germany) software with a FDR p-value cut-off at 0.05 to predict downstream pathways and functions. IPA provides a widely curated database of human and mammalian gene-association findings that allow for deeper analysis of gene interactions and associated downstream pathways and functions than data currently available for teleost models alone (Jones et al., 2020; Xu et al., 2017a, 2017b). For DEG analysis and pathway analysis, treatment groups were compared to the control group (∑PAH = 0 µg/L, DO = 6 ppm, salinity = 3 ppt, temperature = 20°C). In order to maintain the cardiac related scope of this analysis, only canonical pathways, toxicological functions, and disease/ biofunctions related to cardiac effects were included (Rodgers et al., 2018; Serafin et al., 2019).

3.3.8 RT qPCR analysis

Subsets of RNA isolate samples collected for RNA Seq analysis were also used for real-time qPCR validation (3 pools of 3 larvae each per treatment). Isolated RNA was converted to cDNA using a High-Capacity cDNA Reverse Transcription Kit (Thermo Fisher, Waltham, MA, USA), cDNA concentrations were verified on a NanoDrop 2000 spectrophotometer and associated software (Thermo Fisher, Waltham, MA, USA). RT qPCR was conducted on a Bio-Rad CFX Connect Real-Time PCR System utilizing iQ SYBR Green Supermix (Bio-Rad, Hercules, CA) following the thermal cycling protocol provided by the manufacturer. Primers were supplied by

Integrated DNA Technologies (Coralville, IA). Primer sequences were designed through Primer3Plus software (Untergasser et al., 2007) using NCBI nucleotide sequence data. Full primer sequences and NCBI accession numbers are listed in Table 3.1. Reaction efficiencies for each primer pair were determined through serially diluted standard curves with all reaction efficiencies between 90% and 103% ($R^2 \geq 0.99$). Relative abundance of each gene in relation to the control gene *β-actin* was analyzed using the delta-delta CT method (Vandesompele et al., 2002). Note that *β-actin* is a common housekeeping gene with CT values that remained stable across all conditions tested. Statistical analysis of gene expression data for all treatments was analyzed using one-way ANOVAs and Holm-Sidak pairwise multiple comparison versus control group post-hoc tests with fiducial level of significance of $p \leq 0.05$. All comparisons passed normality (Shapiro-Wilk) and equal variance (Brown-Forsythe) tests. All statistical variables are presented in Supplemental Table 3.1 located at https://doi.org/10.1016/j.scitotenv.2020.142156**.**

3.4 Results

3.4.1 Water quality

While this experiment consisted of a fully factorial design that included up to four environmental stressors, to conserve power within analyses, only treatments that included a single factor deviation from control (oil, hypoxia, salinity, or temperature) and treatments that included binary combinations of oil and a single abiotic factor (i.e. oil + hypoxia) were included in this analysis. Nominal exposure conditions (∑PAH, DO, salinity, and temperature) for all treatments included in analysis are listed in Table 3.2A with associated measurements of water quality parameters in Table 3.2B. Temperatures and salinities were maintained at ± 1°C and ± 1 ppt nominal

concentrations respectively. Over the course of the 48h exposure, DO decreased by an average of 2.2 ± 0.6 ppm under normoxic conditions and 1 ± 0.8 ppm under hypoxic conditions. Initial ∑PAH values for all exposures involving oil were 15.3 ± 1.15 ppb (Serafin et al., 2019). For a detailed description of water quality parameters and PAH decline over the 48h exposure period see Serafin et al. (2019).

3.4.2 Differential expression

Differential expression analysis revealed a total of 494 DEGs within the cardiac-related pathways analyzed across all treatment groups (Supplemental Table 3.2; https://doi.org/10.1016/j.scitotenv.2020.142156). Figure 3.1 shows the hierarchical clustering of all DEGs according to treatments. The most obvious pattern that emerged during clustering was the role of oil in the structuring of the transcriptional response of cardiac-related genes; oil (104 DEGs) and oil + hypoxia (160 DEGs) treatments clustered closely followed by the oil + salinity (225 DEGs) and oil + temperature (338 DEGs) treatments. The hypoxia only (137 DEGs) and salinity only (123 DEGs) treatments clustered closely together and were more similar to the treatments containing oil than the temperature alone treatment. The temperature treatment had the fewest DEGs (44) of all exposure groups and did not cluster closely with any additional treatment groups.

3.4.3 qPCR validation of RNASeq DEGs

Overall, qPCR data for genes involved in xenobiotic metabolism and cardiac function are in agreement to those seen in the RNA Seq data (Figure 3.2). Genes involved in xenobiotic metabolism (*ahrr, ugt1a1,* and *cyp1a)* universally showed upregulation relative to controls in all exposures containing oil either singly or in combination with an abiotic stressor (Figure 3.2A-C).

Expression of *ahrr* was significantly increased in the oil, oil + hypoxia, oil + salinity, and oil + temperature exposures, but its expression was not significantly altered when exposed to an abiotic factor alone (Figure 3.2A). Expression of *ugt1a1* was significantly downregulated in the elevated temperature RNA Seq data; corresponding qPCR data showed a similar, but non-significant trend (Figure 3.2B). Exposure to oil, and to oil + hypoxia, high salinity and high temperature caused an upregulation of *ugt1a1* expression. Although *cyp1a* which was not differentially upregulated from the RNA Seq data, upregulation from qPCR data followed a similar trend with the previous two genes, with an upregulation in all treatments involving oil exposure and in any single abiotic stressor treatment + oil (Figure 3.2C).

Expression trends in genes involved in cardiac formation and function were also similar between the qPCR and RNA Seq data. Expression of *fbxo32* was not significantly impacted under oil only, elevated temperature, or the combination of oil + temperature (Figure 3.2D). In contrast, under hypoxic and elevated salinity conditions, RNA Seq measurements showed a significant decrease in *fbxo32* transcripts; similarly, qPCR measurements showed reduced, but non-significant *fbxo32* expression. *fbxo32* expression was significantly upregulated in the combination treatments of oil + hypoxia and oil + salinity. Expression of *fgf7* was not significantly impacted under elevated temperature or elevated salinity (Figure 3.2E). Exposure to hypoxia in the absence of oil significantly increased the number of *fgf7* transcripts measured through RNA Seq and although not significant, the qPCR expression of *fgf7* was also increased relative to control. All exposures involving oil exhibited significantly increased expression of *fgf7* with the combined exposure of oil + temperature having qPCR expression levels significantly higher than oil alone. Similarly, all exposures including oil induced significant increases in expression of *mb* with the oil + temperature exposure significantly higher than the

oil alone exposure (Figure 3.2F). Hypoxia alone also induced a significant increase in *mb* in the qPCR data and a non-significant increase in the RNA Seq data. There were no differences from control in *mb* expression in the elevated salinity and temperature exposures.

3.4.4 Canonical pathway analysis

Analyses conducted through IPA included only those predicted pathways and functions that showed both a significant response ($p < 0.05$) and directional response (activation z-score $\neq 0$) in at least one treatment. Pathway analysis showed DEGs involved in 18 cardiac-related canonical pathways exhibiting a significant transcriptional response in at least one treatment (Figure 3.3). Impacted pathways have roles in several cardiac functions including vasodilation, blood pressure maintenance, cell proliferation, hypertrophy, and contractility. Inhibition of calcium signaling was the only response that remained consistent among all treatments. Single exposures to abiotic factors tended to inhibit signaling pathways (as indicated by negative activation z-scores and shades of blue in Figure 3.3). Exposure to elevated temperature alone induced almost no changes in canonical pathways except for a slight inhibition in calcium signaling. Combined exposures to oil and abiotic factors tended to activate pathways involved in cell proliferation and hypertrophy (positive activation z-scores and shades of orange in Figure 3.3) as well as reduced angiogenesis.

3.4.5 Toxicological function analysis

Further analysis through IPA identified 26 toxicological functions across all treatments that were both significantly impacted and showed directionality (Figure 3.4). Toxicological functions were identified using the human orthologs of DEGs and as such, interpretation of results must be done with caution. Additionally, variants of several functions appear multiple times within the

resulting list of impacted toxicological functions (i.e. congenital heart disease and familial congenital heart disease). These 26 functions can be grouped together and reduced to represent 9 broad toxicological functions: Heart malformations, congenital heart defects, congestive heart failure/ pericardial edema, cardiomyocyte proliferation, cardiomyocyte death, heart damage, hypertrophy, arrythmia, and heart dysfunction/ failure.

In general, toxicological function analysis aligns well with canonical pathway analysis. Similar to the results from the canonical pathway analysis, general trends in increased cellular proliferation and hypertrophy and inhibited contractility were identified by the toxicological function analysis. Exposure to oil alone resulted in activation of congenital cardiac defects, cardiac hypertrophy, and increased cardiac dysfunction/ failure. Exposure to hypoxia or elevated salinity resulted in similar responses of increased cardiac malformations and congenital cardiac defects. Like the DEG and canonical pathway results, elevated temperature alone resulted in few impacted toxicological functions. Broadly, trends in combined oil + hypoxia and oil + salinity responses followed those seen in their respective single abiotic factor responses. The combined effects of oil and elevated temperature, however, did not follow trends in either oil alone or temperature alone treatments; responses included activation of cardiomyocyte proliferation and hypertrophy, inhibition of cardiomyocyte death, and inhibition of cardiac malformations and congenital defects.

3.4.6 Diseases/ biofunction analysis

IPA analysis into diseases and biofunctions revealed an overall trend in activation across exposures with most responses occurring in oil alone, hypoxia, and oil + hypoxia exposures (total of 26 functions impacted, Figure 3.5). As with previously discussed IPA analyses, elevated temperature alone resulted in few impacted functions. Increased salinity and the

combination of oil + salinity also showed little response at this level of analysis. Responses included effects on vasculature development, fatty plaque formations, and blood pressure disorders. Diseases involved in development of vasculature (vascular lesions, outgrowth of vasculature, and others) were activated in all exposures involving oil, which aligns with the inhibition of angiogenesis seen in the canonical pathway analysis (Figure 3.5). Responses that suggest increases in fatty plaque formations (atherosclerosis, foam cells, and hypertriglyceridemia) were only present in oil, hypoxia, and oil + hypoxia exposures. Impacts on blood pressure disorders were seen in all exposures involving oil. These results are supported by those from the canonical pathway analysis in that the inhibition of blood pressure disorders seen in the combined oil + abiotic factors align with the activation of signaling pathways involved in blood pressure maintenance (Aldosterone, Apelin, and Renin-Angiotensin).

3.5 Discussion

This study aimed to characterize the combined effects of oil exposure and sub-optimal abiotic factors on the transcription of cardiac related genes in early life history *F. grandis*. While other studies have described the effects of oil on the cardiac system of fish (Carls et al., 2008; Incardona et al., 2014, 2011, 2009; Jayasundara et al., 2015; Khursigara et al., 2017), to our knowledge none have expanded their assessment to include how dynamic environmental parameters (which are common in estuaries) influence these effects. Importantly, abiotic factors such as DO, salinity, and temperature have been shown to impact cardiac function independent of oil exposure through changes in heart rate, blood pressure, vasodilation, and cardiac remodeling – implying that environmental conditions play a key role in the development and function of the cardiac system in early life fish stages (Claireaux et al., 1995; Farrell, 2007; Keen et al., 2017; Klaiman et al., 2011; Randall and Smith, 1967). In addition, the cardiac

transcriptome of early life stage fish has been shown to be responsive to the presence of oil and perturbations in environmental conditions (Xu et al., 2017a, 2016). Therefore, this study used the analysis of transcriptional changes in conjunction with predicted downstream pathway analysis to elucidate the impacts of both oil and sub-optimal abiotic factors on the cardiovascular system of larval *F. grandis*. Results presented here appear to support our hypothesis that exposure to PAHs and abiotic factors result in changes to cardiac related transcriptional responses. Further, there appears to be some evidence that combined exposure to oil and abiotic factors enhances these responses.

Analysis of the differential gene expression data suggests that the presence of oil is the strongest factor influencing transcriptional responses in the cardiac system under our exposure conditions. All exposures that included oil clustered closely together under the hierarchical clustering model, whereas exposures to individual abiotic factors did not cluster closely with any exposures involving oil. Within the oil cluster, the oil treatment alone and the oil + hypoxia treatment clustered most closely together, a trend that is reflected in downstream analyses through IPA. The combination of oil and an abiotic factor resulted in slightly more DEGs than exposure to any individual stressor, hinting that there may be a synergistic response when exposed to multiple stressors. This is most prominently seen in the oil + temperature exposure which resulted in more than triple the number of DEGs than the oil only exposure and a more than 7-fold increase in DEGs relative to the temperature alone exposure. While these results suggest a more than additive effect in DEG expression, a definitive statistical analysis could not be completed due to small sample sizes and additional exposures will need to be performed in order to verify the trends in the data. However, these DEG results suggest complex interactions between oil and abiotic factors are involved in mediating transcriptional cardiac responses.

A number of DEGs involved in xenobiotic metabolism and cardiac function were chosen for further analysis through qPCR. *ahrr* (aryl-hydrocarbon receptor repressor) is an important feedback modulator in the aryl-hydrocarbon receptor signaling cascade and has roles in regulating cell growth and differentiation (Clark et al., 2010). *ugt1a1* (UDP glucuronosyltransferase 1a1) encodes an enzyme in the glucuronidation pathway that metabolizes lipophilic xenobiotics into water-soluble metabolites (Schlenk et al., 2008). *cyp1α* (cytochrome p450 1a) is a member of the cytochrome p450 family of enzymes which catalyzes reactions involved in xenobiotic metabolism; its expression is induced by the presence of PAHs (Schlenk et al., 2008). qPCR results for these genes involved in xenobiotic metabolism universally followed the same trends as those seen in the DEG analysis of RNA Seq data. As expected (Kim et al., 2018; Mimura et al., 1999; Shimada and Fujii-Kuriyama, 2004), each gene was significantly upregulated in every treatment involving oil exposure. *cyp1α* expression profiles resulting from qPCR analysis followed expected trends as those seen in *ahrr* and *ugt1a1* expression. Interestingly, *cyp1α* did not exhibit significant differential expression in the RNA Seq dataset. Similarly, a lack of significant differential *cyp1α* expression was observed in RNA Seq data for PAH exposed *F. grandis* analyzed using the Tuxedo protocol (Serafin, 2017). These parallel results suggest that the discrepancy between qPCR and RNA Seq analyses are not due to errors induced by the RNA Seq pipeline; rather, they highlight the different sensitivities between RNA Seq and qPCR methodologies. The *cyp1α* qPCR product in this study is only 258 bp, while the RNA Seq methods attempt to map reads to the whole gene of 2708 bp. It is possible that the *cyp1α* gene is not highly conserved between these two *Fundulus* species and the qPCR method caught the conserved region while much of the true *F. grandis cyp1α* reads could

not be mapped to the non-conserved *F. heteroclitus cyp1α* region. This would result in the non-mapped reads being discarded and not appearing as DEGs in the downstream analysis.

Additional genes involved in cardiac development and function (*fbxo32, fgf7,* and *mb*) were assessed and the resulting qPCR trends, much like those involved in xenobiotic metabolism, matched closely with those seen in the RNA Seq data. *fbxo32* (f-box protein 32) was only significantly upregulated in the combined oil + hypoxia and oil + salinity treatments. As *fbxo32* is highly expressed during muscle atrophy (Cleveland and Evenhuis, 2010), its upregulation may suggest an increase in cellular death and dysfunction of the cardiac system under these combined conditions. Similarly, mammalian models have shown increased *fbxo32* expression and associated muscle atrophy under hypoxic conditions (Bodine and Baehr, 2014; De Theije et al., 2015). *fgf7* (fibroblast growth factor 7), which has roles in embryonic development, cell proliferation and differentiation, as well as cardiac morphogenesis (Zinkle and Mohammadi, 2019) was significantly upregulated in all treatments involving oil as well as the hypoxia only exposure. The expression pattern seen here is similar to *fgf7* expression patterns observed in polar cod exposed to PAHs, suggesting that *fgf7* expression may also be sensitive to the presence of PAHs in the environment (Andersen et al., 2015). *mb* (myoglobin) expression followed similar patterns to *fgf7* and was upregulated in hypoxia and all exposures involving oil in both qPCR and RNA Seq datasets. As *mb'*s primary function is intracellular oxygen storage (Bailey and Driedzic, 1986), this may be indicative of an increased oxygen demand under oil and/ or hypoxia conditions. Indeed, in many fish species, exposure to hypoxia resulted in upregulation of myoglobin in muscle tissues (for a review, see Zhu et al., 2013). qPCR results presented here validate the trends seen in the RNA Seq differential gene expression analysis and further confirm that exposure to oil and abiotic environmental stressors are capable of eliciting

responses in the expression of genes involved in detoxification and cardiac function/development in fish early life stages.

IPA identified 18 canonical pathways that were both significantly impacted and showed directionality in their responses. Impacted pathways affected are involved in regulating a number of cardiovascular functions including vasodilation, blood pressure maintenance, cell proliferation, cardiac hypertrophy, and contractility. Alone, exposure to abiotic factors largely resulted in the inhibition of many pathways including vasodilatory responses, blood pressure maintenance, contractility of the heart, and cardiomyocyte proliferation, which align with previous studies showing that hypoxia, salinity, and temperature can result in changes in heart rate, blood pressure, vasodilation, and cardiac remodeling (Claireaux et al., 1995; Farrell, 2007; Keen et al., 2017; Klaiman et al., 2011; Randall and Smith, 1967). When co-exposed with oil, responses appear to shift, and many pathways become activated. For instance, exposure to both oil and hypoxia results in increases in cell proliferation, cardiac hypertrophy, and contractility, and reduced angiogenesis; suggesting that cell growth may be increased in the heart but reduced throughout the rest of the cardiovascular system. Similar results were seen when fish were co-exposed to oil and salinity stress, i.e., increased signaling of cellular proliferation, hypertrophy, and cardiac tissue remodeling and reductions in contractility, angiogenesis, and vasodilation. These results again are suggestive of increased cardiomyocyte growth but reduced cellular proliferation throughout the rest of the cardiovascular system. This likely puts additional stress on the heart as increased cardiomyocyte proliferation and cardiac hypertrophy thickens the walls of the heart resulting in reduced elasticity and contractility. Much like results from the DEG analysis, exposure to elevated temperature alone elicited almost no response in the canonical pathway analysis, but when combined with oil exposure, elevated temperature resulted in the

strongest canonical pathway responses. These pathways, especially those that were not impacted in either the oil alone or temperature alone exposures - such as the activation of Aldosterone and Apelin signaling pathways - suggests that exposure to multiple stressors can induce complex responses in developing fish. Responses in the combined oil and temperature exposure were similar to other binary exposures and included increased cardiomyocyte proliferation, cardiac hypertrophy, and contractility as well as reduced angiogenesis. Further suggesting that cardiac impairment occurs through morphological changes in the cardiac musculature that then drives alterations in the function of the cardiac system.

Further analysis through IPA into impacted toxicological functions yielded results similar to those seen in the canonical pathway analysis. It is important to note that IPA runs analysis on the human orthologs of the DEGs identified in the RNA Seq data and therefore, the functional analysis is based on human/ mammalian functions. As such, a number of functions identified in this analysis are repetitious – for example "Congenital heart disease" and "Familial congenital heart disease" were both identified as functions impacted by the exposures (Figure 3.4). Trends generally follow those seen in canonical pathway analysis for functions involving increases in cardiomyocyte proliferation, inhibited contractility, and increased hypertrophy across treatments, strengthening the conclusion that cardiac impairment is driven by thickening of the heart walls. Additionally, the functions most strongly impacted appear to switch from activation states to inhibition states when going from a single abiotic stressor to combined exposures with oil (i.e. "Congenital heart disease", Figure 3.4). This corresponds well with results from the clustering analysis that suggests that the presence of oil is the primary driver of responses across treatments. Functions with weaker responses overall tended to be more variable and did not exhibit clear reversals in responses when co-exposed with oil (i.e. "Cell death of ventricular

myocytes", Figure 3.4). This suggests that there are complex interactions driving the effects seen at the functional level and that co-exposure to oil and an abiotic stressor may exacerbate effects seen in exposures to an individual stressor. Interrogation into predicted diseases and bio functions resulted in widescale activation with oil, hypoxia, and the co-exposure of oil and hypoxia treatments eliciting the most cardiovascular effects (Figure 3.5), again suggesting that the presence of oil modulates the responses seen across treatments. Processes involved in the development of the vasculature were activated in all treatments involving oil but reduced in the hypoxia only treatment. This response aligns well with the "Inhibition of angiogenesis by TSP1" seen in the canonical pathway analysis (Figure 3.3). TSP1 (thrombospondin 1) is an angiogenesis inhibitor that works by inducing endothelial cell apoptosis and is induced under hypoxic conditions (Moulton and Folkman, 2004; Phelan et al., 1998). It is therefore unsurprising that exposure to hypoxia resulted in inhibition of development of vasculature and other vasculogenesis/ angiogenesis processes (Figure 3.5). Processes involved in blood pressure disorders were largely inhibited in all treatments involving oil, with a slight activation in the hypoxia only treatment. These results correlate well with effects seen in pathways involved in blood pressure maintenance. Specifically, the inhibition of blood pressure disorders in the combined oil and abiotic factor treatments (Figure 3.5) align with the activation of signaling pathways involved in blood pressure maintenance (Aldosterone, Apelin, and Renin-Angiotensin, Figure 3.3). Along with evidence supporting changes in structural morphology of the developing cardiac system, these results provide a holistic view of the impacts of multiple stressors on the cardiovascular system. The data suggests that processes regulating blood pressure maintenance are increased in response to inhibited cardiovascular function which

appears to be driven by increased cardiomyocyte proliferation and reduced development of the systemic vasculature.

This study is one of the first to concomitantly examine the effects of oil and environmental abiotic stressors through the lens of transcriptomic changes related to cardiac development and function. Trends apparent throughout the multiple levels of analysis in this study support previous findings regarding environmental influences on the cardiac transcriptomes of early life history fish when exposed to a single stressor (Carls et al., 2008; Claireaux et al., 1995; Farrell, 2007; Incardona et al., 2014, 2011, 2009; Jayasundara et al., 2015; Keen et al., 2017; Khursigara et al., 2017; Klaiman et al., 2011; Lin et al., 1994; Randall and Smith, 1967). Work presented here expands that knowledge to include trends apparent when fish are co-exposed to oil and abiotic stressors. Overall, responses appear to be structured through complex interactions and the transcriptomic responses to binary exposures do not appear to be the additive result of responses to two single exposures. The presence of oil in combination with abiotic stressors impacted signaling pathways and cardiovascular functions through changes in cardiomyocyte proliferation, cardiac hypertrophy, alterations in contractility, and modulation of blood pressure maintenance. Further, the development of systemic vasculature appears to be heavily impacted by combined exposures of oil and sub-optimal abiotic conditions. Predominant trends across all levels of predictive downstream analysis suggests that cardiac impairment due to co-exposure to oil and an abiotic stressor presents as cardiac hypertrophy driven by increased cardiac proliferation and results in reduced contractility and modulation of blood pressure.

3.6 References

Andersen, Ø., Frantzen, M., Rosland, M., Timmerhaus, G., Skugor, A., Krasnov, A., 2015. Effects of crude oil exposure and elevated temperature on the liver transcriptome of polar cod (*Boreogadus saida*). Aquat. Toxicol. 165, 9–18. https://doi.org/10.1016/j.aquatox.2015.04.023

Andrews, S., 2010. FastQC: a quality control tool for high throughput sequence data.

Bailey, J.R., Driedzic, W.R., 1986. Function of myoglobin in oxygen consumption by isolated perfused fish hearts. Am. J. Physiol. - Regul. Integr. Comp. Physiol. 251, R1144-R1150. https://doi.org/10.1152/ajpregu.1986.251.6.r1144

Bennett, W.A., Beitinger, T.L., 1997. Temperature Tolerance of the Sheepshead Minnow. Copeia. pp. 77–87.

Beyer, J., Trannum, H.C., Bakke, T., Hodson, P. V., Collier, T.K., 2016. Environmental effects of the Deepwater Horizon oil spill: A review. Mar. Pollut. Bull. 110, 28–51. https://doi.org/10.1016/j.marpolbul.2016.06.027

Bodine, S.C., Baehr, L.M., 2014. Skeletal muscle atrophy and the E3 ubiquitin ligases MuRF1 and MAFbx/atrogin-1. Am. J. Physiol. - Endocrinol. Metab. 307, E469–E484. https://doi.org/10.1152/ajpendo.00204.2014

Bolger, A.M., Lohse, M., Usadel, B., 2014. Trimmomatic: A flexible trimmer for Illumina sequence data. Bioinformatics. 30, 2114–2120. https://doi.org/10.1093/bioinformatics/btu170

Borowiec, B.G., Darcy, K.L., Gillette, D.M., Scott, G.R., 2015. Distinct physiological strategies are used to cope with constant hypoxia and intermittent hypoxia in killifish (*Fundulus heteroclitus*). J. Exp. Biol. 218, 1198–1211. https://doi.org/10.1242/jeb.114579

Camilli, R., Di Iorio, D., Bowen, A., Reddy, C.M., Techet, A.H., Yoerger, D.R., Whitcomb, L.L., Seewald, J.S., Sylva, S.P., Fenwick, J., 2012. Acoustic measurement of the Deepwater Horizon Macondo well flow rate. Proc. Natl. Acad. Sci. 109, 20235–20239. https://doi.org/10.1073/pnas.1100385108

Carls, M.G., Holland, L., Larsen, M., Collier, T.K., Scholz, N.L., Incardona, J.P., 2008. Fish embryos are damaged by dissolved PAHs, not oil particles. Aquat. Toxicol. 88, 121–127. https://doi.org/10.1016/j.aquatox.2008.03.014

Carvalho, P.S.M., Kalil, D. da C.B., Novelli, G.A.A., Bainy, A.C.D., Fraga, A.P.M., 2008. Effects of naphthalene and phenanthrene on visual and prey capture endpoints during early stages of the dourado *Salminus brasiliensis*. Mar. Environ. Res. 66, 205–207. https://doi.org/10.1016/j.marenvres.2008.02.059

Claireaux, G., Webber, D.M., Kerr, S.R., Boutilier, R.G., 1995. Physiology and behaviour of free-swimming Atlantic cod (*Gadus morhua*) facing fluctuating temperature conditions. J. Exp. Biol. 198, 49–60.

Clark, B.W., Matson, C.W., Jung, D., Di Giulio, R.T., 2010. AHR2 mediates cardiac teratogenesis of polycyclic aromatic hydrocarbons and PCB-126 in Atlantic killifish (*Fundulus heteroclitus*). Aquat. Toxicol. 99, 232–240. https://doi.org/10.1016/j.aquatox.2010.05.004

Cleveland, B.M., Evenhuis, J.P., 2010. Molecular characterization of atrogin-1/F-box protein-32 (FBXO32) and F-box protein-25 (FBXO25) in rainbow trout (*Oncorhynchus mykiss*): Expression across tissues in response to feed deprivation. Comp. Biochem. Physiol. - B Biochem. Mol. Biol. 157, 248–257. https://doi.org/10.1016/j.cbpb.2010.06.010

Collier, T.K., Anulacion, B.F., Arkoosh, M.R., Dietrich, J.P., Incardona, J.P., Johnson, L.L., Ylitalo, G.M., Myers, M.S., 2013. Effects on fish of polycyclic aromatic hydrocarbons (PAHs) and naphthenic acid exposures, First Edit. ed, Fish Physiology. Elsevier Inc. pp.195-255. https://doi.org/10.1016/B978-0-12-398254-4.00004-2

De Theije, C.C., Langen, R.C.J., Lamers, W.H., Gosker, H.R., Schols, A.M.W.J., Köhler, S.E., 2015. Differential sensitivity of oxidative and glycolytic muscles to hypoxia-induced muscle atrophy. J. Appl. Physiol. 118, 200–211. https://doi.org/10.1152/japplphysiol.00624.2014

Edmunds, R.C., Gill, J.A., Baldwin, D.H., Linbo, T.L., French, B.L., Brown, T.L., Esbaugh, A.J., Mager, E.M., Stieglitz, J., Hoenig, R., Benetti, D., Grosell, M., Scholz, N.L., Incardona, J.P., 2015. Corresponding morphological and molecular indicators of crude oil toxicity to the developing hearts of mahi mahi. Sci. Rep. 5, 1–18. https://doi.org/10.1038/srep17326

Esbaugh, A.J., Mager, E.M., Stieglitz, J.D., Hoenig, R., Brown, T.L., French, B.L., Linbo, T.L., Lay, C., Forth, H., Scholz, N.L., Incardona, J.P., Morris, J.M., Benetti, D.D., Grosell, M., 2016. The effects of weathering and chemical dispersion on Deepwater Horizon crude oil toxicity to mahi-mahi (*Coryphaena hippurus*) early life stages. Sci. Total Environ. 543, 644–651. https://doi.org/10.1016/j.scitotenv.2015.11.068

Farrell, A.P., 2007. Tribute to P. L. Lutz: A message from the heart - Why hypoxic bradycardia in fishes? J. Exp. Biol. 210, 1715–1725. https://doi.org/10.1242/jeb.02781

Forth, H.P., Mitchelmore, C.L., Morris, J.M., Lay, C.R., Lipton, J., 2017a. Characterization of dissolved and particulate phases of water accommodated fractions used to conduct aquatic toxicity testing in support of the Deepwater Horizon natural resource damage assessment. Environ. Toxicol. Chem. 36, 1460–1472. https://doi.org/10.1002/etc.3803

Forth, H.P., Mitchelmore, C.L., Morris, J.M., Lipton, J., 2017b. Characterization of oil and water accommodated fractions used to conduct aquatic toxicity testing in support of the Deepwater Horizon oil spill natural resource damage assessment. Environ. Toxicol. Chem. 36, 1450–1459. https://doi.org/10.1002/etc.3672

Greely, M.S., MacGregor, R., 1983. Annual and Semilunar Reproductive Cycles of the Gulf killifish, *Fundulus grandis*, on the Alabama Gulf coast. Copeia. 711–718.

Green, C., 2013. Intensive (non-pond) culture of Gulf killifish. SRAC Publ. no. 2012.

Greer, C.D., Hodson, P. V., Li, Z., King, T., Lee, K., 2012. Toxicity of crude oil chemically dispersed in a wave tank to embryos of Atlantic herring (*Clupea harengus*). Environ. Toxicol. Chem. 31, 1324–1333. https://doi.org/10.1002/etc.1828

Haney, D.C., Nordlie, F.G., 1997. Influence of environmental salinity on routine metabolic rate and critical oxygen tension of *Cyprinodon variegatus*. Physiol. Zool. 70, 511–518. https://doi.org/10.1086/515867

Hedgpeth, B.M., Griffitt, R.J., 2016. Simultaneous exposure to chronic hypoxia and dissolved polycyclic aromatic hydrocarbons results in reduced egg production and larval survival in the sheepshead minnow (*Cyprinodon variegatus*). Environ. Toxicol. Chem. 35, 645–651. https://doi.org/10.1002/etc.3207

Incardona, J.P., Carls, M.G., Day, H.L., Sloan, C.A., Bolton, J.L., Collier, T.K., Schoiz, N.L., 2009. Cardiac arrhythmia is the primary response of embryonic Pacific herring (*Clupea pallasi*) exposed to crude oil during weathering. Environ. Sci. Technol. 43, 201–207. https://doi.org/10.1021/es802270t

Incardona, J.P., Collier, T.K., Scholz, N.L., 2011. Oil spills and fish health: Exposing the heart of the matter. J. Expo. Sci. Environ. Epidemiol. 21, 3–4. https://doi.org/10.1038/jes.2010.51

Incardona, J.P., Gardner, L.D., Linbo, T.L., Brown, T.L., Esbaugh, A.J., Mager, E.M., Stieglitz, J.D., French, B.L., Labenia, J.S., Laetz, C.A., Tagal, M., Sloan, C.A., Elizur, A., Benetti, D.D., Grosell, M., Block, B.A., Scholz, N.L., 2014. Deepwater Horizon crude oil impacts the developing hearts of large predatory pelagic fish. Proc. Natl. Acad. Sci. 111, E1510–E1518. https://doi.org/10.1073/pnas.1320950111

Jasperse, L., Levin, M., Rogers, K., Perkins, C., Bosker, T., Griffitt, R.J., Sepúlveda, M., De Guise, S., 2019. Hypoxia and reduced salinity exacerbate the effects of oil exposure on sheepshead minnow (*Cyprinodon variegatus*) reproduction. Aquat. Toxicol. 212, 175–185. https://doi.org/10.1016/j.aquatox.2019.05.002

Jayasundara, N., Van Tiem Garner, L., Meyer, J.N., Erwin, K.N., Di Giulio, R.T., 2015. AHR2-mediated transcriptomic responses underlying the synergistic cardiac developmental toxicity of PAHs. Toxicol. Sci. 143, 469–481. https://doi.org/10.1093/toxsci/kfu245

Jones, E.R., Simning, D., Serafin, J., Sepúlveda, M.S., Griffitt, R.J., 2020. Acute exposure to oil induces age and species-specific transcriptional responses in embryo-larval estuarine fish. Environ. Pollut. 263, 1-10. https://doi.org/10.1016/j.envpol.2020.114325

Keen, A.N., Klaiman, J.M., Shiels, H.A., Gillis, T.E., 2017. Temperature-induced cardiac remodelling in fish. J. Exp. Biol. 220, 147–160. https://doi.org/10.1242/jeb.128496

Khursigara, A.J., Perrichon, P., Martinez Bautista, N., Burggren, W.W., Esbaugh, A.J., 2017. Cardiac function and survival are affected by crude oil in larval red drum, *Sciaenops ocellatus*. Sci. Total Environ. 579, 797–804. https://doi.org/10.1016/j.scitotenv.2016.11.026

Kim, K., Jeon, H.J., Choi, S.D., Tsang, D.C.W., Oleszczuk, P., Ok, Y.S., Lee, H.S., Lee, S.E., 2018. Combined toxicity of endosulfan and phenanthrene mixtures and induced molecular changes in adult zebrafish (*Danio rerio*). Chemosphere. 194, 30–41. https://doi.org/10.1016/j.chemosphere.2017.11.128

Klaiman, J.M., Fenna, A.J., Shiels, H.A., Macri, J., Gillis, T.E., 2011. Cardiac remodeling in fish: Strategies to maintain heart function during temperature change. PLoS One. 6, 1-11. https://doi.org/10.1371/journal.pone.0024464

Kolde, R., 2012. Pheatmap: pretty heatmaps.

Lin, H., Pfeiffer, D., Vogl, A., Pan, J., Randall, D., 1994. Immunolocalization of H+-ATPase in the gill epithelia of rainbow trout. J. Exp. Biol. 195, 169–83.

Mager, E.M., Esbaugh, A.J., Stieglitz, J.D., Hoenig, R., Bodinier, C., Incardona, J.P., Scholz, N.L., Benetti, D.D., Grosell, M., 2014. Acute embryonic or juvenile exposure to deepwater horizon crude oil impairs the swimming performance of mahi-mahi (*Coryphaena hippurus*). Environ. Sci. Technol. 48, 7053–7061. https://doi.org/10.1021/es501628k

Magnuson, J.T., Khursigara, A.J., Allmon, E.B., Esbaugh, A.J., Roberts, A.P., 2018. Effects of Deepwater Horizon crude oil on ocular development in two estuarine fish species, red drum (*Sciaenops ocellatus*) and sheepshead minnow (*Cyprinodon variegatus*). Ecotoxicol. Environ. Saf. 166, 186–191. https://doi.org/10.1016/j.ecoenv.2018.09.087

Mauduit, F., Farrell, A.P., Domenici, P., Lacroix, C., Le Floch, S., Lemaire, P., Nicolas-Kopec, A., Whittington, M., Le Bayon, N., Zambonino-Infante, J.-L., Claireaux, G., 2018. Assessing the long-term effect of exposure to dispersant-treated oil on fish health using hypoxia tolerance and temperature susceptibility as ecologically relevant biomarkers. Environ. Toxicol. Chem. 38, 210–221. https://doi.org/10.1002/etc.4271

McNutt, M.K., Camilli, R., Crone, T.J., Guthrie, G.D., Hsieh, P.A., Ryerson, T.B., Savas, O., Shaffer, F., 2012. Review of flow rate estimates of the Deepwater Horizon oil spill. Proc. Natl. Acad. Sci. 109, 20260–20267. https://doi.org/10.1073/pnas.1112139108

Milinkovitch, T., Marras, S., Antognarelli, F., Lefrançois, C., Le Floch, S., Domenici, P., 2020. The effects of hypoxia on aerobic metabolism in oil-contaminated sea bass (*Dicentrarchus labrax*). Chemosphere. 253, 1-7. https://doi.org/10.1016/j.chemosphere.2020.126678

Mimura, J., Ema, M., Sogawa, K., Fujii-Kuriyama, Y., 1999. Identification of a novel mechanism of regulation of Ah (dioxin) receptor function. Genes Dev. 13, 20–25. https://doi.org/10.1101/gad.13.1.20

Moulton, K.S., Folkman, J., 2004. Angiogenesis in cardiovascular disease, in: Molecular basis of cardiovascular disease: A companion to Braunwald's heart disease. Elsevier Inc., pp. 433–454. https://doi.org/10.1016/B978-0-7216-9428-3.50029-9

Muhling, B.A., Roffer, M.A., Lamkin, J.T., Ingram, G.W., Upton, M.A., Gawlikowski, G., Muller-Karger, F., Habtes, S., Richards, W.J., 2012. Overlap between Atlantic bluefin tuna spawning grounds and observed Deepwater Horizon surface oil in the northern Gulf of Mexico. Mar. Pollut. Bull. 64, 679–687. https://doi.org/10.1016/j.marpolbul.2012.01.034

Murphy, D., Gemmell, B., Vaccari, L., Li, C., Bacosa, H., Evans, M., Gemmell, C., Harvey, T., Jalali, M., Niepa, T.H.R., 2016. An in-depth survey of the oil spill literature since 1968: Long term trends and changes since Deepwater Horizon. Mar. Pollut. Bull. 113, 371–379. https://doi.org/10.1016/j.marpolbul.2016.10.028

Norse, E.A., Amos, J., 2010. Impacts, perception, and policy implications of the Deepwater Horizon oil and gas disaster. Environ. Law Report. 40, 11058–11073. https://doi.org/10.1038/nn.2937

Oleksiak, M.F., Karchner, S.I., Jenny, M.J., Franks, D.G., Mark Welch, D.B., Hahn, M.E., 2011. Transcriptomic assessment of resistance to effects of an aryl hydrocarbon receptor (AHR) agonist in embryos of Atlantic killifish (*Fundulus heteroclitus*) from a marine Superfund site. BMC Genomics. 12, 1-18. https://doi.org/10.1186/1471-2164-12-263

Orlando, S.P.J., Rozas, L.P., Ward, G.H., Klein, C.J., 1993. Salinity characteristics of Gulf of Mexico estuaries. Natl. Ocean. Atmos. Adm. Off. Ocean Resour. Conserv. Assess. https://doi.org/10.1016/0004-6981(75)90067-0

Pan, Y.K., Khursigara, A.J., Johansen, J.L., Esbaugh, A.J., 2018. The effects of oil induced respiratory impairment on two indices of hypoxia tolerance in Atlantic croaker (*Micropogonias undulatus*). Chemosphere 200, 143–150. https://doi.org/10.1016/j.chemosphere.2018.02.028

Phelan, M.W., Forman, L.W., Perrine, S.R., Faller, D. V., 1998. Hypoxia increases thrombospondin-1 transcript and protein in cultured endothelial cells. J. Lab. Clin. Med. 132, 519–529. https://doi.org/10.1016/S0022-2143(98)90131-7

Powell, W.H., Morrison, H.G., Weil, E.J., Karchner, S.I., Sogin, M.L., Stegeman, J.J., Hahn, M.E., 2004. Cloning and analysis of the CYP1A promoter from the Atlantic killifish (*Fundulus heteroclitus*). Mar. Environ. Res. 58, 119–124. https://doi.org/10.1016/j.marenvres.2004.03.005

Rabalais, N.N., Turner, R.E., Wiseman, W.J., 2002. Gulf of Mexico hypoxia, A.K.A. "The dead zone." Annu. Rev. Ecol. Syst. 33, 235–263. https://doi.org/10.1146/annurev.ecolsys.33.010802.150513

Randall, D.J., Smith, J.C., 1967. The regulation of cardiac activity in fish in a hypoxic environment. Physiol. Zool. 40, 104–113. https://doi.org/10.1086/physzool.40.2.30152445

Reid, N.M., Proestou, D.A., Clark, B.W., Warren, W.C., Colbourne, J.K., Shaw, J.R., Karchner, S.I., Hahn, M.E., Nacci, D., Oleksiak, M.F., Crawford, D.L., Whitehead, A., 2016. The genomic landscape of rapid repeated evolutionary adaptation to toxic pollution in wild fish. Science. 354, 1305–1308. https://doi.org/10.1126/science.aah4993

Rodgers, M.L., Jones, E.R., Klinkhamer, C., Mahapatra, C.T., Serafin, J., Bosker, T., Perkins, C., Griffitt, R.J., De Guise, S., Sepúlveda, M.S., 2018. Combined effects of Deepwater Horizon crude oil and environmental stressors on *Fundulus grandis* embryos. Environ. Toxicol. Chem. 37, 1916–1925. https://doi.org/10.1002/etc.4153

Rooker, J.R., Kitchens, L.L., Dance, M.A., Wells, R.J.D., Falterman, B., Cornic, M., 2013. Spatial, temporal, and habitat-related variation in abundance of pelagic fishes in the Gulf of Mexico: Potential implications of the Deepwater Horizon oil spill. PLoS One. 8, 1-10. https://doi.org/10.1371/journal.pone.0076080

Sammarco, P.W., Kolian, S.R., Warby, R.A.F., Bouldin, J.L., Subra, W.A., Porter, S.A., 2013. Distribution and concentrations of petroleum hydrocarbons associated with the BP/Deepwater Horizon oil spill, Gulf of Mexico. Mar. Pollut. Bull. 73, 129–143. https://doi.org/10.1016/j.marpolbul.2013.05.029

Schlenk, D., Celander, M., Gallagher, E.P., George, S., James, M., Kullman, S.W., Van Den Hurk, P., Willett, K., 2008. Biotransformation in fishes, in: The toxicology of fishes. CRC Press, pp. 153–234. https://doi.org/10.1201/9780203647295

Schroeder, W.W., Wiseman, W.J., 1986. Low-frequency shelf-estuarine exchange processes in Mobile Bay and other estuarine systems on the Northern Gulf of Mexico, Estuarine Variability. Academic Press, Inc., pp. 355-367. https://doi.org/10.1016/B978-0-12-761890-6.50027-7

Serafin, J., 2017. Combined effects of environmental stressors and crude oil in *Fundulus grandis* development and transcriptome. Purdue University.

Serafin, J., Guffey, S.C., Bosker, T., Griffitt, R.J., De Guise, S., Perkins, C., Szuter, M., Sepúlveda, M.S., 2019. Combined effects of salinity, temperature, hypoxia, and Deepwater Horizon oil on *Fundulus grandis* larvae. Ecotoxicol. Environ. Saf. 181, 106–113. https://doi.org/10.1016/j.ecoenv.2019.05.059

Shimada, T., Fujii-Kuriyama, Y., 2004. Metabolic activation of polycyclic aromatic hydrocarbons to carcinogens by cytochromes P450 1A1 and 1B1. Gann Monogr. Cancer Res. 52, 109–124. https://doi.org/https://doi:10.1111/j.1349-7006.2004.tb03162.x

Simning, D., Sepulveda, M., De Guise, S., Bosker, T., Griffitt, R.J., 2019. The combined effects of salinity, hypoxia, and oil exposure on survival and gene expression in developing sheepshead minnows, *Cyprinodon variegatus*. Aquat. Toxicol. 214, 1-19. https://doi.org/10.1016/j.aquatox.2019.105234

Untergasser, A., Nijveen, H., Rao, X., Bisseling, T., Geurts, R., Leunissen, J.A.M., 2007. Primer3Plus, an enhanced web interface to Primer3. Nucleic Acids Res. 35, W71–W74. https://doi.org/10.1093/nar/gkm306

Vandesompele, J., De Preter, K., Pattyn, F., Poppe, B., Van Roy, N., De Paepe, A., Speleman, F., Åman, P., Semb, H., Powers, D., Aurias, A., Thomas, G., 2002. The multifunctional FUS, EWS and TAF15 proto-oncoproteins show cell type-specific expression patterns and involvement in cell spreading and stress response. Genome Biol. 3, 1-12. https://doi.org/10.1186/gb-2002-3-7-research0034

Whitehead, A., Roach, J.L., Zhang, S., Galvez, F., 2011. Genomic mechanisms of evolved physiological plasticity in killifish distributed along an environmental salinity gradient. Proc. Natl. Acad. Sci. U. S. A. 108, 6193–6198. https://doi.org/10.1073/pnas.1017542108

Xu, E.G., Khursigara, A.J., Magnuson, J., Hazard, E.S., Hardiman, G., Esbaugh, A.J., Roberts, A.P., Schlenk, D., 2017a. Larval red drum (*Sciaenops ocellatus*) sublethal exposure to weathered Deepwater Horizon crude oil: Developmental and transcriptomic consequences. Environ. Sci. Technol. 51, 10162–10172. https://doi.org/10.1021/acs.est.7b02037

Xu, E.G., Mager, E.M., Grosell, M., Hazard, E.S., Hardiman, G., Schlenk, D., 2017b. Novel transcriptome assembly and comparative toxicity pathway analysis in mahi-mahi (*Coryphaena hippurus*) embryos and larvae exposed to Deepwater Horizon oil. Sci. Rep. 7, 1–13. https://doi.org/10.1038/srep44546

Xu, E.G., Mager, E.M., Grosell, M., Pasparakis, C., Schlenker, L.S., Stieglitz, J.D., Benetti, D., Hazard, E.S., Courtney, S.M., Diamante, G., Freitas, J., Hardiman, G., Schlenk, D., 2016. Time- and oil-dependent transcriptomic and physiological responses to Deepwater Horizon oil in mahi-mahi (*Coryphaena hippurus*) embryos and larvae. Environ. Sci. Technol. 50, 7842–7851. https://doi.org/10.1021/acs.est.6b02205

Zhu, C.D., Wang, Z.H., Yan, B., 2013. Strategies for hypoxia adaptation in fish species: A review. J. Comp. Physiol. B Biochem. Syst. Environ. Physiol. 183, 1005–1013. https://doi.org/10.1007/s00360-013-0762-3

Zinkle, A., Mohammadi, M., 2019. Structural biology of the FGF7 subfamily. Front. Genet. 10, 1–8. https://doi.org/10.3389/fgene.2019.00102

Table 3.1. Primer sequences and NCBI accession numbers for all genes analyzed using qPCR. All sequences are listed 5' to 3'. Reverse primers (R) are reverse complements of the genetic sequence.

Gene name		Sequence (5'-3')	Efficiency	NCBI accession #	Product Length
β-actin	*F*	GCT CTG TGC AGA ACA ACC ACA CAT	90%	XM_012850364	136 bp
	R	TAA CGC CTC CTT CAT CGT TCC AGT			
ahrr	*F*	AGC TAT GCA GTC AAC AAC GG	98.8%	NM_001309962.1	385 bp
	R	CTC TCT CTC ATT GCA TGT AAA CG			
ugt1a1	*F*	AGG ATG GCA TGT CTT ACA AGG	102%	XM_012854427.1	321 bp
	R	GCA CAT CTT TGG GTA AAT CGC			
cyp1a	*F*	TGT TGC CAA TGT GAT CTG TG	93%	NM_001310009	258 bp
	R	CGG ATG TTG TCC TTG TCA AA			
fbxo32	*F*	AAA ACA ACA ACG TCT CTG TGG	99.7%	XM_012864657.1	178 bp
	R	TGA ACG TAA ATC CAC TTC TCC			
fgf7	*F*	GTC ACT CAG AAC ACA TTG ACG	97.6%	XM_012877162.1	604 bp
	R	AGT CAT CAA TCG TGA GGA ACC			
mb	*F*	ATG ATA TGG TTC TCA AGC ACT GG	104%	XM_012850507.1	111 bp
	R	GGA ACA GCT TTT GGG TAT CTG G			

Table 3.2. **(A)** Nominal treatment exposure conditions (Oil concentrations, DO, salinity, and temperature). Conditions that deviate from control are bold. **(B)** Initial (0 h) and Final (48 h) water quality values for each test condition. Values represented as mean ± S.D.

A

Treatment	Oil (ppb ∑PAH)	DO (ppm)	Salinity (ppt)	Temperature (°C)
Control	0	6	3	20
Oil	**15**	6	3	20
Hypoxia	0	**≤ 2**	3	20
Oil & Hypoxia	**15**	**≤ 2**	3	20
Salinity	0	6	**30**	20
Oil & Salinity	**15**	6	**30**	20
Temperature	0	6	3	**30**
Oil & Temperature	**15**	6	3	**30**

B

Condition	Nominal Value	Initial Value (0 h)	Final Value (48 h)
Oil	0 ppb ∑PAH	0 ppb ∑PAH	0 ppb ∑PAH
	15 ppb ∑PAH	15.3 ± 1.15 ppb ∑PAH	1 ± 2.9 ppb ∑PAH
DO	6 ppm	6 ppm	2.2 ± 0.6 ppm
	≤ 2 ppm	2 ppm	1 ± 0.8 ppm
Salinity	3 ppt	3 ± 0.5 ppt	3 ± 0.5 ppt
	30 ppt	30 ± 0.5 ppt	30 ± 0.5 ppt
Temperature	20 °C	20 ± 1 °C	20 ± 1 °C
	30 °C	30 ± 1 °C	30 ± 1 °C

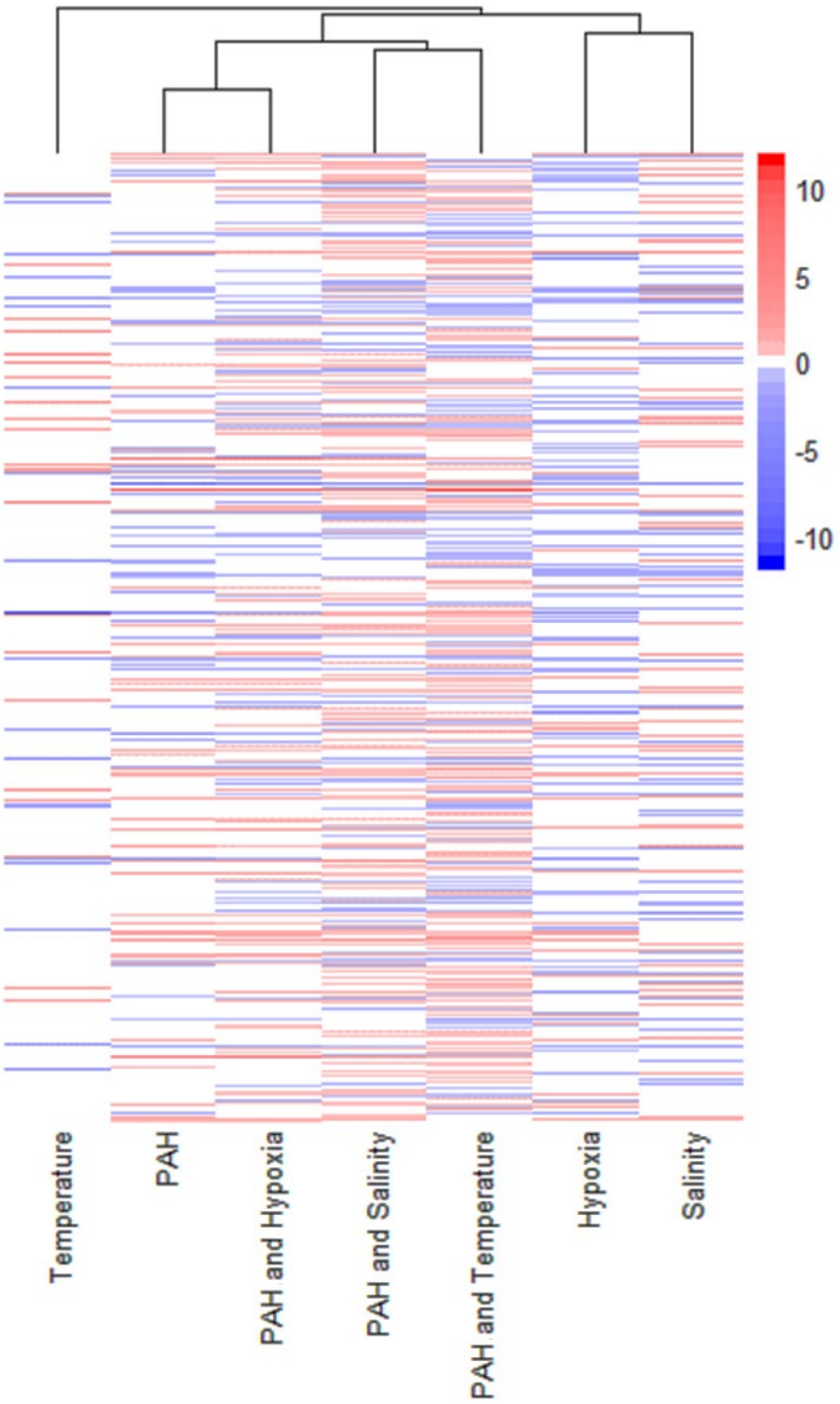

Figure 3.1. Heatmap with hierarchical clustering of cardiac related differentially expressed genes across all treatments relative to control (0 ppb tPAH, 6 ppm DO, 3 ppt, 30° C). Warm shades (reds) indicate increased expression, cool shades (blues) indicate reduced expression.

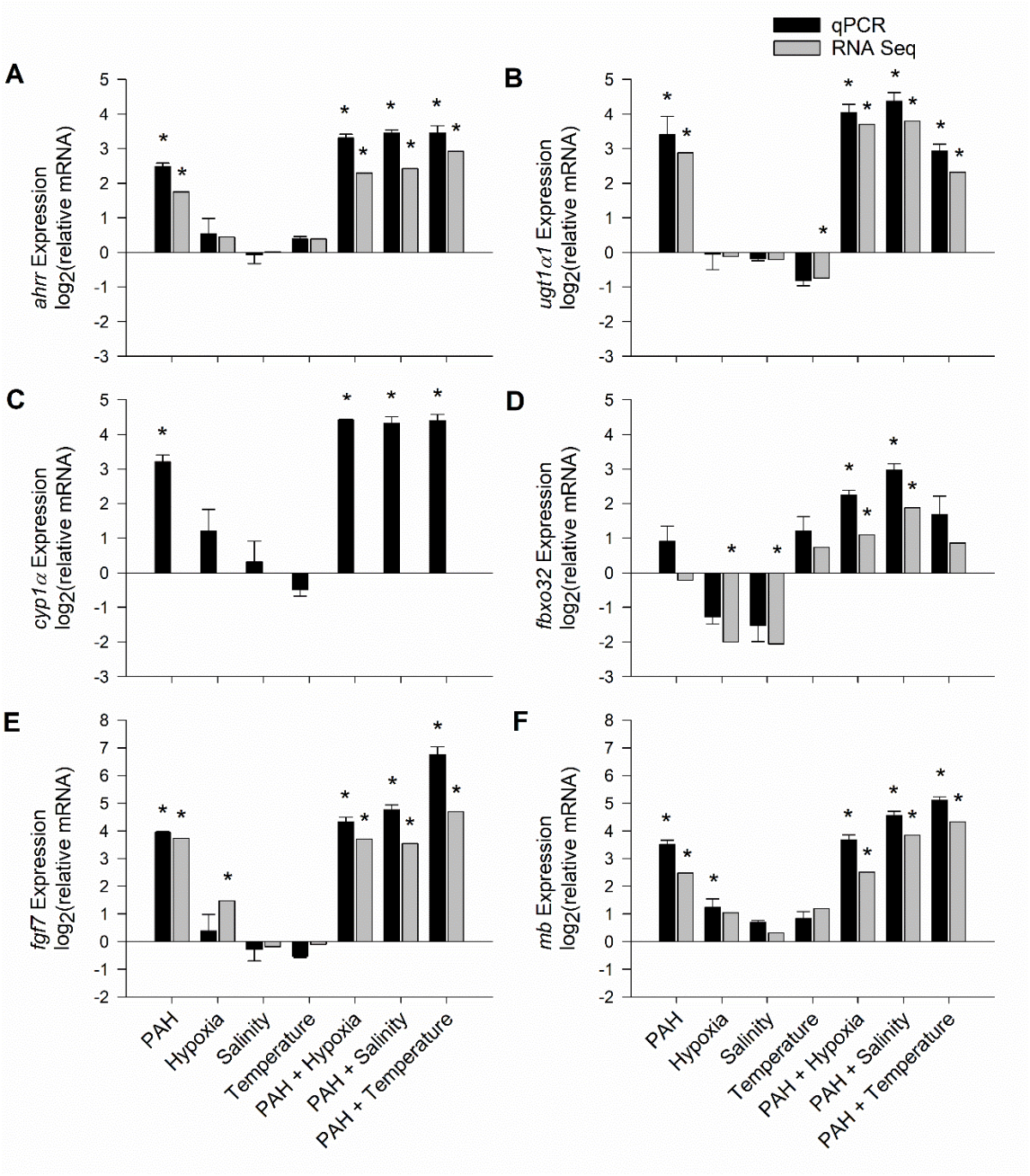

Figure 3.2. qPCR (black bars) and RNA Seq (grey bars) expression values for genes involved in xenobiotic metabolism [ahrr **(A)**, ugt1a1 **(B)**, cyp1α **(C)**] and cardiac development/ function [fbxo32 **(D)**, fgf7 **(E)**, mb **(F)**]. All expression values shown as mean ±SEM log2(relative mRNA) set relative to expression under control conditions (0 ppb tPAH, 6 ppm DO, 3 ppt, 20 °C). Values that are significantly different than control ($p \leq 0.05$) are designated with an asterisk (*).

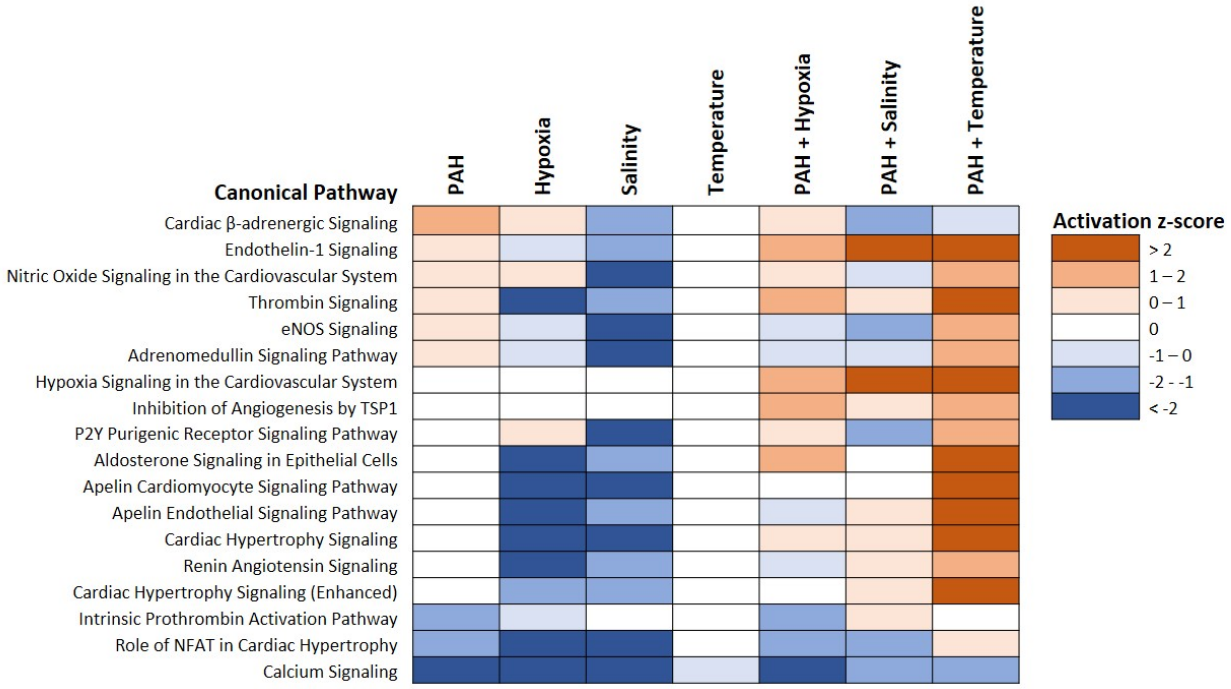

Figure 3.3. IPA analysis of cardiac canonical pathways across all treatment groups that were both significantly impacted ($p \leq 0.05$) and showed directionality (activation z-score $\neq 0$). Warm shades indicate pathway activation, cool shades indicate pathway inhibition.

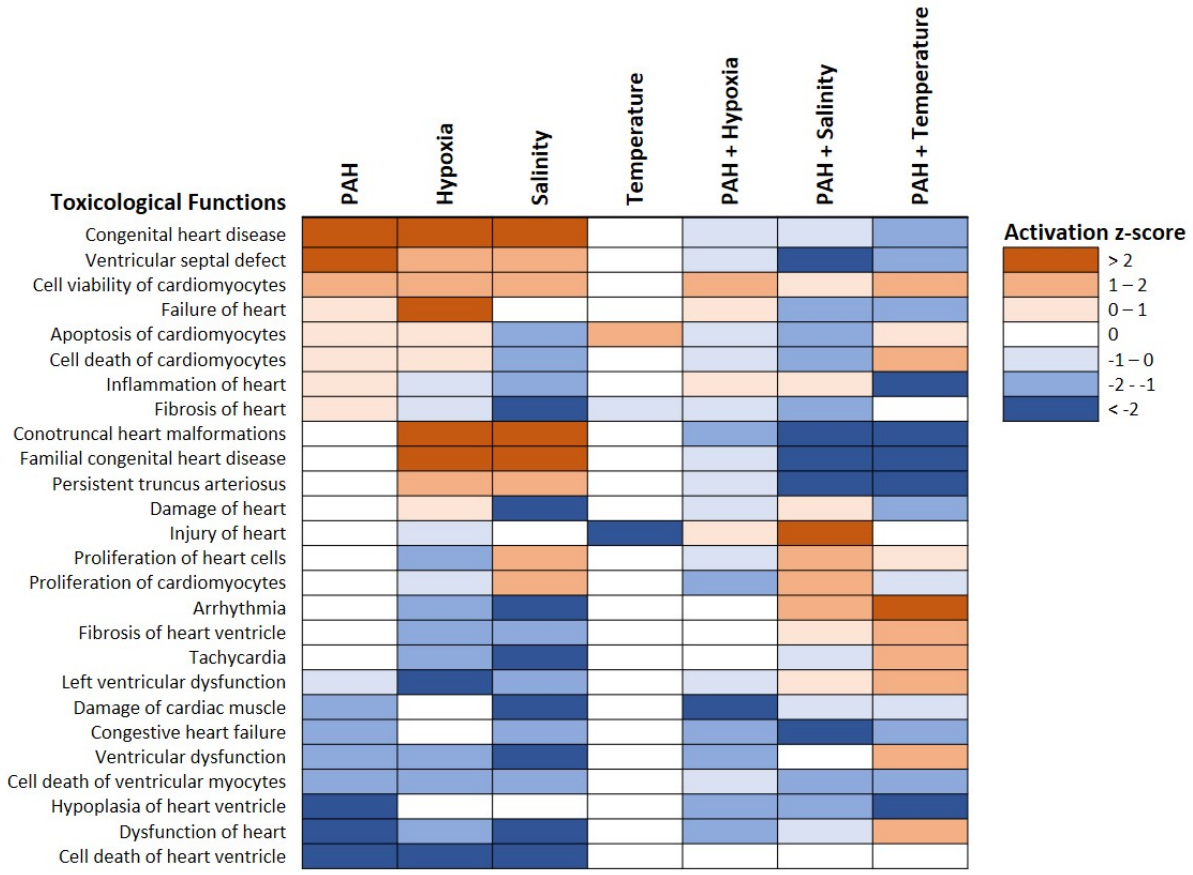

Figure 3.4. IPA analysis of cardiac toxicological functions across all treatment groups that were both significantly impacted ($p \leq 0.05$) and showed directionality (activation z-score $\neq 0$). Warm shades indicate function activation, cool shades indicate function inhibition.

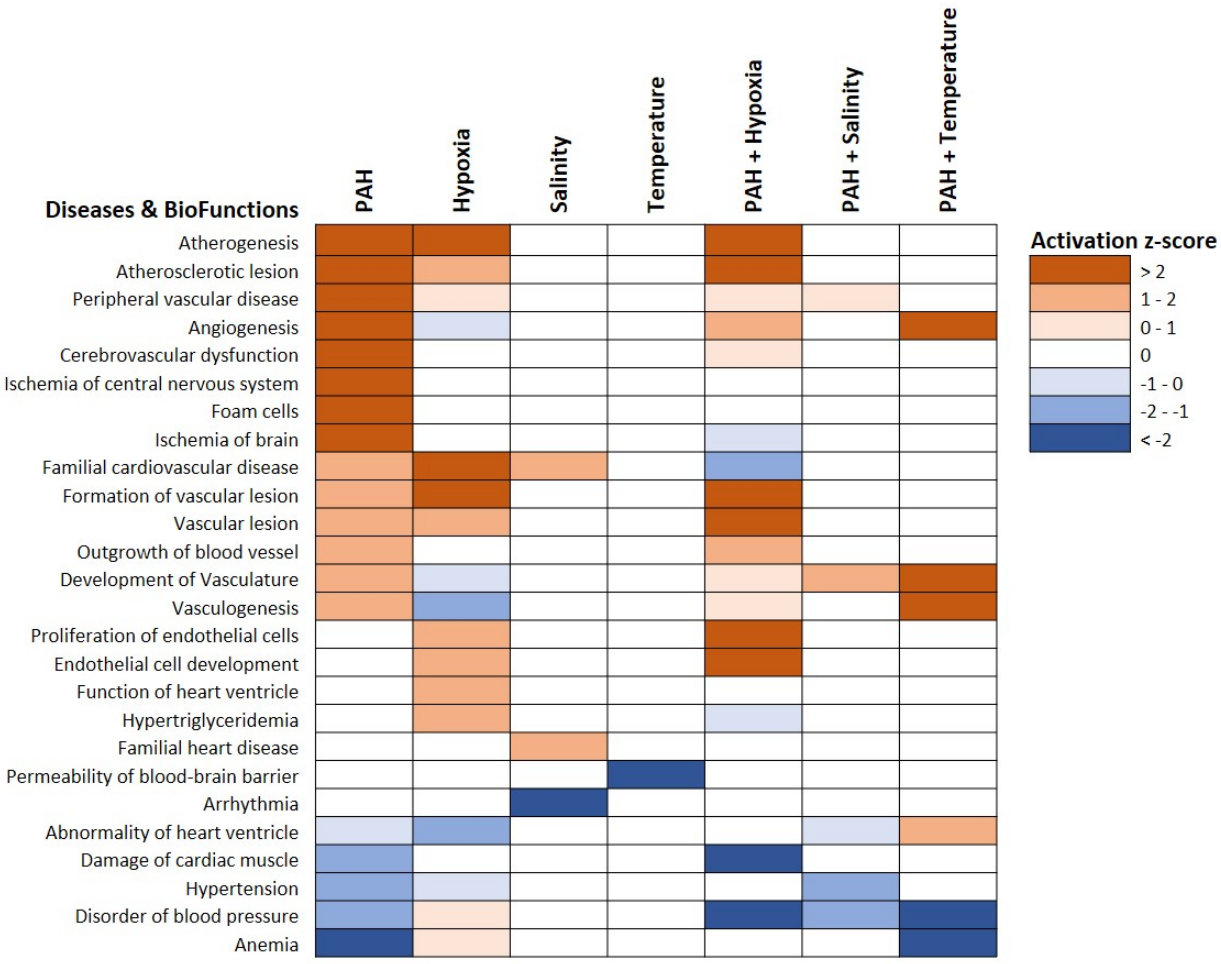

Figure 3.5. IPA analysis of predicted cardiac diseases and impacted bio functions across all treatment groups that were both significantly impacted ($p \leq 0.05$) and showed directionality (activation z-score $\neq 0$). Warm shades indicate disease/ bio function activation, cool shades indicate disease/ bio function inhibition.

CHAPTER 4. OIL INDUCED CARDIAC EFFECTS IN EMBRYONIC SHEEPSHEAD MINNOWS, *CYPRINODON VARIEGATUS*

A version of this chapter has been submitted for publication; reproduced from:
Allmon, E., Walker, G., Griffitt, R., Sepúlveda, M.S. (2021) *Oil induced cardiac effects in embryonic sheepshead minnows, Cyprinodon variegatus*. Manuscript submitted for publication.

4.1 Abstract

Following the Deepwater Horizon oil spill in April 2010, much research has been conducted on the cardiotoxic effects of oil on fish. Sensitive life history stages, such as the embryonic period, have been targeted to elucidate the effects of polycyclic aromatic hydrocarbons (PAHs) on the developing cardiovascular systems of fish. However, much of this research has focused on rapidly developing pelagic species, with little emphasis on estuarine species with longer embryological periods. Moreover, previous studies have used heart rate as the primary endpoint to measure cardiac performance in embryos and larvae; an endpoint that on its own may overlook impairment in cardiac performance. This study aims to fill these knowledge gaps and provide a more holistic approach for assessing the effects of PAHs on cardiac function by exposing sheepshead minnow (*Cyprinodon variegatus*) embryos to two oil doses (150 and 300 µg/L tPAH nominally) throughout embryonic development and measuring cardiac responses through the identification of cardiotoxic phenotypes (pericardial edema) as well as calculation of cardiac output at 4 days post fertilization. Results of this study show significant increases in pericardial edema at both oil doses relative to controls as well as significantly reduced cardiac output – driven by reductions in ventricular stroke volume. This study is one of the first to assess cardiac output in embryonic fish exposed to oil and methods described here allow for more physiologically relevant measures of cardiac performance in early life stages through established and non-invasive measures.

4.2 Introduction

The Gulf of Mexico has been the site of two of the largest marine oil spills in history. The Ixtoc 1 well blowout in the Bay of Campeche, Mexico in June 1979 released 3.4 million barrels of crude oil over the course of 290 days (Soto et al., 2014). As a result, an estimated 33 metric tons of oil were removed from Mexican and Texas shorelines – including environmentally important areas such as coastal lagoons & marshes, mangrove forests, river mouths, and sandy beaches (Jernelöv and Lindén, 1981). In April 2010 off the coast of Louisiana, an explosion on the offshore drilling rig, the Deepwater Horizon, marked the beginning of the largest marine oil spill in United States history (Short, 2017). Over the course of 87 days, an estimated 4.9 million barrels of crude oil was released into the Gulf of Mexico (Camilli et al., 2012; Crone and Tolstoy, 2010) ultimately resulting in over 2100 km of impacted coastal habitat and oiled shorelines in the Northern Gulf of Mexico from Texas to Florida (Nixon et al., 2016). Both disasters resulted in crude oil forming surface slicks that underwent physical, chemical, and biological weathering processes, ultimately resulting in weathered oil being transported to and impacting coastal environments.

The impacts of oil on marine ecosystems are still being investigated, but there is much data available on the toxicity of oil on the fish species inhabiting both pelagic and nearshore environments. Importantly, weathering processes, such as evaporation, photooxidation, dissolution, and biodegradation often change the concentrations of polycyclic aromatic hydrocarbons (PAHs) present within the oil, leading to differing toxicities between crude and weathered oils from the same source (Aeppli et al., 2012; Liu et al., 2012; Neff et al., 2000). Studies on the toxicity of weathered oil from the Deepwater Horizon have shown that weathering processes increase toxicity by concentrating the highly cardiotoxic 3-ring PAHs (Esbaugh et al., 2016; Incardona et al., 2014, 2009, 2004; Mager et al., 2014). Additionally, the Deepwater

Horizon spill occurred coincidentally with the spawning seasons of many commercially important fish species (Block et al., 2005; Rooker et al., 2013, 2012). As such, many studies have been conducted on large pelagic marine species such as bluefin tuna (*Thunnus thynnus*), yellowfin tuna (*Thunnus albacares*), amberjack (*Seriola dumerili*), and mahi-mahi (*Coryphaena hippurus*) to determine the effect on cardiotoxic endpoints following oil exposure during early life stages (Esbaugh et al., 2016; Incardona et al., 2014; Mager et al., 2014; Pasparakis et al., 2019). Similarly, several coastal species – Gulf killifish (*Fundulus grandis*), sheepshead minnow (*Cyprinodon variegatus*), red drum (*Sciaenops ocellatus*), and inland silverside (*Menidia beryllina*) – have shown evidence of cardiotoxicity resulting from oil exposure during embryonic and larval stages (Adeyemo et al., 2015; Allmon et al., 2021; Bosker et al., 2017; Dubansky et al., 2013; Khursigara et al., 2017).

When compared to many pelagic species, the embryonic stage of many coastal and estuarine species is relatively prolonged. Pelagic teleosts are often rapidly developing – for example bluefin tuna and mahi-mahi hatch within 36 hours post-fertilization (hpf) (Mager et al., 2017; Miyashita et al., 2000) - while many estuarine species undergo extended embryonic periods ranging from approximately 6 days post fertilization (dpf) in the sheepshead minnow to up to 30 dpf in the inland silverside (Bosker et al., 2017; Kuntz, 1916; Middaugh and Hemmer, 1992). Early life stage fish have been shown to be particularly susceptible to contaminants and adverse effects during development have been shown to carry over into long-term toxicity (Hutchinson et al., 1998; McKim, 1977). Prolonged development in the embryonic stage may leave estuarine species vulnerable to cardiotoxicity induced by exposure to oil. Conversely, the dynamic biogeochemical processes that regularly occur within estuaries may impart a level of resiliency to the species that reside there. Northern Gulf of Mexico estuaries regularly undergo

fluctuations in dissolved oxygen, salinity, and temperatures (Bianchi et al., 1999; NOAA, 2021) requiring fish species and their developing embryos to be capable of maintaining homeostasis under a wide range of environmental conditions.

The sheepshead minnow is an estuarine fish found along the Atlantic coast of the United States from the Chesapeake Bay to south Florida as well as throughout the Gulf of Mexico (USEPA, 2009). It is an established toxicity model (USEPA, 2009) and it's spawning season, February through October (Kuntz, 1916), directly coincided with the timing of the Deepwater Horizon oil spill, making it an ideal candidate on which to test the effects of oil on the developing cardiac system. While there is much data relating oil exposure to cardiotoxic phenotypes (pericardial edema) (Beyer et al., 2016; Carls et al., 2008) and generalized fish cardiac performance (arrhythmias, changes in heart rate, and contractility) (Edmunds et al., 2015; Incardona et al., 2011, 2009; Mager et al., 2014), literature surrounding the effects of oil on the development of the cardiac system in estuarine species is sparse with heart rate being the most commonly measured cardiotoxic endpoint (Adeyemo et al., 2015; Bosker et al., 2017; Dubansky et al., 2013; Khursigara et al., 2017). Only one study expanded their assessment of cardiac performance to include cardiac output as a function of stroke volume (Khursigara et al., 2017). Many fish have been shown to manipulate stroke volume to control cardiac output (Anttila et al., 2013; Farrell, 1991; Webber et al., 1998), therefore, assessment of heart rate without accounting for changes in cardiac output may be overlooking a significant marker of cardiovascular function. To our knowledge, holistic cardiac performance in response to oil exposure has not been directly measured in estuarine teleosts with prolonged embryonic periods. This study aims to assess cardiac development and function in response to oil exposure by characterizing cardiotoxic phenotypes and measuring cardiac output in sheepshead minnow embryos. We

hypothesize that embryos exposed to oil will exhibit cardiotoxic phenotypes and have a reduced cardiac output resulting from altered heart rates and stroke volumes.

4.3 Materials and Methods

All methods involving animal use were conducted in accordance with relevant guidelines and regulations; methodological protocols have been approved by the Purdue Institutional Animal Care and Use Committee.

4.3.1 Sheepshead minnow husbandry and embryo collection

Wild caught sheepshead minnows (5 females, 3 males) were collected from northern Florida estuaries by the Gulf Specimen Marine Lab (Panacea, FL, USA) in September 2020 and shipped overnight to Purdue University. Adults were housed in sex specific 75 L aquaria as part of a recirculation aquaculture system supplied with constant aeration and maintained at optimal spawning conditions – 25 ppt artificial seawater (prepared with reverse osmosis water and Instant Ocean Sea Salt (Spectrum Brands, Blacksburg, VA, USA) at 25°C on a 16L:8D photoperiod. Fish were fed commercially available brine shrimp flakes twice daily to satiation. Breeding was initiated in the evenings by placing benthic breeding boxes into the female sheepshead minnow tank and the introduction of a single male sheepshead minnow (5 female: 1 male). Spawning occurred overnight (10 h) before the male sheepshead minnow was moved back to the male tank and breeding boxes containing embryos were removed. Embryos were then washed in clean seawater to remove pathogens and/ or parasites, gently rolled on fine mesh to remove embryonic microvilli (USEPA, 2009), and visually assessed for fertilization under a Nikon SMZ1500 stereomicroscope (Nikon Instruments Inc., Melville, NY, USA). Only spawns

with >80% fertilization rates were used in this study. Fertilized embryos were then pooled and immediately moved into exposure chambers.

4.3.2 Exposure design

Sheepshead minnow embryos (<12 hpf, corresponding to the formation of the blastoderm and differentiation of the embryonic shield; Kuntz, 1916) were randomly selected and placed in 1 L borosilicate glass beakers (n = 20/beaker) supplied with 300 mL exposure solutions (0 µg/L tPAH, 150 µg/L tPAH, and 300 µg/L tPAH) which were covered to prevent evaporation and maintained within a temperature controlled environmental chamber at optimal rearing conditions – 25 ppt artificial seawater (prepared as described above), 30°C, and 16L: 8D photoperiod (USEPA, 2009). Exposures were replicated 4 times resulting in n = 80 embryos/exposure condition. Controls (0 µg/L tPAH) consisted only of 300 mL artificial seawater while low oil conditions (nominal 150 µg/L tPAH) and high oil conditions (nominal 300 µg/L tPAH) were achieved by manipulating volumes of artificial seawater and 100% HEWAF to achieve desired PAH concentrations. Mortality and embryo viability were assessed daily. Exposure solutions were refreshed every 24 h to maintain static exposure to nominal PAH concentrations throughout exposures. Embryos were transferred to fresh exposure solutions daily by pipetting. Exposures continued until embryos were sampled for cardiac imaging at 4 dpf. Following imaging, 4 dpf embryos were flash-frozen, and stored at -80°C until processed for RNA extraction and subsequent qPCR analysis to verify exposure to PAHs.

4.3.3 HEWAF preparation & PAH quatification

Naturally weathered oil from the surface slick (referred to as OFS) of the Deepwater Horizon oil spill was collected on August 15, 2011 and was subsequently stored at 4°C until initiation of

exposures. Oil exposure solutions were prepared using standard protocols for the generation of high energy water accommodated fractions (HEWAF) (Esbaugh et al., 2016; Incardona et al., 2013) at a loading rate of 1 g OFS per 1 L 25 ppt seawater. Prior to initiation of sheepshead minnow exposures, four representative replicates of 100% HEWAF were sampled for immediate in-house fluorescence analysis (using standard techniques described by Greer et al. (2012) and Serafin et al. (2019) then shipped at 4°C to the commercial analytical lab ALS Environmental for total PAH analysis. The combination of both techniques allowed for full quantification of the total PAHs (tPAH) within the HEWAF as well as immediate measurement of tPAH concentration within each HEWAF. This allowed for the adjustment in volume of 100% HEWAF needed to create each exposure solution to maintain consistent tPAH dosing throughout the exposure period. In-house fluorescence analysis was conducted on a Turner Designs AU-10 Fluorometer (Turner Designs, San Jose, CA, USA). Immediately following preparation, fluorescence of 100% HEWAF was measured to determine volume needed to create exposure solutions (150 µg/L tPAH and 300 µg/L tPAH respectively). Volumes of 100% HEWAF needed to achieve each concentration varied with each HEWAF due to differences in the efficiency of the HEWAF preparation. Initial (0 h) and final (24 h) fluorescence of exposure solutions were measured from each treatment throughout exposure period.

4.3.4 Water quality

Initial (0 h) and final (24 h) values were recorded for all water quality parameters during exposure solution renewals throughout the course of the exposure period. Parameters were only measured from control solutions (0 µg/L tPAH) to avoid PAH contamination of probes/equipment. Water temperature and dissolved oxygen were measured with a YSI PRO1020 multi-parameter meter (YSI Incorporated, Yellow Springs, OH, USA), salinity was

measured with a Pentair Vital Sine SR6 handheld refractometer (Pentair Aquatic Eco-Systems, Inc., Cary, NC, USA), and pH and ammonia were measured using an API colorimetric test kit (API Fishcare, Chalfont, PA, USA).

4.3.5 Image & video collection

At 4 dpf, 10 embryos were randomly selected from each beaker for cardiac imaging (total n = 40/treatment). Imaging was conducted on a Nikon SMZ1500 stereomicroscope affixed with a Nikon Ds-Ri2 camera and Nikon NIS-Elements D software (Nikon Instruments Inc., Melville, NY, USA). Embryos were mounted in a 3% methylcellulose solution and still frame images and videos were captured for each individual. Images were captured at 8x magnification in the left lateral view. Videos (30 s) were captured at 8x magnification at 10.9 frames per second (fps) in the frontal view.

4.3.6 Cardiac morphology & function analysis

Cardiotoxic phenotypes were determined from still images in the left lateral view imported into ImageJ (Schneider et al., 2012). The freehand tool was used to outline and define the area of the pericardial cavity for each individual. Individuals were determined to exhibit either a cardiotoxic or control phenotype with the cardiotoxic phenotype defined as a pericardial area greater than 3 standard deviations from the mean pericardial area of the control (0 μg/L tPAH) (Figure 4.1). Video sequences were used to determine heart rate (HR), stroke volume (SV), and calculate cardiac output (CO) for each individual. HR was visually determined from the video sequences for each individual. Video sequences were loaded into ImageJ and the ventricle was measured at peak systole and diastole from the same heartbeat for a total of 3 heartbeats per individual. The ventricle was traced using the freehand tool to define the ventricular area and the length of the

longitudinal and width axes of the ventricle were measured using the straight-line measurement tool (Figure 4.2). These measurements were used to calculate the volume of the ventricle at peak systole and peak diastole following techniques described in Khursigara et al., 2017 using the following formula (Bagatto and Burggren, 2006)

$$V = \frac{4}{3}\pi ab^2$$

where *a* is the longitudinal axis and *b* is the width axis. SV was defined as the difference in volume between peak systole and peak diastole for each heartbeat. CO was calculated by multiplying the HR and SV for each individual. Pericardial area, HR, SV, and CO were compared using one-way ANOVAs with Holm-Sidak multiple comparison versus control group post-hoc tests and a fiducial level of significance of $p \leq 0.05$.

4.3.7 qPCR analysis

Following imaging, 4 dpf embryos were washed in clean seawater to remove residual methylcellulose, flash-frozen, and stored at -80°C until processed for RNA extraction. Whole embryos were used for RNA extraction and due to low RNA yields from a single embryo, 4 embryos were pooled to constitute a single biological replicate resulting in n = 10 biological replicates per tPAH concentration. RNA extractions were performed using a Qiagen RNeasy mini kit according to manufacturer protocols. Quantification and quality of extracted RNA were measured using a NanoDrop 2000C spectrophotometer (Thermo Scientific, Waltham, MA, USA). Total RNA was treated for potential DNA contamination through incubation with DNase 1 (Thermo Scientific, Waltham, MA, USA) and subsequent cDNA synthesis was performed with 100 ng total RNA starting material and SuperScript III reverse transcriptase (Invitrogen,

Carlsbad, CA, USA) according to manufacturer protocols. Resulting cDNA was stored at -20°C until qPCR analysis.

Real time PCR primers were developed for sheepshead minnow genes *β-actin* and *cyp1α* and were supplied by Integrated DNA Technologies (IDT, Coralville, IA, USA). Primer sequences were derived from published NCBI nucleotide data for each gene and designed through Primer3Plus software (Untergasser et al., 2007). RT qPCR was performed on a Bio-Rad CFX Connect Real-Time PCR System with iQ SYBR Green Supermix (Bio-Rad, Hercules, CA, USA) following thermal cycling protocols provided by the manufacturer. Reaction efficiencies for each primer pair were determined through serially diluted standard curves. For full primer sequences, NCBI accession numbers, and reaction efficiencies see Table 4.1. Expression of *cyp1α* relative to the housekeeping gene *β-actin* was analyzed using the delta delta CT method (Pfaffl, 2004). Statistical analysis of *cyp1α* expression across treatments was done using a one-way ANOVA and Holm-Sidak multiple comparison versus control group post-hoc test at a fiducial level of significance of $p \leq 0.05$.

4.4 Results

4.4.1 HEWAF analysis

The measured concentrations of all constituent PAHs measured in each individual 100% HEWAF sent to ALS Environmental for analysis are presented in Supplemental Table 4.1 and can be accessed through the Purdue University Research Repository, doi: 10.4231/SN4J-5570. The average relative PAH composition of these samples can be seen in Figure 4.3. Overwhelmingly, HEWAFs used in this study were comprised of 3 and 4 ring PAHs

(constituting 68% and 25% of the total PAHs, respectively) with 2 ring PAH comprising 4% and 5 ring or larger PAHs accounting for 3% of the total PAHs present.

4.4.2 Water quality

Nominal oil concentrations (150 µg/L and 300 µg/L) used in this study are consistent with previous studies involving sheepshead minnows (Bosker et al., 2017; Jones et al., 2020; Magnuson et al., 2018; Simning et al., 2019). tPAH exposure conditions as well as all measured water quality parameters can be found in Table 4.2. Low oil exposures (150 µg/L nominally) had initial tPAH values of 164.40 ± 13.63 µg/L which decreased to 117.68 ± 18.39 µg/L over the 24 h exposure period between solution renewal. High oil exposures (300 µg/L nominally) had initial tPAH values of 327.75 ± 10.51 µg/L which decreased to 190.56 ± 20.55 µg/L over the 24 h exposure period before solutions were renewed. Seawater controls had no measurable tPAH concentrations at any point during the experiment. For all PAH conditions, water temperatures and salinities were maintained at 30 ± 0.3°C and 25 ppt, respectively. Dissolved oxygen levels remained at 8.10 ± 0.02 mg/L throughout the experiment. pH remained stable at 8.0 and ammonia remained below detectable limits throughout the course of the experiment.

4.4.3 *cyp1α* expression

Expression of *cyp1α* significantly increased relative to controls in both the low and high oil doses (Figure 4.4). While there appeared to be a trend toward a dose dependent increase in expression of *cyp1α* with tPAH concentration, the differences in relative expression were not significant between the two oil doses.

4.4.4 Cardiac morphology & function

Cardiotoxic phenotypes, manifested as pericardial edema, were present at both low and high oil exposures. The mean pericardial area increased significantly from 42.6 $mm^2 10^{-3}$ under control conditions to 57.5 $mm^2 10^{-3}$ when exposed to low oil conditions and to 60.2 $mm^2 10^{-3}$ when exposed to high oil conditions (Figure 4.5). HR was not significantly altered by oil exposure (Figure 4.6A), however SV significantly decreased from 0.070 nL under control conditions to 0.041 nL when exposed to low oil and to 0.046 nL when exposed to high oil (Figure 4.6B). This decrease in SV led to a significant decrease in CO under both oil exposures – decreasing from 9.624 nL/min under control conditions to 5.298 nL/min under low oil conditions and to 6.425 nL/min under high oil conditions (Figure 4.6C). There was no significant difference observed in any cardiotoxic endpoints between the two oil doses.

4.5 Discussion

Studies on the effects of oil on embryonic and larval fish have been extensive following the Deepwater Horizon oil spill (see Pasparakis et al., 2019 for full review). While many of these studies have focused on cardiac endpoints, a disproportionate number have focused on fast developing pelagic species (Brette et al., 2014; Edmunds et al., 2015; Incardona et al., 2014; Mager et al., 2014; Pasparakis et al., 2016) leaving the cardiotoxic effects of oil on longer developing coastal and estuarine species under-represented in the current literature. Of the few studies that do address oil cardiotoxicity in estuarine species, the primary cardiotoxic endpoint measured is heart rate (Adeyemo et al., 2015; Bosker et al., 2017; Dubansky et al., 2013; Khursigara et al., 2017) which may not fully capture changes in cardiac function induced by oil exposure. This study expands on the current literature and provides a more comprehensive assessment of embryologic cardiac function in an estuarine teleost.

Previous studies have shown that weathering processes tend to concentrate 3 and 4 ring PAHs in oil, making them more cardiotoxic relative to their crude oil progenitors (Esbaugh et al., 2016; Incardona et al., 2004). As expected, tPAH analysis of OFS HEWAF used in this study revealed high concentrations of 3 and 4 ring PAHs with phenanthrene analogues being the most prevalent. This general oil composition is consistent with previous work using OFS from the Deepwater Horizon (Johansen and Esbaugh, 2019; Khursigara et al., 2017; Magnuson et al., 2018; Pasparakis et al., 2016) and tPAH concentrations used in this study are consistent with those used in previous work assessing sheepshead minnow's response to oil exposure across multiple life history stages (Bosker et al., 2017; Jones et al., 2020; Magnuson et al., 2018; Simning et al., 2019) as well as previous work assessing embryonic and larval endpoints in estuarine species (Adeyemo et al., 2015; Allmon et al., 2021; Serafin et al., 2019; Simning et al., 2019). Phenanthrene and it's analogs comprised a total of 37% of the HEWAF tPAH; phenanthrene exposure has been shown to induce pericardial edema, bradycardia, arrythmias, and reduce circulatory capacity in early life history fish (Incardona et al., 2004). It is therefore unsurprising that cardiotoxic endpoints such as pericardial edema and reduced cardiac performance were observed in this study.

The chorion of fish embryos provides a degree of protection from external environmental conditions as the embryo develops (Cotelli et al., 1988). However, chorions of aquatic species must also be permeable enough to facilitate respiratory gas exchange, the removal of metabolic wastes, and maintain ionic and osmotic balance within the embryo (Groot and Alderdice, 1985). This is especially true of estuarine species who regularly encounter variability in salinity in their environment. Work conducted by Carls et al. (2008) in zebrafish showed that oil toxicity in embryos is due to dissolved PAHs in the water and not direct contact with suspended oil micro-

droplets within the water column. However, work done by Khursigara et al. (2017) on the estuarine species red drum, showed a significant decrease in embryonic survival in embryos exposed to unfiltered versus filtered HEWAF solutions – suggesting that the presence of oil micro-droplets play an important role in toxicity. This dichotomy in responses may be due to differences in characteristics of the chorions in freshwater and estuarine species (Philibert et al., 2019). To verify trans-chorionic exposure to PAHs, expression of *cyp1α* was measured in 4 dpf embryos. *cyp1α* is used as a biomarker of PAH exposure and is a first line detoxification mechanism involved in the metabolism of PAHs (Goksøyr, 1995; Kim et al., 2013; Nilson et al., 1998; Sarasquete and Segner, 2000). Expression of *cyp1α* was highly upregulated in both low oil and high oil exposures relative to control embryos, confirming that individuals in both oil doses were exposed to PAHs. However, our experimental design cannot determine if the exposure is solely due to dissolved PAHs in the water or through direct contact between embryos and oil micro-droplets. While not statistically significant, there appears to be a dose dependent trend in *cyp1α* upregulation with oil exposure.

As expected, and consistent with findings of previous studies (Incardona et al., 2014, 2011, 2004; Khursigara et al., 2017; Mager et al., 2014) exposure to oil increased the incidence of embryos expressing a cardiotoxic phenotype. Pericardial edema, the collection of fluid within the pericardial space, can have damaging effects on the developing cardiac system and is often regarded as an early sign of cardiac failure (Carls et al., 2008; Dong et al., 2010; Incardona et al., 2014; Incardona and Scholz, 2016). The buildup of fluid increases pressure on the developing heart and impacts its function by reducing blood flow through decreased contractility (Incardona et al., 2005). Additionally, pericardial edema has been linked to delays in or failure to complete looping of the tubular heart (Carls et al., 2008; Hicken et al., 2011; Incardona et al., 2005).

These interruptions in cardiac function and morphological development often lead to cardiac failure and death of the individual. While no direct mortality stemming from cardiac failure was observed during the embryonic exposures in this study, additional work should be done to trace the lethal and sublethal effects of the observed pericardial edema on post-hatch and juvenile individuals.

Cardiac performance has been measured in response to oil exposure in many species, both pelagic and estuarine. In juvenile and adult individuals, assessment of swimming performance and aerobic scope are often used as proxies for cardiac performance. Pelagic species, such as cobia (*Rachycentron canadum*) (Nelson et al., 2017) and mahi-mahi (Mager et al., 2018, 2014; Stieglitz et al., 2016), as well as estuarine species, including red drum (Ackerly and Esbaugh, 2020; Johansen and Esbaugh, 2019, 2017) and Atlantic croaker (*Micropogoias undulatus*) (Pan et al., 2018), have been used in respirometry studies after oil exposure on developed cardiac systems and have shown a consistent respiratory impairment following acute oil exposure. Direct measurements of cardiac performance in early life stages, however, are sparse and often rely heavily on heart rate measurements. Bradycardia is a common cardiac response to oil exposure and has been reported in embryonic and larval estuarine species including red drum, sheepshead minnow, and Gulf killifish following oil exposure (Bosker et al., 2017; Dubansky et al., 2013; Khursigara et al., 2017). Data from this study however do not show a reduction in heart rate following exposure to weathered oil from the Deepwater Horizon. This data more closely aligns with observations of inland silverside embryos in which exposure to oil alone did not alter heart rate, but exposure to dispersants and combined exposure to oil and dispersants resulted in significant bradycardia (Adeyemo et al., 2015). As suggested by Khursigara et al. (2017), heart rate may not be the most reliable endpoint for assessing cardiac

performance. Instead, cardiac output – which takes into account both heart rate and stroke volume – may be a more complete and physiologically relevant indicator of cardiac function. Indeed, this study highlights the need for comprehensive cardiac assessment rather than single endpoint analysis as interrogation into heart rate alone would have overlooked reductions in cardiac output driven by reduction in stroke volume in sheepshead minnow embryos exposed to oil. The assessment of stroke volume as conducted in this study allows for a non-intrusive measure of cardiac output that can be conducted earlier in development and is sensitive to subtle changes in cardiac performance.

Data presented in this study are some of the first to comprehensively address embryonic cardiac performance in response to oil exposure in an estuarine fish. Here, the cardiotoxic phenotype – pericardial edema – is measured in conjunction with cardiac output to assess impairments to the developing cardiovascular system in embryonic sheepshead minnows. The extent of pericardial edema and reductions in cardiac output did not differ between oil concentrations, suggesting that toxicologically relevant EC_{50} concentrations fall below the low oil dose (nominal 150 µg/L tPAH) used in this study. Conversely, no embryologic mortality was recorded during the exposures, suggesting that LC_{50} values for sheepshead minnows in the embryo stage fall above the high oil dose, 300 µg/L tPAH. The presence of both pericardial edema and reduced stroke volume are evidence of impaired cardiac performance. However, whether pericardial edema arises from impaired cardiac function, or increased pressure within the pericardial cavity causes reduced stroke volume is unknown. Additional studies are needed to address the causality between these two metrics of cardiotoxicity. Further, there is a need for follow-up studies on the long-term physiologic impacts of embryonic exposure to oil. Work with zebrafish have shown that PAH induced pericardial edema can be attenuated or reversed

after transfer of embryos to PAH free water (Incardona et al., 2004). The persistent effects on cardiac performance stemming from embryologic impairment in sheepshead minnows remains to be seen.

4.6 References

Ackerly, K.L., Esbaugh, A.J., 2020. The additive effects of oil exposure and hypoxia on aerobic performance in red drum (*Sciaenops ocellatus*). Sci. Total Environ. 737, 140174. https://doi.org/10.1016/j.scitotenv.2020.140174

Adeyemo, O.K., Kroll, K.J., Denslow, N.D., 2015. Developmental abnormalities and differential expression of genes induced in oil and dispersant exposed *Menidia beryllina* embryos. Aquat. Toxicol. 168, 60–71. https://doi.org/10.1016/j.aquatox.2015.09.012

Aeppli, C., Carmichael, C.A., Nelson, R.K., Lemkau, K.L., Graham, W.M., Redmond, M.C., Valentine, D.L., Reddy, C.M., 2012. Oil weathering after the Deepwater Horizon disaster led to the formation of oxygenated residues. Environ. Sci. Technol. 46, 8799–8807. https://doi.org/10.1021/es3015138

Allmon, E., Serafin, J., Chen, S., Rodgers, M.L., Griffitt, R., Bosker, T., de Guise, S., Sepúlveda, M.S., 2021. Effects of polycyclic aromatic hydrocarbons and abiotic stressors on *Fundulus grandis* cardiac transcriptomics. Sci. Total Environ. 752, 142156. https://doi.org/10.1016/j.scitotenv.2020.142156

Anttila, K., Dhillon, R.S., Boulding, E.G., Farrell, A.P., Glebe, B.D., Elliott, J.A.K., Wolters, W.R., Schulte, P.M., 2013. Variation in temperature tolerance among families of atlantic salmon (*Salmo salar*) is associated with hypoxia tolerance, ventricle size and myoglobin level. J. Exp. Biol. 216, 1183–1190. https://doi.org/10.1242/jeb.080556

Bagatto, B., Burggren, W., 2006. A three-dimensional functional assessment of heart and vessel development in the larva of the zebrafish (*Danio rerio*). Physiol. Biochem. Zool. 79, 194–201. https://doi.org/10.1086/498185

Beyer, J., Trannum, H.C., Bakke, T., Hodson, P. V., Collier, T.K., 2016. Environmental effects of the Deepwater Horizon oil spill: A review. Mar. Pollut. Bull. 110, 28–51. https://doi.org/10.1016/j.marpolbul.2016.06.027

Bianchi, T.S., Pennock, J.R., Twilley, R.R. (Eds.), 1999. Biogeochemistry of Gulf of Mexico estuaries. John Wiley & Sons, Inc., New York.

Block, B.A., Teo, S.L.H., Walli, A., Boustany, A., Stokesbury, M.J.W., Farwell, C.J., Weng, K.C., Dewar, H., Williams, T.D., 2005. Electronic tagging and population structure of Atlantic bluefin tuna. Nature. 434, 1121–1127. https://doi.org/10.1038/nature03463

Bosker, T., van Balen, L., Walsh, B., Sepúlveda, M.S., DeGuise, S., Perkins, C., Griffitt, R.J., 2017. The combined effect of Macondo oil and corexit on sheepshead minnow (*Cyprinodon variegatus*) during early development. J. Toxicol. Environ. Heal. - Part A Curr. 80, 477–484. https://doi.org/10.1080/15287394.2017.1340208

Brette, F., Machado, B., Cros, C., Incardona, J.P., Scholz, N.L., Block, B.A., 2014. Crude oil impairs cardiac excitation-contraction coupling in fish. Science. 343, 772–776. https://doi.org/10.1126/science.1242747

Camilli, R., Di Iorio, D., Bowen, A., Reddy, C.M., Techet, A.H., Yoerger, D.R., Whitcomb, L.L., Seewald, J.S., Sylva, S.P., Fenwick, J., 2012. Acoustic measurement of the Deepwater Horizon Macondo well flow rate. Proc. Natl. Acad. Sci. 109, 20235–20239. https://doi.org/10.1073/pnas.1100385108

Carls, M.G., Holland, L., Larsen, M., Collier, T.K., Scholz, N.L., Incardona, J.P., 2008. Fish embryos are damaged by dissolved PAHs, not oil particles. Aquat. Toxicol. 88, 121–127. https://doi.org/10.1016/j.aquatox.2008.03.014

Cotelli, F., Andronico, F., Brivio, M., Lamia, C.L., 1988. Structure and composition of the fish egg chorion (*Carassius auratus*). J. Ultrastruct. Res. Mol. Struct. Res. 99, 70–78. https://doi.org/10.1016/0889-1605(88)90034-1

Crone, T.J., Tolstoy, M., 2010. Magnitude of the 2010 Gulf of Mexico oil leak. Science. 330, 634–634. https://doi.org/10.1126/science.1195840

Dong, W., Matsumura, F., Kullman, S.W., 2010. TCDD induced pericardial edema and relative Cox-2 expression in medaka (*Oryzias latipes*) embryos. Toxicol. Sci. 118, 213–223. https://doi.org/10.1093/toxsci/kfq254

Dubansky, B., Whitehead, A., Miller, J.T., Rice, C.D., Galvez, F., 2013. Multitissue molecular, genomic, and developmental effects of the deepwater horizon oil spill on resident Gulf killifish (*Fundulus grandis*). Environ. Sci. Technol. 47, 5074–5082. https://doi.org/10.1021/es400458p

Edmunds, R.C., Gill, J.A., Baldwin, D.H., Linbo, T.L., French, B.L., Brown, T.L., Esbaugh, A.J., Mager, E.M., Stieglitz, J., Hoenig, R., Benetti, D., Grosell, M., Scholz, N.L., Incardona, J.P., 2015. Corresponding morphological and molecular indicators of crude oil toxicity to the developing hearts of mahi mahi. Sci. Rep. 5, 1–18. https://doi.org/10.1038/srep17326

Esbaugh, A.J., Mager, E.M., Stieglitz, J.D., Hoenig, R., Brown, T.L., French, B.L., Linbo, T.L., Lay, C., Forth, H., Scholz, N.L., Incardona, J.P., Morris, J.M., Benetti, D.D., Grosell, M., 2016. The effects of weathering and chemical dispersion on Deepwater Horizon crude oil toxicity to mahi-mahi (*Coryphaena hippurus*) early life stages. Sci. Total Environ. 543, 644–651. https://doi.org/10.1016/j.scitotenv.2015.11.068

Farrell, A.P., 1991. From Hagfish to Tuna: A Perspective on Cardiac Function in Fish. Physiol. Zool. 64, 1137–1164. https://www.jstor.org/stable/30156237

Goksøyr, A., 1995. Use of cytochrome P450 1A (CYP1A) in fish as a biomarker of aquatic pollution. Arch. Toxicol. Suppl. 17, 80–95. https://doi.org/10.1007/978-3-642-79451-3_7

Greer, C.D., Hodson, P. V., Li, Z., King, T., Lee, K., 2012. Toxicity of crude oil chemically dispersed in a wave tank to embryos of Atlantic herring (*Clupea harengus*). Environ. Toxicol. Chem. 31, 1324–1333. https://doi.org/10.1002/etc.1828

Groot, E., Alderdice, D., 1985. Fine structure of the external egg membrane of five species of Pacific salmon and steelhead trout. Can. J. Zool. 63, 552–566.

Hicken, C.E., Linbo, T.L., Baldwin, D.H., Willis, M.L., Myers, M.S., Holland, L., Larsen, M., Stekoll, M.S., Rice, S.D., Collier, T.K., Scholz, N.L., Incardona, J.P., 2011. Sublethal exposure to crude oil during embryonic development alters cardiac morphology and reduces aerobic capacity in adult fish. Proc. Natl. Acad. Sci. U. S. A. 108, 7086–7090. https://doi.org/10.1073/pnas.1019031108

Hutchinson, T.H., Solbé, J., Kloepper-Sams, P.J., 1998. Analysis of the ECETOC Aquatic Toxicity (EAT) database. III - Comparative toxicity of chemical substances to different life stages of aquatic organisms. Chemosphere 36, 129–142. https://doi.org/10.1016/S0045-6535(97)10025-X

Incardona, J.P., Carls, M.G., Day, H.L., Sloan, C.A., Bolton, J.L., Collier, T.K., Schoiz, N.L., 2009. Cardiac arrhythmia is the primary response of embryonic pacific herring (*Clupea pallasi*) exposed to crude oil during weathering. Environ. Sci. Technol. 43, 201–207. https://doi.org/10.1021/es802270t

Incardona, J.P., Carls, M.G., Teraoka, H., Sloan, C.A., Collier, T.K., Scholz, N.L., 2005. Aryl hydrocarbon receptor-independent toxicity of weathered crude oil during fish development. Environ. Health Perspect. 113, 1755–1762. https://doi.org/10.1289/ehp.8230

Incardona, J.P., Collier, T.K., Scholz, N.L., 2011. Oil spills and fish health: Exposing the heart of the matter. J. Expo. Sci. Environ. Epidemiol. 21, 3–4. https://doi.org/10.1038/jes.2010.51

Incardona, J.P., Collier, T.K., Scholz, N.L., 2004. Defects in cardiac function precede morphological abnormalities in fish embryos exposed to polycyclic aromatic hydrocarbons. Toxicol. Appl. Pharmacol. 196, 191–205. https://doi.org/10.1016/j.taap.2003.11.026

Incardona, J.P., Gardner, L.D., Linbo, T.L., Brown, T.L., Esbaugh, A.J., Mager, E.M., Stieglitz, J.D., French, B.L., Labenia, J.S., Laetz, C.A., Tagal, M., Sloan, C.A., Elizur, A., Benetti, D.D., Grosell, M., Block, B.A., Scholz, N.L., 2014. Deepwater Horizon crude oil impacts the developing hearts of large predatory pelagic fish. Proc. Natl. Acad. Sci. 111, E1510–E1518. https://doi.org/10.1073/pnas.1320950111

Incardona, J.P., Scholz, N.L., 2016. The influence of heart developmental anatomy on cardiotoxicity-based adverse outcome pathways in fish. Aquat. Toxicol. 177, 515–525. https://doi.org/10.1016/j.aquatox.2016.06.016

Incardona, J.P., Swarts, T.L., Edmunds, R.C., Linbo, T.L., Aquilina-Beck, A., Sloan, C.A., Gardner, L.D., Block, B.A., Scholz, N.L., 2013. Exxon Valdez to Deepwater Horizon: Comparable toxicity of both crude oils to fish early life stages. Aquat. Toxicol. 142, 303–316. https://doi.org/10.1016/j.aquatox.2013.08.011

Jernelöv, A., Lindén, O., 1981. Ixtoc I: A case study of the Wwrld's largest oil spill. Ambio 10, 299–306. https://www.jstor.org/stable/4312725

Johansen, J.L., Esbaugh, A.J., 2019. Oil-induced responses of cardiac and red muscle mitochondria in red drum (*Sciaenops ocellatus*). Comp. Biochem. Physiol. Part - C Toxicol. Pharmacol. 219, 35–41. https://doi.org/10.1016/j.cbpc.2019.02.003

Johansen, J.L., Esbaugh, A.J., 2017. Sustained impairment of respiratory function and swim performance following acute oil exposure in a coastal marine fish. Aquat. Toxicol. 187, 82–89. https://doi.org/10.1016/j.aquatox.2017.04.002

Jones, E.R., Simning, D., Serafin, J., Sepúlveda, M.S., Griffitt, R.J., 2020. Acute exposure to oil induces age and species-specific transcriptional responses in embryo-larval estuarine fish. Environ. Pollut. 263, 1–10. https://doi.org/10.1016/j.envpol.2020.114325

Khursigara, A.J., Perrichon, P., Martinez Bautista, N., Burggren, W.W., Esbaugh, A.J., 2017. Cardiac function and survival are affected by crude oil in larval red drum, *Sciaenops ocellatus*. Sci. Total Environ. 579, 797–804. https://doi.org/10.1016/j.scitotenv.2016.11.026

Kim, R.O., Kim, B.M., Hwang, D.S., Au, D.W.T., Jung, J.H., Shim, W.J., Leung, K.M.Y., Wu, R.S.S., Rhee, J.S., Lee, J.S., 2013. Evaluation of biomarker potential of cytochrome P450 1A (CYP1A) gene in the marine medaka, *Oryzias melastigma* exposed to water-accommodated fractions (WAFs) of Iranian crude oil. Comp. Biochem. Physiol. - C Toxicol. Pharmacol. 157, 172–182. https://doi.org/10.1016/j.cbpc.2012.11.003

Kuntz, A., 1916. Notes on the embryology and larval development of five species of teleostean fishes. Bull. Bur. Fish. 34, 409–429.

Liu, Z., Liu, J., Zhu, Q., Wu, W., 2012. The weathering of oil after the Deepwater Horizon oil spill: Insights from the chemical composition of the oil from the sea surface, salt marshes and sediments. Environ. Res. Lett. 7. https://doi.org/10.1088/1748-9326/7/3/035302

Mager, E.M., Esbaugh, A.J., Stieglitz, J.D., Hoenig, R., Bodinier, C., Incardona, J.P., Scholz, N.L., Benetti, D.D., Grosell, M., 2014. Acute embryonic or juvenile exposure to Deepwater Horizon crude oil impairs the swimming performance of mahi-mahi (*Coryphaena hippurus*). Environ. Sci. Technol. 48, 7053–7061. https://doi.org/10.1021/es501628k

Mager, E.M., Pasparakis, C., Schlenker, L.S., Yao, Z., Bodinier, C., Stieglitz, J.D., Hoenig, R., Morris, J.M., Benetti, D.D., Grosell, M., 2017. Assessment of early life stage mahi-mahi windows of sensitivity during acute exposures to Deepwater Horizon crude oil. Environ. Toxicol. Chem. 36, 1887–1895. https://doi.org/10.1002/etc.3713

Mager, E.M., Pasparakis, C., Stieglitz, J.D., Hoenig, R., Morris, J.M., Benetti, D.D., Grosell, M., 2018. Combined effects of hypoxia or elevated temperature and Deepwater Horizon crude oil exposure on juvenile mahi-mahi swimming performance. Mar. Environ. Res. 139, 129–135. https://doi.org/10.1016/j.marenvres.2018.05.009

Magnuson, J.T., Khursigara, A.J., Allmon, E.B., Esbaugh, A.J., Roberts, A.P., 2018. Effects of Deepwater Horizon crude oil on ocular development in two estuarine fish species, red drum (*Sciaenops ocellatus*) and sheepshead minnow (*Cyprinodon variegatus*). Ecotoxicol. Environ. Saf. 166, 186–191. https://doi.org/10.1016/j.ecoenv.2018.09.087

McKim, J.M., 1977. Evaluation of tests with early life stages of fish for predicting long-term toxicity. J. Fish. Res. Board Canada 34, 1148–1154. https://doi.org/10.1139/f77-172

Middaugh, D.P., Hemmer, M.J., 1992. Reproductive ecology of the inland silverside, *Menidia beryllina*, (Pisces: Atherinidae) from Blackwater Bay, Florida. Copeia 1992, 53. https://doi.org/10.2307/1446535

Miyashita, S., Tanaka, Y., Sawada, Y., Takii, K., Mukai, Y., Kumai, H., 2000. Embryonic development and effects of water temperature on hatching of the bluefin tuna, *Thunnus thynnus*. Aquacult. Sci. 48, 199-207. https://doi.org/10.11233/aquaculturesci1953.48.199

Neff, J.M., Ostazeski, S., Gardiner, W., Stejskal, I., 2000. Effects of weathering on the toxicity of three offshore Australian crude oils and a diesel fuel to marine animals. Environ. Toxicol. Chem. 19, 1809–1821. https://doi.org/10.1002/etc.5620190715

Nelson, D., Stieglitz, J.D., Cox, G.K., Heuer, R.M., Benetti, D.D., Grosell, M., Crossley, D.A., 2017. Cardio-respiratory function during exercise in the cobia, *Rachycentron canadum*: The impact of crude oil exposure. Comp. Biochem. Physiol. Part - C Toxicol. Pharmacol. 201, 58–65. https://doi.org/10.1016/j.cbpc.2017.08.006

Nilson, B., Berg, K., Goksøyr, A., 1998. Induction of cytochrome P450 1A (CYP1A) in fish. Methods Mol. Biol. 107, 423–438.

Nixon, Z., Zengel, S., Baker, M., Steinhoff, M., Fricano, G., Rouhani, S., Michel, J., 2016. Shoreline oiling from the Deepwater Horizon oil spill. Mar. Pollut. Bull. 107, 170–178. https://doi.org/10.1016/j.marpolbul.2016.04.003

NOAA National Estuarine Research Reserve System (NERRS). 2021. System-wide monitoring program. Data accessed from the NOAA NERRS Centralized Data Management Office website: http://www.nerrsdata.org; accessed 12 February 2021.

Pan, Y.K., Khursigara, A.J., Johansen, J.L., Esbaugh, A.J., 2018. The effects of oil induced respiratory impairment on two indices of hypoxia tolerance in Atlantic croaker (*Micropogonias undulatus*). Chemosphere 200, 143–150. https://doi.org/10.1016/j.chemosphere.2018.02.028

Pasparakis, C., Esbaugh, A.J., Burggren, W., Grosell, M., 2019. Impacts of deepwater horizon oil on fish. Comp. Biochem. Physiol. Part - C Toxicol. Pharmacol. 224, 108558. https://doi.org/10.1016/j.cbpc.2019.06.002

Pasparakis, C., Mager, E.M., Stieglitz, J.D., Benetti, D., Grosell, M., 2016. Effects of Deepwater Horizon crude oil exposure, temperature and developmental stage on oxygen consumption of embryonic and larval mahi-mahi (*Coryphaena hippurus*). Aquat. Toxicol. 181, 113–123. https://doi.org/10.1016/j.aquatox.2016.10.022

Pfaffl, M., 2001. A new Mathematical model for relative quantification in real-time RT-PCR. Nucleic Acids Res. 29, e45. https://doi.org/10.1093/nar/29.9.e45

Philibert, D.A., Lyons, D., Philibert, C., Tierney, K.B., 2019. Field-collected crude oil, weathered oil and dispersants differentially affect the early life stages of freshwater and saltwater fishes. Sci. Total Environ. 647, 1148–1157. https://doi.org/10.1016/j.scitotenv.2018.08.052

Rooker, J.R., Kitchens, L.L., Dance, M.A., Wells, R.J.D., Falterman, B., Cornic, M., 2013. Spatial, temporal, and habitat-related variation in abundance of pelagic fishes in the Gulf of Mexico: Potential implications of the Deepwater Horizon oil spill. PLoS One 8, 1–10. https://doi.org/10.1371/journal.pone.0076080

Rooker, J.R., Simms, J.R., David Wells, R.J., Holt, S.A., Holt, G.J., Graves, J.E., Furey, N.B., 2012. Distribution and habitat associations of billfish and swordfish larvae across mesoscale features in the Gulf of Mexico. PLoS One 7. https://doi.org/10.1371/journal.pone.0034180

Sarasquete, C., Segner, H., 2000. Cytochrome P4501A CYP1A in teleostean fishes. Sci. Total Environ. 247, 313–332. https://doi.org/10.1016/S0048-9697(99)00500-8

Schneider, C.A., Rasband, W.S., Eliceiri, K.W., 2012. NIH Image to ImageJ: 25 years of image analysis. Nat. Methods 9, 671–675. https://doi.org/10.1038/nmeth.2089

Serafin, J., Guffey, S.C., Bosker, T., Griffitt, R.J., De Guise, S., Perkins, C., Szuter, M., Sepúlveda, M.S., 2019. Combined effects of salinity, temperature, hypoxia, and Deepwater Horizon oil on *Fundulus grandis* larvae. Ecotoxicol. Environ. Saf. 181, 106–113. https://doi.org/10.1016/j.ecoenv.2019.05.059

Short, J.W., 2017. Advances in understanding the fate and effects of oil from accidental spills in the United States beginning with the Exxon Valdez. Arch. Environ. Contam. Toxicol. 73, 5–11. https://doi.org/10.1007/s00244-016-0359-4

Simning, D., Sepúlveda, M., De Guise, S., Bosker, T., Griffitt, R.J., 2019. The combined effects of salinity, hypoxia, and oil exposure on survival and gene expression in developing sheepshead minnows, *Cyprinodon variegatus*. Aquat. Toxicol. 214, 1–19. https://doi.org/10.1016/j.aquatox.2019.105234

Soto, L.A., Botello, A. V., Licea-Durán, S., Lizárraga-Partida, M.L., Yáñez-Arancibia, A., 2014. The environmental legacy of the Ixtoc-I oil spill in Campeche Sound, southwestern Gulf of Mexico. Front. Mar. Sci. 1, 1–9. https://doi.org/10.3389/fmars.2014.00057

Stieglitz, J.D., Mager, E.M., Hoenig, R.H., Benetti, D.D., Grosell, M., 2016. Impacts of Deepwater Horizon crude oil exposure on adult mahi-mahi (*Coryphaena hippurus*) swim performance. Environ. Toxicol. Chem. 35, 2613–2622. https://doi.org/10.1002/etc.3436

United States Environmental Protection Agency, 2009. Whole effluent toxicity - Saltwater Series: Sheepshead Minnow (*Cyprinodon variegatus*) and Inland Silverside (*Menidia beryllina*) Larval Survival and Growth Toxicity Tests. Test Method 1004.0. EPA 833-C-09-001

Untergasser, A., Nijveen, H., Rao, X., Bisseling, T., Geurts, R., Leunissen, J.A.M., 2007. Primer3Plus, an enhanced web interface to Primer3. Nucleic Acids Res. 35, W71–W74. https://doi.org/10.1093/nar/gkm306

Webber, D.M., Boutilier, R.G., Kerr, S.R., 1998. Cardiac output as a predictor of metabolic rate in cod *Gadus morhua*. J. Exp. Biol. 201, 2779–2789.

Table 4.1. List of sheepshead minnow primers used for real time PCR. All sequences are 5' to 3' and reverse primers are reverse compliments of the genetic sequence.

Gene	NCBI Accession #	Orientation	Sequence	Efficiency	Length
β-actin	FJ754999.1	F	AACACTGTGCTGTCTGGAGGTA	97.9%	133 bp
		R	AGACGGAGTATTTACGCTCTGG		
cyp1α	EF535032.1	F	GAGTCTTTCATCCTGGAGCTGT	98.0%	180 bp
		R	GATGAACGAAGATGGGTCTTTC		

Table 4.2. **(A)** Nominal and measured tPAH concentrations for each treatment at onset of exposure (0 h) and immediately preceding refreshment of exposure solutions (24 h). **(B)** Measured water quality parameters at onset of exposure (0 h) and immediately preceding refreshment of exposure solutions (24 h). Values represented as mean ± SD. Water quality parameters **(B)** measured only for control solutions. **(A)** n = 20 per time point, **(B)** n = 20.

A

Condition	Nominal Value	Initial Value (0 h)	Final Value (24 h)
Control	0 µg/L tPAH	0 µg/L	0 µg/L
Low oil	150 µg/L tPAH	164.40 ± 13.63 µg/L	117.68 ± 18.39 µg/L
High oil	300 µg/L tPAH	327.75 ± 10.51 µg/L	190.56 ± 20.55 µg/L

B

Parameter	Initial Value (0 h)	Final Value (24 h)
Temperature	30 ± 0.3°C	30 ± 0.3°C
Dissolved Oxygen	8.11 ± 0.02 mg/L	8.08 ± 0.02 mg/L
Salinity	25 ppt	25 ppt
pH	8.0	8.0
Ammonia	0 ppm	0 ppm

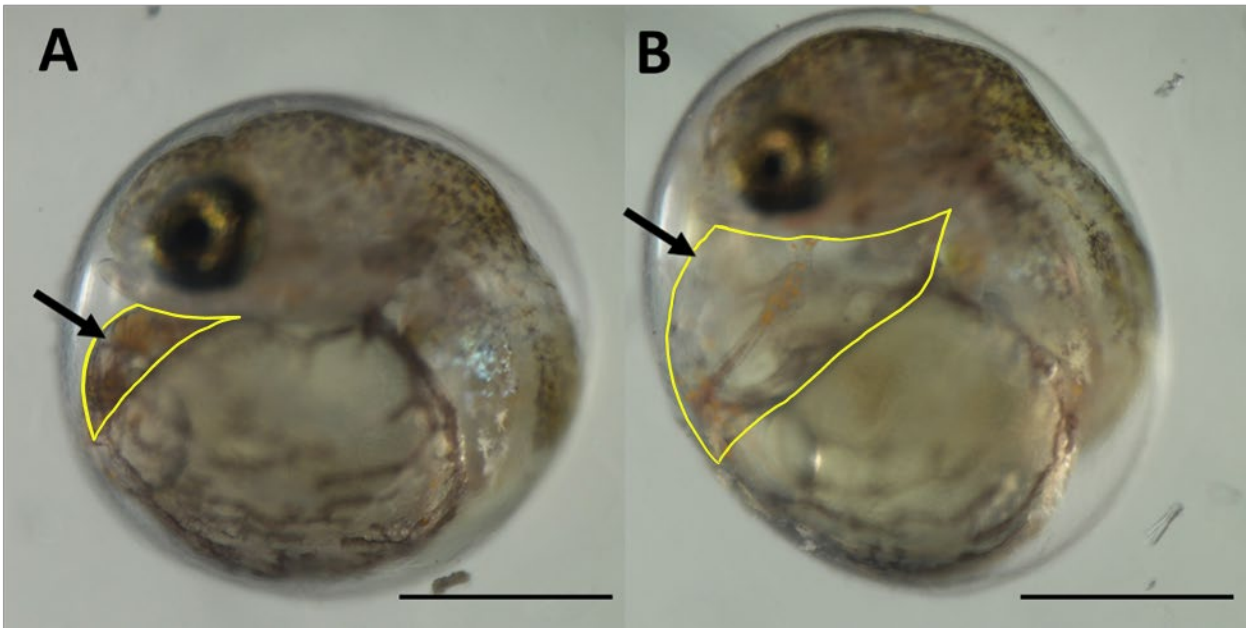

Figure 4.1. Representative images of (A) control and (B) oil exposed (300 µg/L tPAH) 4 dpf sheepshead minnow embryos. Arrows point to pericardial area (outlined in yellow), note the pericardial edema and tubular heart present in embryos exposed to oil (B). Scale bars = 500 µm.

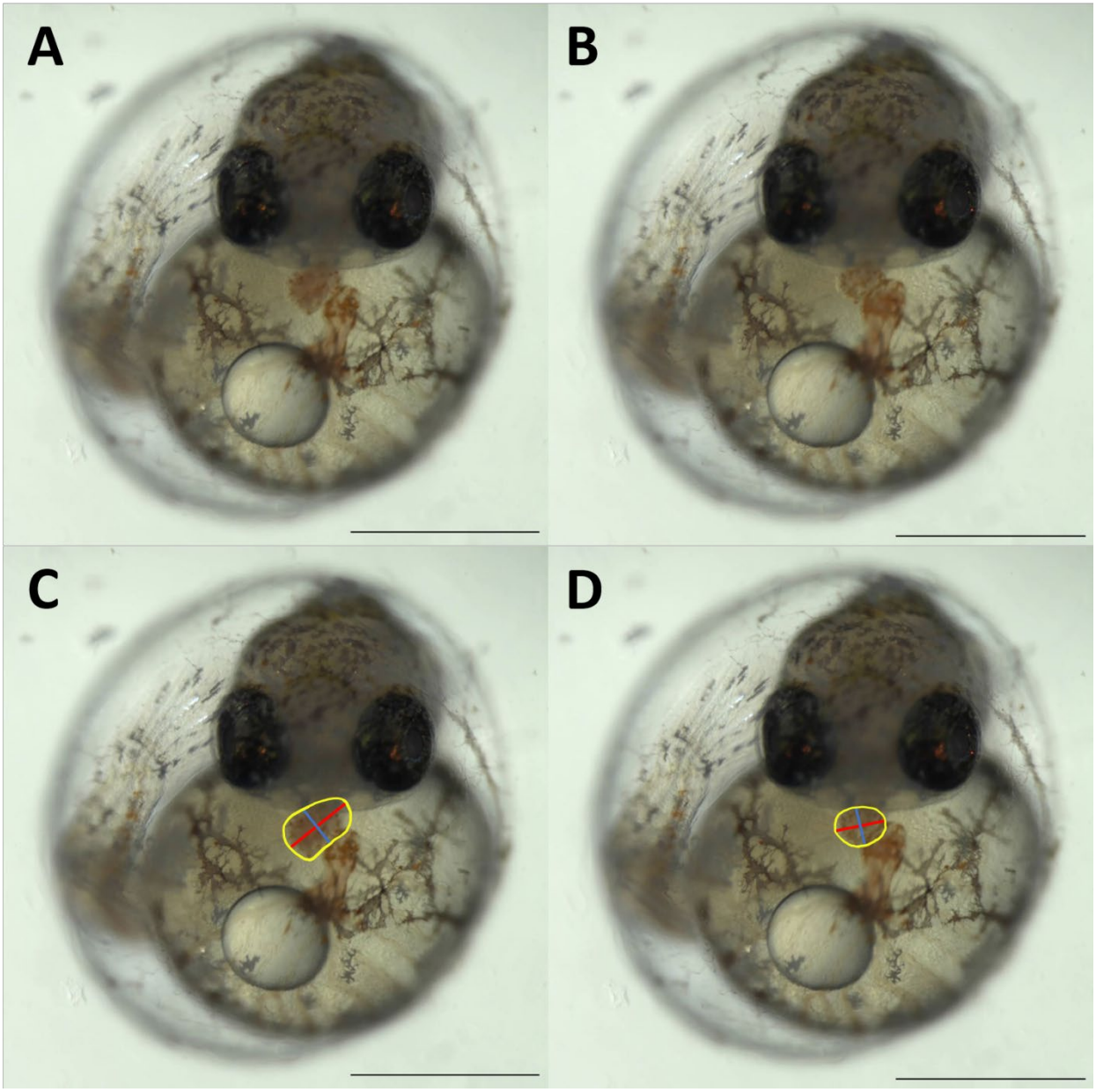

Figure 4.2. Representative images of **(A)** peak diastole and **(B)** peak systole in control 4 dpf sheepshead minnow embryos. Ventricular outlines (yellow), ventricular longitudinal axis (red), and ventricular width axis (blue) are shown at **(C)** peak diastole and **(D)** peak systole. Scale bars = 500 µm.

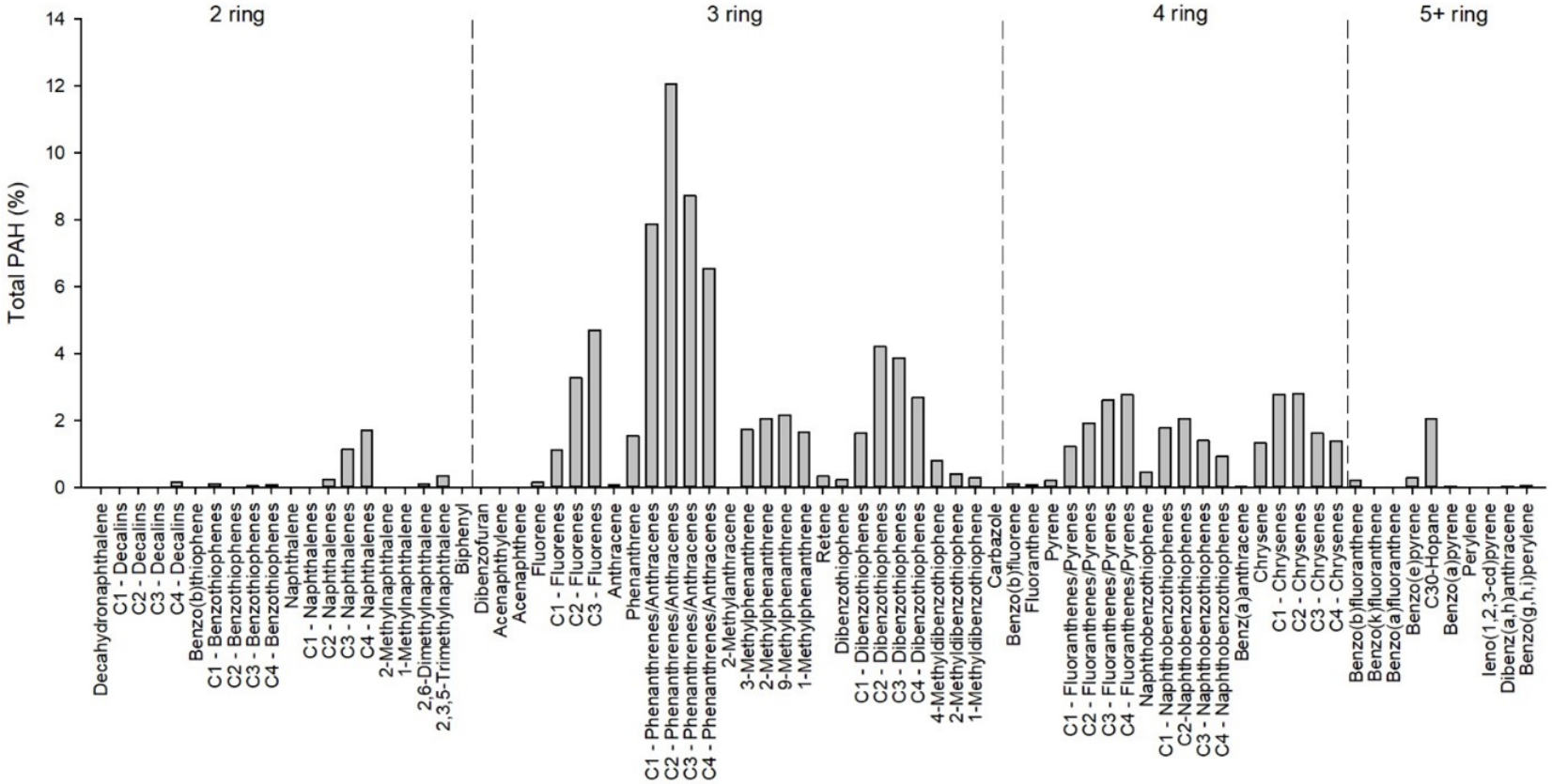

Figure 4.3. Average relative PAH composition of 100% HEWAF stock solution made with naturally weathered OFS. Dotted lines separate subclasses of PAHs based on number of aromatic rings present within each compound. n = 4.

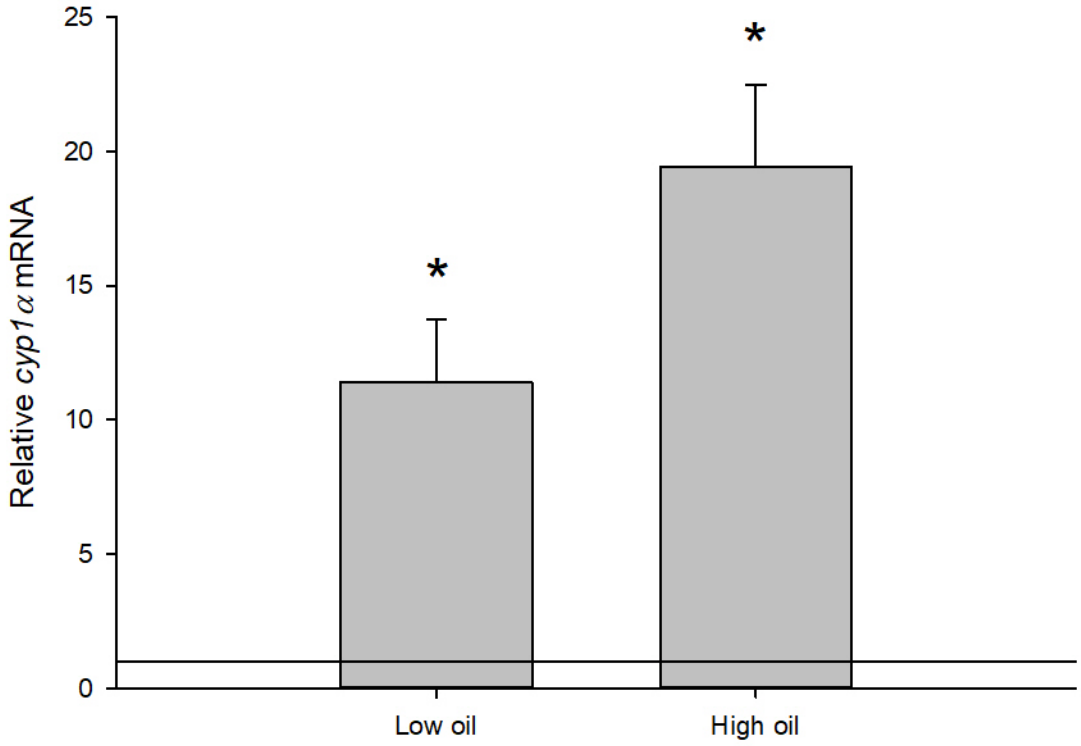

Figure 4.4. *cyp1α* expression in 4dpf sheepshead minnow embryos exposed to low (150 µg/L tPAH) and high (150 µg/L tPAH) concentrations of naturally weathered OFS. Values set relative to controls denoted by solid line at 1.0. Bars represent mean ± SEM. Asterisks denote significant differences from controls ($p \leq 0.05$). n = 8-10 per treatment.

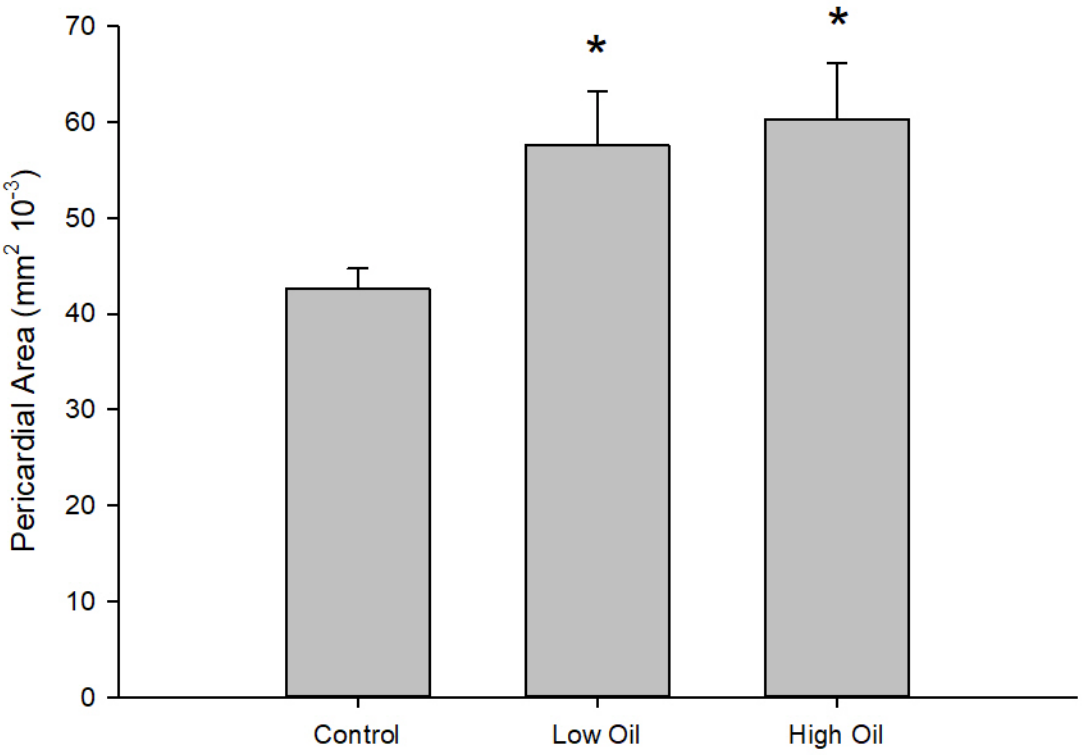

Figure 4.5. Mean pericardial area of 4 dpf sheepshead minnow embryos exposed to low (150 µg/L tPAH) and high (150 µg/L tPAH) concentrations of naturally weathered OFS. Bars represent mean ± SEM. Asterisks denote significant differences from controls ($p \leq 0.05$). n = 40 per treatment.

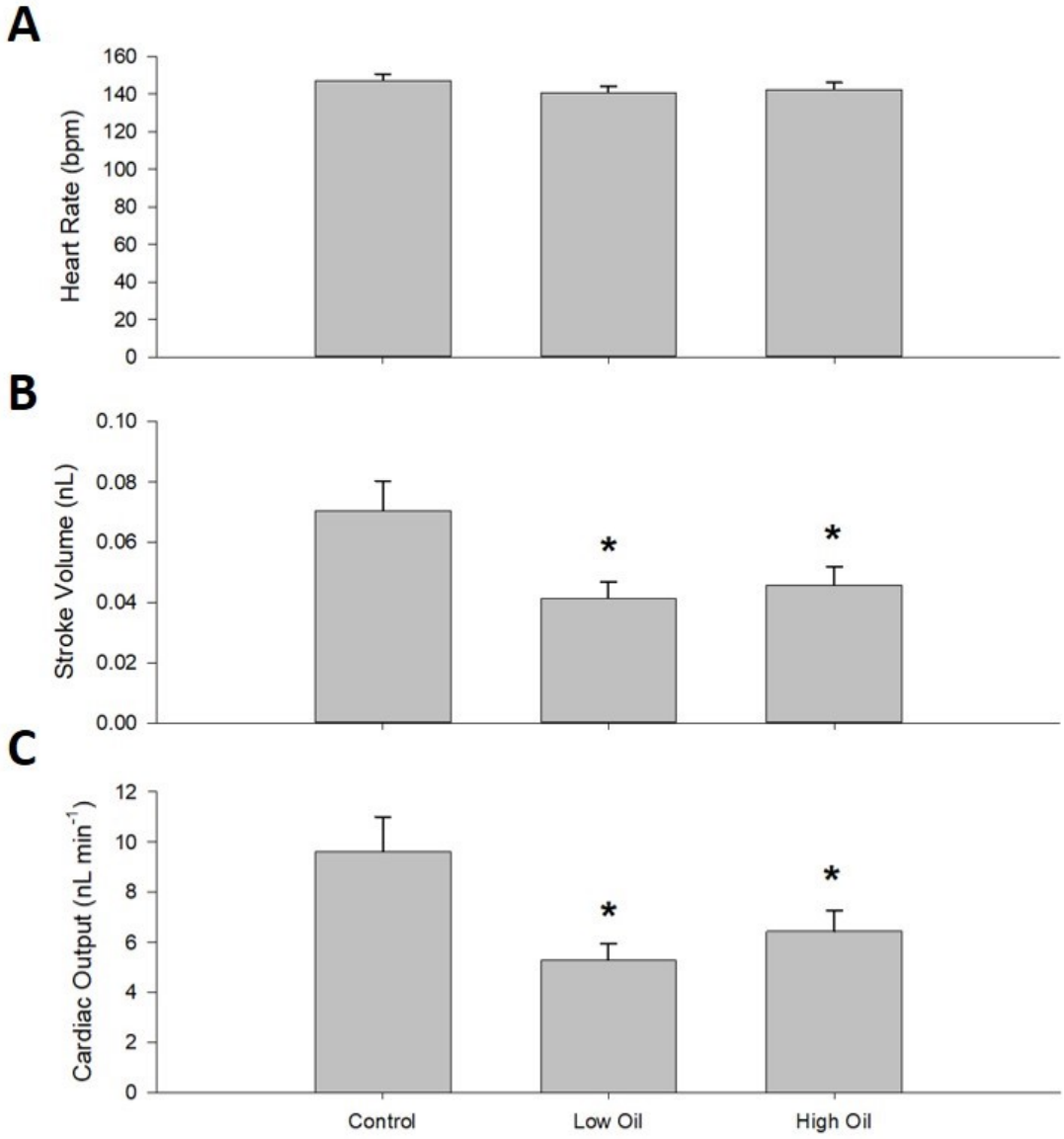

Figure 4.6. Cardiac function in 4 dpf sheepshead minnow embryos as assessed by **(A)** heart rate, **(B)** stroke volume, and **(C)** cardiac output following exposure to control, low (150 µg/L tPAH), or high (300 µg/L tPAH) oil concentrations. Bars represent mean ± SEM. Asterisks denote significant differences from controls ($p \leq 0.05$). n = 38-40 per treatment.

CHAPTER 5. HEMODYNAMIC DEPENDENCE OF MECHANO-GENETIC EVOLUTION OF THE CARDIOVASCULAR SYSTEM IN JAPANESE MEDAKA

A version of this chapter has been submitted for publication; reproduced from:
Chakraborty, S., Allmon, E., Sepúlveda, M.S., Vlachos, P. (2021) *Hemodynamic dependence of mechano-genetic evolution of the cardiovascular system in Japanese medaka*. Manuscript submitted for publication.

5.1 Abstract

The progression of the cardiac gene expression-wall shear stress (WSS) interplay is critical to identify developmental defects during cardiovascular morphogenesis. However, mechano-genetics from the embryonic to larval stages are poorly understood in vertebrates. We quantify peak WSS in the heart and tail vessels of Japanese medaka from 3 days post fertilization (dpf) to 14 dpf using in-vivo micro particle image velocimetry (μPIV) flow measurements, and in parallel analyzed the expression of five cardiac genes (*fgf8, hoxb6b, bmp4, nkx2.5*, *smyd1*). Here, for the first time, we report that WSS in the atrioventricular canal (AVC), ventricle outflow tract (OFT), and the caudal vessels in medaka peak with inflection points at 6 dpf and 10-11 dpf instead of a monotonic trend. In addition, all genes were upregulated at 3 dpf and 7 dpf indicating a possible correlation between the two, with the cardiac gene upregulation preceding WSS increase in order to facilitate cardiac wall remodeling.

5.2 Introduction

Wall shear stress (WSS) fluctuations experienced by vascular endothelial cells and endocardial cells are linked with changes in cardiac specific gene expression and changes in cellular phenotypes (1-4) that modulate cardiovascular morphogenesis (5-8). The flow mechanics of the embryonic heart strongly influences the pulsatility and the topology of the

peripheral vascular network (9-11). Small teleost models such as zebrafish (*Danio rerio*) and the Japanese medaka (*Oryzias latipes*) have been extensively imaged to capture non-intrusive, accurate flow velocity and WSS measurements at varying stages of cardiovascular development (12-19). The modulation of key genes responsible for cardiac anomalies in these species have previously been investigated by mutating genes or introducing perturbation in the blood circulation (20-26). However, baseline longitudinal studies tracking the evolution of cardiovascular flow metrics and cardiovascular specific gene expressions at discrete 24 h intervals are scarce in the vertebrate embryogenesis literature (27, 28).

Cardiac valves located in the atrioventricular canal (AVC) and the outflow tract (OFT) of the ventricle experience the highest flow velocity and WSS (12, 29-31). The dynamic WSS variation in these regions control developmental landmarks like valve cushion formation as well as valve leaflet formation and direction during age progression (7, 32-35). However, in two separate studies with zebrafish, peak WSS was shown to increase from 72 hours post fertilization (hpf) to 6 days post fertilization (dpf) at the AVC (31, 36) while the reverse trend is seen at the OFT (29, 37). Since both regions morphologically expand during chamber formation and subsequently undergo an area reduction after valve cushions form (38), opposite peak WSS trends in the AVC and OFT seem counterintuitive. Imaging intervals of 12 h or 24 h are too large for zebrafish which undergo rapid development with ventricle lengths increasing at a rate of 125 μm/day during the first 60 dpf (39). Consequently, possible inflection points in peak WSS progression with age may have been missed in previous studies. Previous studies investigating aortic arch and cardiac outflow tract morphogenesis in chicken embryos have shown an inflection point in peak WSS progression (40, 41) with age that correlated with the expression of

some developmental genes (41). Hence, in order to capture the cardiac developmental landmarks in more detail, we chose the Japanese medaka as the vertebrate model in the current study.

Japanese medaka grows faster compared to higher mammalian vertebrate models (like mice, rabbits, pigs, humans) but is two times slower compared to zebrafish (39, 42). Additionally, the larger size and lack of pigmentation in medaka embryos until 14 dpf (42) when compared to zebrafish allows for better optical imaging. Multiple comparisons of the cardiac ontogeny in zebrafish and Japanese medaka can be found in the literature (39, 42, 43); a relevant illustration outlining the onset of analogous cardiac events in the two species is presented by Taneda et al. (43). Significant ontogenetic events of cardiac development central to this study include those such as the formation of the tubular heart (1 dpf in zebrafish (44) and 1.5 dpf in Japanese medaka (42)), the onset of blood circulation (1.25 dpf in zebrafish (44) and 3 dpf in Japanese medaka (42)), and endocardial cushion formation (1.75 dpf in zebrafish (45) and 5 dpf in Japanese medaka (42, 46)) as well as post-hatch cardiac remodeling such as valvulogenesis (15). For a more detailed comparison between the two species, see Table 5.1.

Multiple measurements of vascular WSS along caudal and dorsal vessels of larval teleosts have shown that arteries have higher pulsatility and flow velocities than veins. Owing to low velocity (~0.3-2 mm/s) of the cardiovascular flow in teleosts (11, 13, 47), the vascular WSS reported is low (5-30 dyne/cm^2) compared to humans and other vertebrates (18, 48-50). However, little attention has been given to the cross-sectional variation of these vessels from embryonic to larval stages that eventually separates them into arteries and veins (11, 51). The vessel cross-section is critical in regulating flow velocities (11) which can subsequently lower the WSS below the critical value required for cell proliferation in vessels (52-55). Calculation of WSS is non-trivial due to the difficulty in measuring spatially resolved velocity gradients near

the cardiac wall. Velocity fields in the fish heart can be measured non-invasively through 2-dimensional imaging by using micro–Particle Image Velocimetry (μPIV) which cross-correlates red blood cell (RBC) patterns in successive time-lapse images separated by a known time interval (36, 56, 57). Velocity gradients of higher accuracy are then calculated from the spatially and temporally resolved velocity field instead of assuming a linear/parabolic velocity profile near the cardiac wall as done in previous studies (6, 8, 58). Variations in blood viscosity with increasing shear rate and varying hematocrit in developing teleost embryos have rarely been accounted for (36, 59). Previous studies have assumed blood dynamic viscosity to be constant at all fish ages and used values ranging from 3cP to 8 cP to calculate WSS in zebrafish heart (29, 31, 36, 60). A recent experimental investigation has shown the blood viscosity in embryonic zebrafish changes with time and therefore should not be assumed to be fixed (59).

WSS induced mechano-transduction is known to influence embryonic cardiovascular development through the induction of late-onset genes (61-63). Molecular genetic approaches, such as qPCR, have been used with teleost embryos to identify molecular pathways and to study the functions of specific genes related to cardiovascular abnormalities/development. One well established genetic pathway in the growing zebrafish heart is activated in the AVC to control the atrio-ventricular (AV) valve morphogenesis. The Kruppel-like factor 2a (*klf2a*) gene responsible for this phenomenon is known to be expressed strongly in regions of high shear that impacts endocardial cushion differentiation leading to AV valve formation (5, 7, 10, 32). Fibroblast growth factor 8 (*fgf8*) and bone morphogenetic factor-4 (*bmp4*) are cardiac genes required for development of teleost heart precursors (64, 65) and contribute to anterior heart field development in mouse (66). The gene homeobox B6b (*hoxb6b*) is responsible for anterior/posterior patterning in the medaka was reported to disrupt morphogenesis in a toxic

environment exposed to silver nanocolloids (67). NK2 homeobox 5 (*nkx2.5*) is a cardiac transcription factor that modulates the formation of the secondary heart field (68, 69) and was reported to peak between 48 hpf and 96 hpf in zebrafish embryos followed by a decrease at 120 hpf (26). SET and MYND Domain-1 (*smyd1*) is a protein coding gene that aids in cardiac muscle differentiation (65) and its knockdown in zebrafish results in disrupted myofibril growth and loss of a heartbeat (70). These genes, in addition to many others, play important roles in the early development of the teleost heart and therefore position themselves as potential target genes to trace the ontogenetic processes involved in early life history cardiac development.

This overview of the literature highlights the need for a baseline framework for vertebrate embryonic models that investigates variation of cardiovascular WSS with cardiac gene expressions along developmental stages. In this work, we conducted a series of live experiments to image the Japanese medaka heart and peripheral vessels under a microscope followed by subsequent μPIV analysis for flow quantification along with gene expression profiling across development in embryo/larva in absence of any perturbation. We report peak WSS measurements in two cardiac valve regions at the AVC and OFT. Concomitantly, we calculated peak WSS values in four vessel locations: dorsal artery (DA), dorsal vein (DV), caudal artery (CA) and caudal vein (CV) along the tail. We also performed qPCR analysis to compare gene expressions of five cardiac genes *fgf8, hoxb6b, nkx2.5, smyd1,* and *bmp4* in relation to peak WSS variation from 3 dpf to 12 dpf. To our knowledge, this is the first study with fish early life-stages that attempts to identify a correlation between the peak cardiac WSS variation and cardiac specific gene expression during development.

5.3 Materials and Methods

All methods were carried in accordance with relevant guidelines and regulations and method protocols have been approved by the Purdue Animal Care and Use Committee (PACUC).

5.3.1 Japanese medaka husbandry and embryo/ larvae collection

Wild type adult Japanese medaka obtained from US EPA (Duluth, MN, USA) were mated in 2 L transparent tanks with continuous oxygen supply under artificial reproductive conditions (14L:10D photoperiod; 28°C). Spawning was initiated daily at 9am and fertilized embryos were collected, immersed in embryo medium (diluted saline solution containing 2 ppm methylene blue), and housed in an environmental chamber at 28°C with continuous oxygen supply by 5pm. A total of 150 embryos were collected from 9 clutches originating from 5 different spawning pairs. Hatching from all clutches occurred between 8 and 9 dpf, sampling continued until 14 dpf to account for hemodynamic and/or gene expression changes that may occur after hatching. Embryos/ larvae were randomly collected for gene expression every 12 h from 0.5 dpf until 3 dpf and every 24 h from 4 dpf until 12 dpf (n=10/ time point) and were immediately frozen at -80°C until RNA extraction. The more frequent sampling interval during early embryonic development was chosen to capture the possible rapid changes in the cardiac development induced gene expression. Additional embryos/ larvae were randomly sampled for imaging analysis every 24 h after the onset of blood circulation from 3 dpf until 14 dpf (n=5/ time point).

5.3.2 Flow velocity analysis in heart

2-dimensional images of medaka fish heart and caudal vessels were visualized through a Nikon-Ti microscope with a 60x objective lens and acquired by a high-speed CMOS camera (Phantom Miro-310, 2500x1600 pixels) which resulted in an effective pixel size of 0.16 μm. Brightfield

time-resolved images were captured for 4s at a rate of 400 frames per second. These correspond to 8-10 cycles and approximately 199 image pairs per cycle. The raw images were preprocessed by applying a proper orthogonal decomposition (71-74) across time series of images and retaining the non-dominant modes that represent the fluctuations of RBC patterns across time while substantially removing background artifacts. The RBC movement patterns across time lapse images were cross-correlated and a phase average of the cross-correlations were used to obtain velocities in the heart and vessels as shown in Figure 5.1. The heart rate (HR) was measured from the Fourier transform of the instantaneous velocity waveforms. The Reynolds number ($Re = \frac{\rho V d}{\mu}$) and Womersley number ($Wo = d\sqrt{\frac{\rho\omega}{\mu}}$) were calculated for each sample and each age based on the atrial inlet diameter (d), blood density (ρ) as 1025 kg/m^3, blood dynamic viscosities (μ) that change with age and $\omega = 2\pi HR/60$. The EF is a function of ventricle volumes at diastole and systole and is defined in Eqn 5.1.

$$A = \pi L D_1 ; \; Vol = \frac{\pi}{4} L D_1 D_2 ; \; D_1 = D_2 ;$$
$$\text{EF} = \frac{End\_diastolic\_Vol - End\_systolic\_Vol}{End\_diastolic\_Vol} \qquad \textbf{Eqn 5.1}$$

5.3.3 µPIV analysis

The instantaneous velocity field at a time point in the heart cycle was obtained from the standard cross correlation (SCC) of two successive image pairs as mentioned previously (75). Each image region was subdivided into windows before cross-correlating. Cross-correlation vectors were obtained using an initial window size of 96x96 pixels (window resolution : 48x48 pixels) with a 50% overlap between windows, followed by another pass of window size of 64x64 pixels (window resolution : 32x32 pixels) with 50% overlap and finally followed by another pass of

window size of 64x64 pixels (window resolution : 32x32 pixels) with 75% overlap (76). In the first, second, and third pass, each window of each image contained approximately 10-15 RBC patterns, 6-8 RBC patterns, and 5-7 RBC patterns respectively. In each pass there were minimum 3 and maximum 6 iterations of window deformation weighted by a Blackman filter that minimized the loss of information due to in-plane motion of the particles (77, 78). The correlation planes at each phase of the cycle were averaged across all cycles to get an ensemble correlation plane (79). The peak location of the correlation plane denotes the displacement between images at that time point. An accurate velocity estimate at each cycle phase was obtained by fitting sub-pixel resolution curves to the correlation peak using a three point Gaussian estimator (75, 80). Universal outlier detection was done between passes to eliminate erroneous velocity vectors (81). An additional median filtering with a window size of 3x3 pixels spatially was done to the vectors in the final pass (1, 82). All calculation steps were done using the in-house PIV software, PRANA (83).

5.3.4 Hematocrit (Ht) calculation

Ventricle images were cropped to retain a small area around the ventricle center. RBC pattern count (Nrbc) was calculated from the average auto-correlation plane of all the time-lapse ventricle images for each medaka heart as discussed in (84). The ventricle volume (Vvol) was calculated by multiplying the area of the images with the depth of focus. Then the Ht in percentage was calculated using Eqn 5.2.

$$Ht = 100 * Volume\ of\ a\ RBC * \frac{Nrbc}{Vvol} \qquad \textbf{Eqn 5.2}$$

5.3.5 WSS analysis in AVC and OFT

Endocardial wall boundaries were detected from the velocity contour maps by identification of edges where the velocity gradient is maximum. WSS is a product of the fluid dynamic viscosity (μ) and the flow shear rate (γ) at the wall location as shown in Eqn 5.3.

$$WSS = [\mu\gamma]_{walllocation} \quad \textbf{Eqn 5.3}$$

Blood dynamic viscosity in teleosts is ill-defined. We modelled the medaka heart blood viscosity as a function of both hematocrit (Ht) and wall shear rate (γ) according to the Walburn-Schneck equation (85). Velocity gradients were calculated using a high accuracy gradient calculation technique namely the Compact-Richardson method (86) in accordance to second order polynomial fitting done in previous studies (30, 36). Shear rate (γ) at the AVC and OFT were derived from the velocity gradient field using Eqn 5.4 where $\vec{V}$ is the flow velocity vector, $\vec{n}$ is the unit vector normal to the cardiac wall surface and $\frac{d\vec{V}}{d\vec{n}}$ is the directional derivative of the velocity in the direction normal to the cardiac wall surface.

$$\boldsymbol{\gamma = \frac{d\vec{V}}{d\vec{n}}} \quad \textbf{Eqn 5.4}$$

5.3.6 Flow and WSS analysis in vessels

Vessel diameters were calculated from the images using a combination of thresholding and edge detection techniques. The RBC dimension (w) is of the same order as the vessel diameter (d) through which it flows. So, the flow velocity (V) was calculated assuming time-dependent plug flow. This assumption has been used in previous studies with zebrafish (18, 50). Due to a column of RBC at the center of the vessel, there exists a thin plasma layer devoid of cells near the

vascular wall that exerts the WSS. Hence the plasma viscosity (μ) of 1.2 cP has been used for vascular WSS calculations as shown in Eqn 5.5.

$$WSS = \mu \frac{V}{h}, \text{ where } h = \frac{d - w}{2} \qquad \textbf{Eqn 2.5}$$

5.3.7 qPCR analysis

Real time PCR primers were developed for the genes *fgf8, hoxb6b, nkx2.5, smyd1*, and *bmp4*, and control gene *18S mRNA* (Table 5.2). The identified sequences were verified against the NCBI database using a standard Blast search. To ensure sufficient quantities of quality RNA, total RNA isolation was performed on whole embryos using Qiagen RNeasy mini kit according to manufacturer protocols and quantified using a NanoDrop 2000C spectrophotometer (Thermo Scientific). Due to low RNA yield from single embryos at the earliest sampling points, samples between 0.5 dpf and 3 dpf consisted of pooled RNA from 2 embryos collected from the same clutch; all samples for all remaining time points consisted of total RNA from single embryos/ larvae. Total RNA was treated for potential DNA contamination by incubating with DNase 1 (Thermo Scientific) according to manufacturer protocols. cDNA synthesis was performed on 50 ng of total RNA using SuperScript III reverse transcriptase (Invitrogen), according to manufacturer protocols. Samples were stored at -20ºC until qPCR analysis. qPCR analysis was performed using the iQ SYBR Green Supermix (Bio-Rad) and reactions were prepared according to the manufacturer's protocols. All reactions were processed using a CFX Connect qPCR machine (Bio-Rad) with accompanying software. For all genes, cDNA free reactions and no reverse-transcriptase control reactions were performed to check for self-annealing sites and non-target DNA contamination. A serial dilution was used for standard curves to determine the reaction efficiency of each primer pair. The Ct values for each sample were used to assess

relative abundance of each gene in relation to the control gene using the delta-delta Ct method (87).

5.3.8 Statistical analysis

Statistical significance was tested for all the cardiac function and geometry parameters by using Tukey-Kramer Honest Significant Difference (HSD) tests. The p-values for cardiac function and geometry parameters (HR, Re, Wo, A, EF and t_{diast}/T) between a pair of dpf are listed in Supplementary Table 5.1 and can be accessed through the Purdue University Research Repository, doi:10.4231/GGB2-WG59. The p-values that denote difference of mean values of the shear dependent parameters (hematocrit, viscosity, peak shear rate at AVC, peak WSS at AVC and OFT) between a pair of dpf are listed in Supplementary Table 5.2, doi:10.4231/3RX2-WR09. Statistical tests of the relative gene expression across developmental stages were performed using commercial software JMP. Tukey-Kramer HSD test examined statistical differences with p value <0.05 considered significant. The number of samples for each gene in each dpf was 8-10 except for one sample expressing *smyd1* at 0.5 dpf. The p-values that denote difference of mean values of the relative cardiac gene expressions (*fgf8, hoxb6b, nkx2.5, bmp4* and *smyd1*) between a pair of time points are listed in Supplementary Table 5.3, doi:10.4231/ADDK-QB60.

5.4 Results and Discussion

5.4.1 Cardiac function and geometry

The variation of cardiac function parameters and end-diastole ventricle area (A) with age progression of medaka is shown in Figure 5.2. The HR increases from a mean value of 78.5 beats per minute (bpm) to 173.6 bpm with age progression and plateaus at 12-14 dpf in the larval stage

(Figure 5.2A). The trend is similar to other vertebrates in utero (88, 89) but the range is different for each type of adult vertebrate (e.g., zebrafish: 120-180 bpm; human: 60-90 bpm; mouse: 300-600 bpm) (90). Reynolds number (Re) is defined as the ratio of inertial forces and viscous forces (91, 92). Wormersley number (Wo) is defined as the ratio of transient inertial forces and viscous forces (92). Both the Re and Wo are dimensionless, much less than 1 and increase with age within a small range [Re ~ 0.01-0.02; Wo ~ 0.02-0.04] (Figure 5.2B and Figure 5.2C). For higher vertebrates like humans, pigs and frogs the peak Re and peak Wo are much greater than 1 (91, 93, 94), however embryonic stages of chicks and mice fall within the same range as teleosts (91, 95). The end-diastolic area (A) in Figure 5.2D increases from a mean value of 1143 μm^2 at 3 dpf to 4884 μm^2 at 14 dpf with age progression. The same trend is seen in all vertebrates but to a higher degree in higher vertebrates (91). The ejection fraction (EF) does not show any monotonic trend across age progression (Figure 5.2E) but resembles the ventricle ejection fraction of humans (96). The EF undergoes a transient non-significant spike at 5 dpf but decreases again before increasing after hatching at 9 dpf after which it plateaus from 10-14 dpf. T is defined as the time period of a single heart cycle while t_{diast} is the time taken for the ventricle to fill. The fractional time of ventricle diastole (t_{diast}/T) seen in Figure 5.2F initially increases from a mean value of 0.33 at 3 dpf to 0.41 at 6 dpf then declines to 0.34 until 8 dpf. It remains constant (~ 0.3) until hatching and later declines again to 0.21 at 13-14 dpf. In human fetuses the same trend of decreasing ventricle filling time with age is observed as heart rate increases from 90 bpm at 20 weeks to above 120 bpm at 40 weeks with isovolumic contraction time decreasing from 20% to ~ 0 % respectively (97, 98).

5.4.2 Hematocrit, viscosity, and shear rate in the ventricle

The viscosity at each dpf is a function of both hematocrit and the shear rate. Figure 5.3A shows an initial increase in shear rate from 3 dpf (200 s^{-1}) to 5 dpf (332 s^{-1}) peaking at 6 dpf (1124 s^{-1}). It decreases to 491 s^{-1} at 7 dpf and then stays almost constant with little variations from 8 dpf (553 s^{-1}) to 14 dpf (497 s^{-1}). There were no significant differences in hematocrit variation over time as shown in Figure 5.3B. Hematocrit increased from a mean value of 38.5% at 3 dpf to 48% at 6 dpf followed by a reduction to 35% at 8 dpf and remained fairly constant around that value from 9 dpf (34%) to 14 dpf (37%). The resultant mean viscosity shown in Figure 5.3C shows little variation from 3-7 dpf (4.3±0.2 cP) and then drops before hatching at 8 dpf where it plateaus to a value of 3.7±0.2 cP from 9-14 dpf. Although there is a statistically significant increase in shear rate and a non-significant increase in mean hematocrit at 6 dpf, no substantial change was observed in the blood viscosity value at 6 dpf due to relatively low sample size (n=5) and high variability. Additionally, 6 dpf corresponds to stage 36 in medaka development during which there is considerable heart development including the flexion of the atrioventricular region (42) and increased concentric cardiac chamber growth (43). This period of rapid growth and morphological change may account for the increased variation in WSS at the AVC and OFT measured at 6dpf.

5.4.3 Velocity and WSS measurement in AVC and OFT

Velocity variation within an entire heart beat cycle at each dpf is plotted at the AVC and the OFT in Figure 5.4. The pink shaded region between the minimum and maximum time variations at each dpf depicts the bounds within which the profiles fluctuate. The median profile for each dpf is shown by the black solid line. The median peak velocity after the onset of circulation during 3 dpf at the OFT (Figure 5.4B: 2.5 mm/s) is substantially higher than that at the AVC (Figure

5.4A: 1.1 mm/s). The AVC peak stays the same at 4 dpf and increases at 5 dpf but the OFT (2.7-3.0 mm/s) still reports higher peak velocity magnitude than the AVC (1.1-2.3 mm/s). The median peak velocity values increase substantially at 6 dpf (AVC: 4.2 mm/s; OFT: 3.6 mm/s) and decrease progressively at 7 dpf (AVC: 3.4 mm/s; OFT: 2.7 mm/s). At 8 dpf peak AVC velocity decreases while the OFT peak velocity increases (AVC: 2.8 mm/s; OFT: 3.1 mm/s). After hatching, the median peak velocity values remain fairly constant from 9 dpf (AVC: 4.1 mm/s; OFT: 3.6 mm/s) to 14 dpf (AVC: 3.8 mm/s; OFT: 3.5 mm/s). At the AVC, high median negative velocities observed from 6 dpf (-1.3 mm/s) until 14 dpf (-1.4 mm/s) denote presence of retrograde flow back into atrium at the end of ventricle diastole. After ventricular systole, initially a small negative velocity is observed at the OFT during 3 dpf (-0.1 mm/s) which reduces considerably at 4dpf (-0.04 mm/s) and 5 dpf (-0.05 mm/s). It increases gradually at 6 dpf (-0.1 mm/s) and 7dpf (-0.2 mm/s). The negative velocity increases considerably at 8dpf (-0.8 mm/s). Post-hatch it fluctuates between -0.4 mm/s (13 dpf) to -1.5 mm/s (11 dpf) until 14 dpf (-0.8 mm/s).

WSS variation with an entire heart cycle in each dpf is plotted at the AVC and the OFT in Figure 5.5. The median peak WSS values (Figure 5.5A and Figure 5.5B**)** reflect the combined effects of changing blood viscosity and shear rate at each time point. Similar to the peak velocity variation with time, the median peak WSS peaks at 6 dpf (AVC: 47 dyne/cm^2; OFT: 34.4 dyne/cm^2), declines at 7 dpf (AVC: 17 dyne/cm^2; OFT: 19.8 dyne/cm^2) and increases again at 8 dpf (AVC: 23.8 dyne/cm^2; OFT: 24.4 dyne/cm^2). It continues increasing after hatching and fluctuates around a small range of values from 9 dpf (AVC: 33.6 dyne/cm^2; OFT: 30.4 dyne/cm^2) to 14 dpf (AVC: 26.7 dyne/cm^2; OFT: 22 dyne/cm^2). Retrograde flow at AVC and OFT is

evident from high median negative WSS magnitudes from 6dpf (AVC: -17.5 dyne/cm^2; OFT: -1.9 dyne/cm^2) through 14 dpf (AVC: -4.3 dyne/cm^2; OFT: -2.7 dyne/cm^2).

5.4.4 Area, velocity, and WSS measurements in tail vessels

The caudal vessels and dorsal vessels undergo reduction in their cross-sectional areas as fish develop (Figure 5.6). In the embryonic stage (3-8 dpf), the dorsal vessels could not be imaged and hence Figure 5.6A shows only the area reduction of the caudal vessels from 3 dpf to 7 dpf. The veins and arteries are not differentiated at 3 dpf (633.1 μm^2) and 4 dpf (459.7 μm^2) as evident from the similar mean cross-sectional areas. From 5 dpf (CV: 411.7 μm^2; CA: 213.7 μm^2) to 7 dpf (CV: 373.1 μm^2; CA: 145.2 μm^2) the caudal artery reduces faster in area than the caudal vein. At 8 dpf, as the embryo prepares to hatch by decompressing and the areas increase slightly (CV: 475.1 μm^2; CA: 169.6 μm^2). The caudal vessels continue to decrease in cross-section from 9 dpf (CV: 452.2 μm^2; CA: 169.6 μm^2) to 14 dpf (CV: 248.7 μm^2; CA: 80.1 μm^2) as seen in Figure 5.6B. The DA and DV, located upstream of the CA and CV respectively, depict the same trend of area variation with cross-section but interestingly at each time point the dorsal vessel areas are larger than the caudal vessel areas (Figure 5.6B).

The velocity and WSS variation in the vessels over time reflects the effect of vessel area variation with time (Figure 5.7). The pulsatility in the veins are dampened faster over time than the arteries. After hatching, a time-dependent flow continues in the CA while the CV exhibits steady flow. The peak velocity magnitude remains similar for both CA and CV from 3-5 dpf (Figure 5.7A). The peak WSS in the CA and CV are similar at 3 dpf and 4 dpf. At 5 dpf the peak WSS is slightly higher in the CA than the CV (Figure 5.7B). At 6 dpf, both the peak velocity and peak WSS magnitude of the CA are considerably increased, followed by a decline at 7 dpf and subsequent slight increase at 8 dpf. This increase in velocity corresponds to the increase in cross-

sectional area of the CA. Interestingly, the peak velocity and peak WSS of the CV progressively decreases from 6-8 dpf as it undergoes a less drastic change in cross-section. After hatching the velocity and WSS of the DA and DV are higher than the CA and CV respectively (the difference is greater for the arteries at 9 dpf and 12 dpf). There is no trend in the variation of peak values from 11-14 dpf. It is interesting to note that the arterial flows are subjected to low WSS during most of the cycle from 3-8 dpf even though peak values are higher. WSS values <10 dynes/cm^2 for unsteady flows and WSS values < 1 dynes/cm^2 for steady flows are known to cause cell proliferation and vascular remodeling along endothelial layers of the vasculature (51). Post-hatch the baseline WSS in the CA and DA at each time point are at least 15 dynes/cm^2, indicating stable flow-structure dynamics in the tail vessels.

5.4.5 Gene expression and cardiac morphology

PCR efficiencies for all primers were ≥ 88.6% with an $R^2 \geq 0.86$. The relative expression of five cardiac specific genes (*fgf8, hoxb6b, nkx2.5, bmp4, smyd1*) across developmental time are plotted in Figure 5.8. Statistical significance between each pair of time points were compared for each gene individually. A sequentially varying control was chosen for these tests instead of a fixed control due to absence of a baseline cardiac event occurring at a fixed dpf. For each gene plot, days not connected by the same letter are significantly different. Elevated levels of expression of *smyd1*, *hoxb6b* and *nkx2.5* at 0.5 dpf may be attributed to the maternal influences on the embryo (99-102). Relative expression of all genes increased significantly at 3 dpf and 7 dpf.

The embryonic medaka heart dynamically develops from a linear tube to chambered heart with valve cushions at inflow and outflow of chambers. Different feedback loops between flow induced forces and gene expressions impact cellular rearrangement throughout cardiac

morphogenesis. The timing of these changes in gene expression corresponds well with known ontogenetic events such as cardiac cushion formation and cardiac remodeling events including chamber differentiation, trabeculation, and valvulogenesis (15, 42, 45, 103). Particularly, *nkx2.5, fgf8, and bmp4* are important molecular signals involved in the endocardial-mesenchymal transition (EMT) that precedes the formation of cardiac cushions at 5 dpf as well as during cardiac remodeling processes such as valve leaflet formation and eventual completion of valvulogenesis post hatch (45, 104-106). Early upregulation of *fgf8* was expected as it is required for signaling the development of cardiac precursors during cardiomyocyte differentiation that ultimately coalesce to form the outflow tract at the arterial pole of the ventricle (65, 107). Increases in expression of *smyd1* follow predictable trends with increases at the onset of blood circulation at 3 dpf and cardiac remodeling events as this gene is important in cardiac muscle differentiation and cardiac muscle contraction (65, 70). Finally, elevated expression of *hoxb6b* – a gene important in cardiac morphogenesis and morphological patterning (67) – intuitively undergoes increases in expression during periods of morphological change in the cardiac system such as cardiac looping (2.5 dpf), chamber differentiation (3 dpf), and cardiac remodeling post-hatch (42). The extent of flexion in the atrioventricular region is at maximum during 6dpf to 7dpf (65) and all gene undergoing a second, transient upregulation at 7dpf may be a manifestation of this cardiac event.

5.4.6 Correlation between peak WSS and cardiac gene expression during development

Peak WSS was non-invasively quantified in the heart and tail vessels of the embryonic and larval medaka and compared with the expressions of five cardiac genes (Figure 5.9). Figure 5.9A shows the expressions of five cardiac genes. Both the WSS-AVC and WSS-OFT increase significantly at 6 dpf likely representing a functional change in response to the genetic changes

observed at 3 dpf (Figure 5.9B). As noted previously, possible invagination of endocardial cells in the AVC region at 6dpf narrows the valvular area leading to an increase in the wall velocity gradient and the peak WSS. Similar results have been reported in developing zebrafish (108, 109). With concentric chamber growth in subsequent time points, the valve regions expand resulting in the reduction and plateau of peak WSS. An interesting difference from zebrafish is that the AVC formation in zebrafish depends on retrograde flows more than on the magnitude of WSS (7). The opposite is seen in this work where there is a drastic increase in peak WSS in the medaka AVC and OFT but little to no retrograde flow occurring at 6-7 dpf. Figure 5.9C compares the peak WSS in tail vessels (CA, DA, CV and DV) varying with time. The CV peak WSS follows the trend expressed in the CA until 5 dpf, before decreasing and eventually plateauing between 7 dpf and 14 dpf. The peak WSS is similar in magnitude at both the DV and the CV after hatching. The peak WSS in the CA displays the same trend as that in the AVC and OFT from 3-8 dpf. Post-hatch, the peak WSS continues to increase (owing to the progressive reduction in vessel cross-section with time) in both the DA and CA. The WSS is higher in the DA than in the CA from 9-12 dpf but is same at 13-14 dpf. Summarizing the trends in Figure 5.9, we observe that gene expression spikes at 3 dpf and 7 dpf are followed by an increase in peak WSS in ventricle inflow (AVC), outflow (OFT) and the tail CA at 6 dpf and 10-11 dpf respectively.

The changes in gene expression at 3dpf, followed by increased WSS at 6 dpf correspond well with the formation of cardiac cushions within the Japanese medaka. The timing of cushion formation and valve remodeling have been well described in the zebrafish model (1.75 dpf (44, 106) and 5 dpf (15) respectively). However, descriptions of these cardiac events are sparse for the Japanese medaka - a literature review uncovered information pertaining only to the timing of

the cushion formation (5 dpf) (43, 46) but no information regarding the timing of valve remodeling for the species. Additionally, there have been several studies that have shown the interplay between increased WSS and the initiation of vascular/ cardiac remodeling - including processes such as trabeculation and valvulogenesis in zebrafish, mice, and chick embryos (37, 110-112). Based on the relationship between increased gene expression at 7 dpf and increased WSS data at 10-11 dpf presented in this study as well as analogous timing in post-hatch zebrafish development, it can be inferred that valve formation in Japanese medaka occurs at or around 10-11 dpf although additional studies need to be conducted to verify this timing.

5.4.7 Effect of WSS magnitude and retrograde flow on cardiac morphology

Previous research in zebrafish have shown the importance of shear forces in cardiac tissue remodeling (6) at each stage of its cardiac development (14, 32, 36, 60, 109, 113). Unfortunately for medaka, there is little in-depth study that clearly demarcates onset of cellular processes like EMT, trabeculation, and valve formation in absence of perturbation. So, we compared cardiac events of medaka with zebrafish in Table 5.1 and assumed similar cellular mechanisms regulate cardiac development in both species. A linear heart tube is seen from 3 dpf to 5 dpf where low velocity pulsatile flows occur in a single direction and there is no sharp demarcation between atrium and ventricle. Lower WSS in these stages (95) (Figure 5.5) with concomitant cardiac looping trigger trabeculation (10, 114-116) although it is not evident from the imaging in this study. Large WSS values, as observed at 6 dpf, are known to promote expansion of extracellular matrix and EMT that leads to invagination of cardiac cells (28). Endocardial cushion formation due to invagination of endocardial cells previously seen in the AVC region of zebrafish (108, 109) narrows the valvular area leading to an increase in the wall velocity gradient and the peak WSS at 6 dpf. A similar trend of inflection for the peak WSS in the OFT and aortic arch was

previously reported during cardiac development of chick embryos (40, 41). The AVC formation in zebrafish depends on retrograde flows more than on the magnitude of WSS (5, 7). A weak retrograde flow is observed in the medaka AVC and OFT (Figure 5.4) at 3 dpf, 4 dpf and 5 dpf which maybe within measurement error. The retrograde flow WSS increases considerably at the AVC during 6 dpf and at the OFT during 7dpf. With concentric chamber growth in the following time points (7 dpf-8 dpf), the AVC and OFT regions expand further due to which the peak WSS reduces. After hatching, the pericardium continues to thicken thereby narrowing the AVC and OFT further. There are no valve leaflets formed as evident from the moderate retrograde flows from 9 dpf to 14 dpf (Figures 5.4 & 5.5).

5.4.8 Relation of cardiac flow with vascular flow over time

Viscous forces and changing wall boundaries are the catalysts for the cardiovascular development in teleost embryos. Unlike cardiac vasculature in higher vertebrates, flow rates are so small in growing medaka ($Re << 1$) that there is no inertial contribution to facilitate morphological changes. The medaka heart starts pulsating at stage 24 (1 day 20 h) and a primitive vascular network is present (42, 51). At 2 days 2 hr post fertilization, the valveless heart behaves like an impedance pump (10, 117) and pushes the blood at 78.5±2 beats per minute into the vasculature. The CA and CV have same diameters in this stage and exhibit the same low flow velocities (0.58 mm/s) with high pulsatility. The low vascular WSS values (<10 dynes/cm^2) in conjunction with chemical stimuli are known to cause red blood cell agglomeration and perfusion that leads to self-angiogenesis (118-120). The vascular feedback around 5 dpf causes a prominent cardiac looping in the heart. Due to this, the chambers are separated by well-defined narrow valveless regions that alters the pulsatility rate and mechanism (10). The increased pulsatility drives higher flow velocities into the vasculature from 5 dpf to 8 dpf. The vessel

diameters reduce to accommodate the altered flow within a compressed embryo (11). The CV, the primary vessel returning blood to the heart suffers less diameter reduction than the CA carrying blood from the heart. During hatching from 8 dpf to 9 dpf, the caudal vessels mildly increase in cross-section owing to decompression. The vessel cross-section reduction from 9 dpf to 14 dpf is also evident along its axial location on the tail (from DA to CA). At these stages, the heart has well-defined chambers surrounded by a visibly thick pericardium. The OFT and dorsal aorta act as capacitors downstream of the cardiac flow that dampen the flow pulsatility in vessels that are farthest from the heart (9, 10). The topology of the vasculature like vessel curvature, bifurcations, and network organizations dynamically alter mechanical cues that regulate perfusion throughout the cardiovascular system. Investigating all types of stimuli (chemical, electrical, topological, cellular) and their inter-relationships in a developing cardiovascular system is beyond the scope of this study. Instead, this study highlights for the first time, the occurrence of peak vascular WSS in the CA concomitant to the cardiac AVC and OFT WSS peaks at 6 dpf signaling a major cardiac event when cardiac looping, chamber ballooning and expansion takes place (Figure 5.9).

5.5 Conclusions

To our knowledge, this work is the first to report peak WSS values in the AVC and OFT of a developing Japanese medaka from 3 dpf (onset of blood circulation) to 14 dpf. The influence of the cardiac flow on the vascular geometry and WSS downstream were concomitantly explored. This type of longitudinal study over a significant period of cardiovascular development relating the WSS to gene-expressions is scarce in all vertebrates. Contrary to intuition, the tail vessels experienced a reduction in cross-sectional area with age progression. Caudal vessels that are further away from the heart underwent a greater reduction than the dorsal vessels. The salient

feature that stood out from the longitudinal analysis of peak-WSS variation with age is the existence of inflection points instead of a monotonic trend. These inflection points in WSS are preceded by inflection in the expression of cardiac genes at earlier time points. The temporal expressions of these genes correspond with important developmental landmarks in the cardiac morphogenesis like valve area formation, chamber looping, and chamber growth. Thus, identification of these unique trends in the mechano-genetic tapestry of a developing cardiovascular teleost model will provide a baseline framework for future studies that can test causality between gene expression and WSS variations. This baseline framework can be validated by exposing the medaka to cardiotoxic environments. The validated framework can be tested by probing the mechano-genetic evolution in higher vertebrate models. Once the mechano-genetic correlation is established, clinical trials on humans can improve the diagnostic capability and assess the sensitivity of the cardiac tissue damage.

5.6 References

1. Davies PF, Civelek M, Fang Y, Fleming I. The atherosusceptible endothelium: endothelial phenotypes in complex haemodynamic shear stress regions in vivo. Cardiovasc Res. 2013;99(2):315-27.

2. Conway DE, Breckenridge MT, Hinde E, Gratton E, Chen CS, Schwartz MA. Fluid shear stress on endothelial cells modulates mechanical tension across VE-cadherin and PECAM-1. Curr Biol. 2013;23(11):1024-30.

3. Tzima E, Irani-Tehrani M, Kiosses WB, Dejana E, Schultz DA, Engelhardt B, et al. A mechanosensory complex that mediates the endothelial cell response to fluid shear stress. Nature. 2005;437(7057):426-31.

4. Mahler GJ, Frendl CM, Cao Q, Butcher JT. Effects of shear stress pattern and magnitude on mesenchymal transformation and invasion of aortic valve endothelial cells. Biotechnol Bioeng. 2014;111(11):2326-37.

5. Heckel E, Boselli F, Roth S, Krudewig A, Belting HG, Charvin G, et al. Oscillatory Flow Modulates Mechanosensitive klf2a Expression through trpv4 and trpp2 during Heart Valve Development. Curr Biol. 2015;25(10):1354-61.

6. Hove JR, Koster RW, Forouhar AS, Acevedo-Bolton G, Fraser SE, Gharib M. Intracardiac fluid forces are an essential epigenetic factor for embryonic cardiogenesis. Nature. 2003;421(6919):172-7.

7. Vermot J, Forouhar AS, Liebling M, Wu D, Plummer D, Gharib M, et al. Reversing blood flows act through klf2a to ensure normal valvulogenesis in the developing heart. PLoS Biol. 2009;7(11):e1000246.

8. Hierck BP, Van der Heiden K, Poelma C, Westerweel J, Poelmann RE. Fluid shear stress and inner curvature remodeling of the embryonic heart. Choosing the right lane! ScientificWorldJournal. 2008;8:212-22.

9. Anton H, Harlepp S, Ramspacher C, Wu D, Monduc F, Bhat S, et al. Pulse propagation by a capacitive mechanism drives embryonic blood flow. Development. 2013;140(21):4426-34.

10. Boselli F, Freund JB, Vermot J. Blood flow mechanics in cardiovascular development. Cell Mol Life Sci. 2015;72(13):2545-59.

11. Bagatto B, Burggren W. A three-dimensional functional assessment of heart and vessel development in the larva of the zebrafish (*danio rerio*). Physiol Biochem Zool. 2006;79(1):194-201.

12. Baek KI, Ding Y, Chang CC, Chang M, Sevag Packard RR, Hsu JJ, et al. Advanced microscopy to elucidate cardiovascular injury and regeneration: 4D light-sheet imaging. Prog Biophys Mol Biol. 2018.

13. Fieramonti L, Foglia EA, Malavasi S, D'Andrea C, Valentini G, Cotelli F, et al. Quantitative measurement of blood velocity in zebrafish with optical vector field tomography. J Biophotonics. 2015;8(1-2):52-9.

14. Garita B, Jenkins MW, Han M, Zhou C, Vanauker M, Rollins AM, et al. Blood flow dynamics of one cardiac cycle and relationship to mechanotransduction and trabeculation during heart looping. Am J Physiol Heart Circ Physiol. 2011;300(3):H879-91.

15. Hu N, Sedmera D, Yost HJ, Clark EB. Structure and function of the developing zebrafish heart. Anat Rec. 2000;260(2):148-57.

16. Schwerte T, Fritsche R. Understanding cardiovascular physiology in zebrafish and *xenopus* larvae: the use of microtechniques. Comp Biochem Physiol A Mol Integr Physiol. 2003;135(1):131-45.

17. Taylor JM, Girkin JM, Love GD. High-resolution 3D optical microscopy inside the beating zebrafish heart using prospective optical gating. Biomed Opt Express. 2012;3(12):3043-53.

18. Choi W, Kim HM, Park S, Yeom E, Doh J, Lee SJ. Variation in wall shear stress in channel networks of zebrafish models. J R Soc Interface. 2017;14(127).

19. Donnarumma D, Brodoline A, Alexandre D, Gross M. 4D holographic microscopy of zebrafish larvae microcirculation. Opt Express. 2016;24(23):26887-900.

20. Brette F, Shiels HA, Galli GL, Cros C, Incardona JP, Scholz NL, et al. A Novel Cardiotoxic Mechanism for a Pervasive Global Pollutant. Sci Rep. 2017;7:41476.

21. Huang L, Xi Z, Wang C, Zhang Y, Yang Z, Zhang S, et al. Phenanthrene exposure induces cardiac hypertrophy via reducing miR-133a expression by DNA methylation. Sci Rep. 2016;6:20105.

22. Mu J, Wang J, Jin F, Wang X, Hong H. Comparative embryotoxicity of phenanthrene and alkyl-phenanthrene to marine medaka (*oryzias melastigma*). Mar Pollut Bull. 2014;85(2):505-15.

23. Zhang Y, Huang L, Wang C, Gao D, Zuo Z. Phenanthrene exposure produces cardiac defects during embryo development of zebrafish (*danio rerio*) through activation of MMP-9. Chemosphere. 2013;93(6):1168-75.

24. Zhang Z, Yan Q. Comparative toxicity of different crude oils on the cardiac function of marine medaka (*oryzias melastigma*) embryo. International Journal Bioautomation. 2014;18(4):389-96.

25. Padmanabhan A, Lee JS, Ismat FA, Lu MM, Lawson ND, Kanki JP, et al. Cardiac and vascular functions of the zebrafish orthologues of the type I neurofibromatosis gene NFI. Proc Natl Acad Sci U S A. 2009;106(52):22305-10.

26. Matrone G, Wilson KS, Mullins JJ, Tucker CS, Denvir MA. Temporal cohesion of the structural, functional and molecular characteristics of the developing zebrafish heart. Differentiation. 2015;89(5):117-27.

27. Poelmann RE, Gittenberger-de Groot AC, Hierck BP. The development of the heart and microcirculation: role of shear stress. Med Biol Eng Comput. 2008;46(5):479-84.

28. Lindsey SE, Butcher JT, Yalcin HC. Mechanical regulation of cardiac development. Front Physiol. 2014;5:318.

29. Boselli F, Vermot J. Live imaging and modeling for shear stress quantification in the embryonic zebrafish heart. Methods. 2016;94:129-34.

30. Jamison RA, Samarage CR, Bryson-Richardson RJ, Fouras A. In vivo wall shear measurements within the developing zebrafish heart. PLoS One. 2013;8(10):e75722.

31. Lee J, Moghadam ME, Kung E, Cao H, Beebe T, Miller Y, et al. Moving domain computational fluid dynamics to interface with an embryonic model of cardiac morphogenesis. PLoS One. 2013;8(8):e72924.

32. Bulk A, Bark D, Jr., Johnson B, Garrity D, Dasi LP. Mechanisms influencing retrograde flow in the atrioventricular canal during early embryonic cardiogenesis. J Biomech. 2016;49(14):3162-7.

33. Hsu JJ, Vedula V, Baek KI, Chen C, Chen J, Chou MI, et al. Contractile and hemodynamic forces coordinate Notch1b-mediated outflow tract valve formation. JCI Insight. 2019;5.

34. Paolini A, Abdelilah-Seyfried S. The mechanobiology of zebrafish cardiac valve leaflet formation. Curr Opin Cell Biol. 2018;55:52-8.

35. Steed E, Boselli F, Vermot J. Hemodynamics driven cardiac valve morphogenesis. Biochim Biophys Acta. 2016;1863(7 Pt B):1760-6.

36. Bark DL, Jr., Johnson B, Garrity D, Dasi LP. Valveless pumping mechanics of the embryonic heart during cardiac looping: Pressure and flow through micro-PIV. J Biomech. 2017;50:50-5.

37. Yalcin HC, Amindari A, Butcher JT, Althani A, Yacoub M. Heart function and hemodynamic analysis for zebrafish embryos. Dev Dyn. 2017;246(11):868-80.

38. Combs MD, Yutzey KE. Heart valve development: regulatory networks in development and disease. Circ Res. 2009;105(5):408-21.

39. Singleman C, Holtzman NG. Analysis of postembryonic heart development and maturation in the zebrafish, *danio rerio*. Dev Dyn. 2012;241(12):1993-2004.

40. Midgett M, Chivukula VK, Dorn C, Wallace S, Rugonyi S. Blood flow through the embryonic heart outflow tract during cardiac looping in HH13–HH18 chicken embryos. Journal of The Royal Society Interface. 2015;12(111):20150652.

41. Karakaya C, Goktas S, Celik M, Kowalski WJ, Keller BB, Pekkan K. Asymmetry in Mechanosensitive Gene Expression during Aortic Arch Morphogenesis. Sci Rep. 2018;8(1):16948.

42. Iwamatsu T. Stages of normal development in the medaka *oryzias latipes*. Mech Dev. 2004;121(7-8):605-18.

43. Taneda Y, Konno S, Makino S, Morioka M, Fukuda K, Imai Y, et al. Epigenetic control of cardiomyocyte production in response to a stress during the medaka heart development. Dev Biol. 2010;340(1):30-40.

44. Kimmel CB, Ballard WW, Kimmel SR, Ullmann B, Schilling TF. Stages of embryonic development of the zebrafish. Developmental Dynamics. 1995;203:253-310.

45. de Vlaming A, Sauls K, Hajdu Z, Visconti R, Nagy Mehesz A, Levine RA, Slaugenhaupt SA, Hagège A, Chester A, Markwald RR, Norris RA. Differentiation. 2012; 84(1):103-116.

46. Watanabe-Asaka T, Sekiya Y, Wada H, Yasuda T, Okubo I, Mitani H. Regular heartbeat rhythm at the heartbeat initiation stage is essential for normal cardiogenesis at low temperature. BMC Dev Biol. 2014; 14(12):1-13.

47. Parker T, Libourel PA, Hetheridge MJ, Cumming RI, Sutcliffe TP, Goonesinghe AC, et al. A multi-endpoint in vivo larval zebrafish (*danio rerio*) model for the assessment of integrated cardiovascular function. J Pharmacol Toxicol Methods. 2014;69(1):30-8.

48. Schwerte T, Pelster B. Digital motion analysis as a tool for analysing the shape and performance of the circulatory system in transparent animals. J Exp Biol. 2000;203(Pt 11):1659-69.

49. Watkins SC, Maniar S, Mosher M, Roman BL, Tsang M, St Croix CM. High resolution imaging of vascular function in zebrafish. PLoS One. 2012;7(8):e44018.

50. Lee SJ, Choi W, Seo E, Yeom E. Association of early atherosclerosis with vascular wall shear stress in hypercholesterolemic zebrafish. PLoS One. 2015;10(11):e0142945.

51. Fujita M, Isogai S, Kudo A. Vascular anatomy of the developing medaka, *oryzias latipes*: a complementary fish model for cardiovascular research on vertebrates. Dev Dyn. 2006;235(3):734-46.

52. Ando J, Nomura H, Kamiya A. The effect of fluid shear stress on the migration and proliferation of cultured endothelial cells. Microvasc Res. 1987;33(1):62-70.

53. Peiffer V, Sherwin SJ, Weinberg PD. Does low and oscillatory wall shear stress correlate spatially with early atherosclerosis? A systematic review. Cardiovasc Res. 2013;99(2):242-50.

54. Cecchi E, Giglioli C, Valente S, Lazzeri C, Gensini GF, Abbate R, et al. Role of hemodynamic shear stress in cardiovascular disease. Atherosclerosis. 2011;214(2):249-56.

55. Davies PF. Hemodynamic shear stress and the endothelium in cardiovascular pathophysiology. Nat Clin Pract Cardiovasc Med. 2009;6(1):16-26.

56. Sugii Y, Nishio S, Okamoto K. In vivo PIV measurement of red blood cell velocity field in microvessels considering mesentery motion. Physiol Meas. 2002;23(2):403-16.

57. Nakano A, Sugii Y, Minamiyama M, Niimi H. Measurement of red cell velocity in microvessels using particle image velocimetry (PIV). Clin Hemorheol Microcirc. 2003;29(3-4):445-55.

58. Miller LA. Fluid dynamics of ventricular filling in the embryonic heart. Cell Biochem Biophys. 2011;61(1):33-45.

59. Lee J, Chou TC, Kang D, Kang H, Chen J, Baek KI, et al. A rapid capillary-pressure driven micro-channel to demonstrate newtonian fluid behavior of zebrafish blood at high shear rates. Sci Rep. 2017;7(1):1980.

60. Lee J, Fei P, Packard RR, Kang H, Xu H, Baek KI, et al. 4-Dimensional light-sheet microscopy to elucidate shear stress modulation of cardiac trabeculation. J Clin Invest. 2016;126(5):1679-90.

61. Lucitti JL, Jones EA, Huang C, Chen J, Fraser SE, Dickinson ME. Vascular remodeling of the mouse yolk sac requires hemodynamic force. Development. 2007;134(18):3317-26.

62. Teichert AM, Scott JA, Robb GB, Zhou YQ, Zhu SN, Lem M, et al. Endothelial nitric oxide synthase gene expression during murine embryogenesis: commencement of expression in the embryo occurs with the establishment of a unidirectional circulatory system. Circ Res. 2008;103(1):24-33.

63. Udan RS, Vadakkan TJ, Dickinson ME. Dynamic responses of endothelial cells to changes in blood flow during vascular remodeling of the mouse yolk sac. Development. 2013;140(19):4041-50.

64. Reifers F, Walsh EC, Leger S, Stainier DY, Brand M. Induction and differentiation of the zebrafish heart requires fibroblast growth factor 8 (fgf8/acerebellar). Development. 2000;127(2):225-35.

65. Huang Q, Fang C, Wu X, Fan J, Dong S. Perfluorooctane sulfonate impairs the cardiac development of a marine medaka (*oryzias melastigma*). Aquat Toxicol. 2011;105(1-2):71-7.

66. Ilagan R, Abu-Issa R, Brown D, Yang YP, Jiao K, Schwartz RJ, et al. Fgf8 is required for anterior heart field development. Development. 2006;133(12):2435-45.

67. Kashiwada S, Ariza ME, Kawaguchi T, Nakagame Y, Jayasinghe BS, Gartner K, et al. Silver nanocolloids disrupt medaka embryogenesis through vital gene expressions. Environ Sci Technol. 2012;46(11):6278-87.

68. George V, Colombo S, Targoff KL. An early requirement for nkx2.5 ensures the first and second heart field ventricular identity and cardiac function into adulthood. Dev Biol. 2015;400(1):10-22.

69. Guner-Ataman B, Paffett-Lugassy N, Adams MS, Nevis KR, Jahangiri L, Obregon P, et al. Zebrafish second heart field development relies on progenitor specification in anterior lateral plate mesoderm and nkx2.5 function. Development. 2013;140(6):1353-63.

70. Tan X, Rotllant J, Li H, De Deyne P, Du SJ. SmyD1, a histone methyltransferase, is required for myofibril organization and muscle contraction in zebrafish embryos. Proc Natl Acad Sci U S A. 2006;103(8):2713-8.

71. Chatterjee A. An introduction to the proper orthogonal decomposition. Current science. 2000:808-17.

72. Bernero S, Fiedler H. Application of particle image velocimetry and proper orthogonal decomposition to the study of a jet in a counterflow. Experiments in Fluids. 2000;29:S274-S81.

73. Druault P, Guibert P, Alizon F. Use of proper orthogonal decomposition for time interpolation from PIV data. Experiments in Fluids. 2005;39(6):1009-23.

74. Kefayati S, Poepping TL. Transitional flow analysis in the carotid artery bifurcation by proper orthogonal decomposition and particle image velocimetry. Med Eng Phys. 2013;35(7):898-909.

75. Willert CE, Gharib M. Digital particle image velocimetry. Experiments in Fluids. 1991;10(4):181-93.

76. Eckstein A, Vlachos PP. Assessment of advanced windowing techniques for digital particle image velocimetry (DPIV). Measurement Science and Technology. 2009;20(7):075402.

77. Scarano F. Iterative image deformation methods in PIV. Measurement Science and Technology. 2001;13(1):R1.

78. Astarita T. Analysis of weighting windows for image deformation methods in PIV. Experiments in Fluids. 2007;43(6):859-72.

79. Meinhart CD, Wereley ST, Santiago JG. A PIV algorithm for estimating time-averaged velocity fields. J Fluids Eng. 2000;122(2):285-9.

80. Kähler CJ, Scharnowski S, Cierpka C. On the uncertainty of digital PIV and PTV near walls. Experiments in Fluids. 2012;52(6):1641-56.

81. Westerweel J, Scarano F. Universal outlier detection for PIV data. Experiments in Fluids. 2005;39(6):1096-100.

82. Shinneeb A, Bugg J, Balachandar R. Variable threshold outlier identification in PIV data. Measurement Science and Technology. 2004;15(9):1722.

83. Vlachos P. https://sourceforge.net/projects/qi-tools/ 2010.

84. Xue Z, Charonko JJ, Vlachos PP. Particle image pattern mutual information and uncertainty estimation for particle image velocimetry. Measurement Science and Technology. 2015;26(7):074001.

85. Hund S, Kameneva M, Antaki J. A quasi-mechanistic mathematical representation for blood viscosity. Fluids. 2017;2(1):10.

86. Etebari A, Vlachos PP. Improvements on the accuracy of derivative estimation from DPIV velocity measurements. Experiments in Fluids. 2005;39(6):1040-50.

87. Pfaffl MW. A new mathematical model for relative quantification in real-time RT-PCR. Nucleic Acids Res. 2001;29(9):e45.

88. Doubilet PM, Benson CB. Embryonic heart rate in the early first trimester: what rate is normal? J Ultrasound Med. 1995;14(6):431-4.

89. Yu Q, Leatherbury L, Tian X, Lo CW. Cardiovascular assessment of fetal mice by in utero echocardiography. Ultrasound Med Biol. 2008;34(5):741-52.

90. De Luca E, Zaccaria GM, Hadhoud M, Rizzo G, Ponzini R, Morbiducci U, et al. ZebraBeat: a flexible platform for the analysis of the cardiac rate in zebrafish embryos. Sci Rep. 2014;4:4898.

91. Santhanakrishnan A, Miller LA. Fluid dynamics of heart development. Cell Biochem Biophys. 2011;61(1):1-22.

92. Fung Y-c. Biomechanics: motion, flow, stress, and growth: Springer Science & Business Media; 2013.

93. Nakamura M, Wada S, Yokosawa S, ISODA H, TAKEDA H, YAMAGUCHI T. Measurement of blood flow in the left ventricle and aorta using clinical 2D cine phase-contrast magnetic resonance imaging. Journal of Biomechanical Science and Engineering. 2007;2(2):46-57.

94. Vasudevan V, Low AJJ, Annamalai SP, Sampath S, Poh KK, Totman T, et al. Flow dynamics and energy efficiency of flow in the left ventricle during myocardial infarction. Biomech Model Mechanobiol. 2017;16(5):1503-17.

95. Yalcin HC, Shekhar A, McQuinn TC, Butcher JT. Hemodynamic patterning of the avian atrioventricular valve. Dev Dyn. 2011;240(1):23-35.

96. Mankad R, McCreery CJ, Rogers W, Weichmann RJ, Savage EB, Reichek N, et al. Regional myocardial strain before and after mitral valve repair for severe mitral regurgitation. Journal of Cardiovascular Magnetic Resonance. 2001;3(3):257-66.

97. Kiserud T, Acharya G. The fetal circulation. Prenat Diagn. 2004;24(13):1049-59.

98. Leiva MC, Tolosa JE, Binotto CN, Weiner S, Huppert L, Denis AL, et al. Fetal cardiac development and hemodynamics in the first trimester. Ultrasound Obstet Gynecol. 1999;14(3):169-74.

99. Mommens M, Fernandes JM, Bizuayehu TT, Bolla SL, Johnston IA, Babiak I. Maternal gene expression in Atlantic halibut (Hippoglossus hippoglossus L.) and its relation to egg quality. BMC Res Notes. 2010;3:138.

100. Nesan D, Vijayan MM. Embryo exposure to elevated cortisol level leads to cardiac performance dysfunction in zebrafish. Mol Cell Endocrinol. 2012;363(1-2):85-91.

101. Seppola M, Johnsen H, Mennen S, Myrnes B, Tveiten H. Maternal transfer and transcriptional onset of immune genes during ontogenesis in Atlantic cod. Dev Comp Immunol. 2009;33(11):1205-11.

102. Lin H, Hsu S, Hwang P. Maternal transfer of cadmium tolerance in larval Oreochromis mossambicus. Journal of Fish Biology. 2000;57(1):239-48.

103. Rasouli SJ, Stainier DYR. Regulation of cardiomyocyte behavior in zebrafish trabeculation by Neureglin 2a signaling. Nature Communincations. 2017; 8:15281.

104. Stainier DYR. Zebrafish genetics and vertebrate heart formation. Nature Reviews Genetics. 2001; 2:39-48.

105. Yelon D. Cardiac patterning and morphogenesis in zebrafish. Developmental Dynamics. 2001; 222:552-563.

106. Glickman NS, Yelon D. Cardiac development in zebrafish: coordination of form and function. Seminars in Cell & Developmental Biology. 2002; 13(6):507–513.

107. Miura GI, Yelon D. A guide to analysis of cardiac phenotypes in the zebrafish embryo. Methods Cell Biol. 2011;101:161-80

108. Haack T, Abdelilah-Seyfried S. The force within: endocardial development, mechanotransduction and signalling during cardiac morphogenesis. Development. 2016;143(3):373-86.

109. Scherz PJ, Huisken J, Sahai-Hernandez P, Stainier DY. High-speed imaging of developing heart valves reveals interplay of morphogenesis and function. Development. 2008;135(6):1179-87.

110. Kowalski WJ, Dur O, Wang Y, Patrick MJ, Tinney JP, Keller BB, Pekkan K. Critical transitions in early embryonic aortic arch patterning and hemodynamics. PLoS One. 2012; 8(3):e60271.

111. Lee J, Vedula V, In Baek K, Chen J, Hsu JJ, Ding Y, Chang C-C, Kang H, Small A, Fei P, Chuong C, Li R, Demer L, Sevag Packard RR, Marsden AL, Hsiai TK. Spatial and temporal variations in hemodynamic forces initiate cardiac trabeculation. JCI Insight. 2018; 3(12):e96672.

112. Ahuja N, Ostwald P, Bark D, Garrity D. Biochemical cues direct valvulogenesis. Journal of Cardiovascular Development and Disease. 2020; 7(18):1-23.

113. Liu J, Stainier DY. Zebrafish in the study of early cardiac development. Circ Res. 2012;110(6):870-4.

114. Goenezen S, Rennie MY, Rugonyi S. Biomechanics of early cardiac development. Biomech Model Mechanobiol. 2012;11(8):1187-204.

115. Peshkovsky C, Totong R, Yelon D. Dependence of cardiac trabeculation on neuregulin signaling and blood flow in zebrafish. Dev Dyn. 2011;240(2):446-56.

116. Sedmera D, Pexieder T, Vuillemin M, Thompson RP, Anderson RH. Developmental patterning of the myocardium. Anat Rec. 2000;258(4):319-37.

117. Forouhar AS, Liebling M, Hickerson A, Nasiraei-Moghaddam A, Tsai HJ, Hove JR, et al. The embryonic vertebrate heart tube is a dynamic suction pump. Science. 2006;312(5774):751-3.

118. Eelen G, Treps L, Li X, Carmeliet P. Basic and Therapeutic Aspects of Angiogenesis Updated. Circ Res. 2020;127(2):310-29.

119. Nicoli S, Standley C, Walker P, Hurlstone A, Fogarty KE, Lawson ND. MicroRNA-mediated integration of haemodynamics and Vegf signalling during angiogenesis. Nature. 2010;464(7292):1196-200.

120. Li J, Hou B, Tumova S, Muraki K, Bruns A, Ludlow MJ, et al. Piezo1 integration of vascular architecture with physiological force. Nature. 2014;515(7526):279-82.

Table 5.1. Comparison of cardiac development times in zebrafish and Japanese medaka

Cardiac Event	Bilateral Heart Formation	Heart Tube Beating	Onset of Chamber Formation	Onset of Cardiac Looping	Cushions Start Forming	Onset of Concentric Chamber Growth	Pericardial Cavity Formation	References
Zebrafish	18 hpf	22 hpf	30 hpf	36 hpf	56 hpf	64 hpf	96 hpf	15, 26, 29, 30, 39, 43, 109, 113
Medaka	38 hpf	44 hpf	54 hpf	64 hpf	120 hpf	120 hpf	168 hpf	42, 43, 46

Table 5.2. List of Japanese medaka primers used for real time PCR. All sequences are 5′ to 3′ and reverse primers are reverse compliments of the genetic sequence.

Gene	NCBI Accession Number	Orientation	Sequence	Product length (bp)	Primer Efficiency (%)
18s *mRNA*	AB105163.1	F	ACTCCGGTTCTATTTTGTGGGTTTT	92	119.1
		R	CTAGCGGCACAATACGAATGC		
fgf8	XM_004076908.3	F	GTGGAGACTGACACATTTGGAA	102	96.9
		R	GTTTTTCTTGCCAATGAGCTTC		
hoxb6b	AB208002.1	F	CGACCCGTTAAGACACTACTCC	182	113.6
		R	CCTCTGCGTCCTTGTAAAAAGT		
nkx2.5	EF206723.1	F	AGCTTTACCTCTGCGTTTTACG	91	92.6
		R	CATCTTTTCCTCGTTCATCCTC		
bmp4	DQ915174.1	F	TTTACAGGGATCAGGTGAAAGG	108	88.6
		R	AAGCAGGAAGTCCAAACATCTC		
smyd1	XM_004072212.3	F	GGCTTATGCTATCCTCATGGTC	194	121.8
		R	CTTCTTCCACAGACTTGGGTTC		

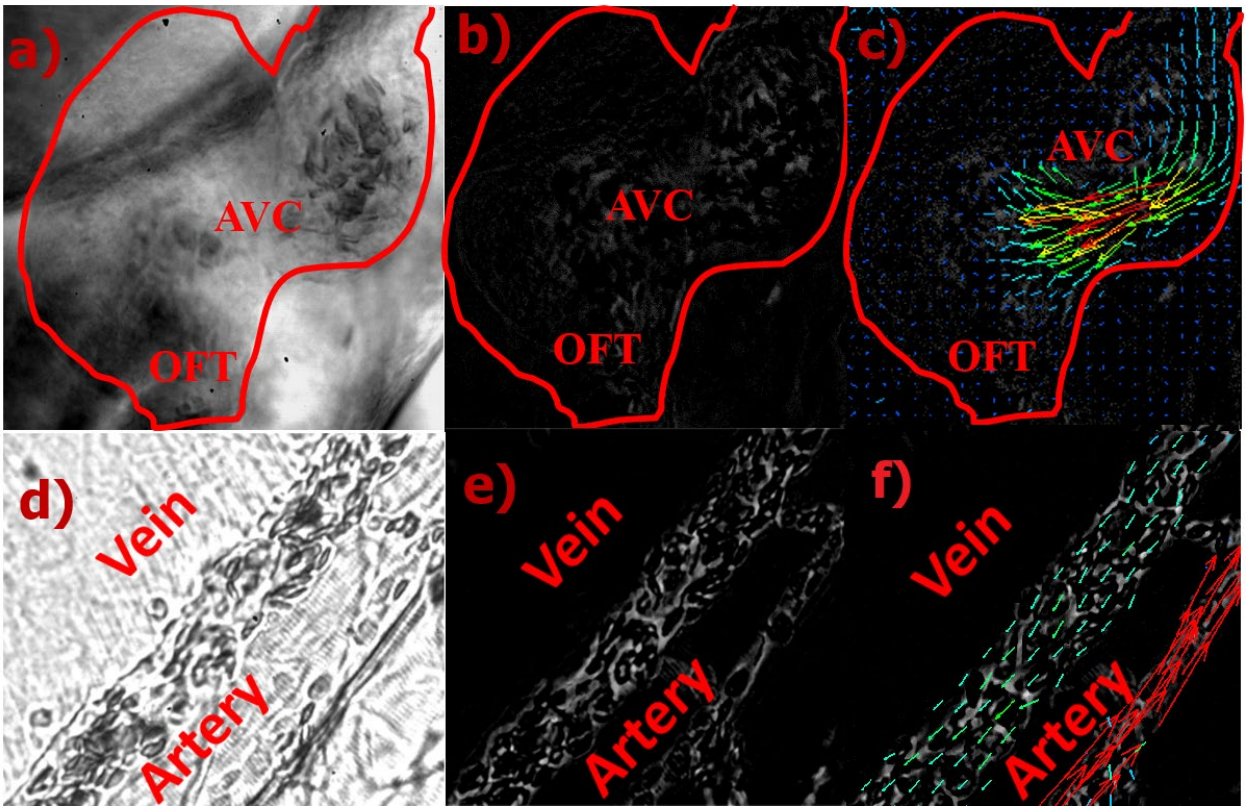

Figure 5.1. Raw images to velocity vector fields. **(A)** raw image **(B)** signal amplified image and **(C)** velocity vectors superimposed on raw image of a 13 dpf Japanese medaka heart during ventricle diastole. AVC = Atrioventricular canal; OFT = ventricle outflow tract. **(D)** raw image **(E)** signal amplified image and **(F)** velocity vectors superimposed on raw image of caudal vein and caudal artery. Red vectors denote higher velocity than green vectors.

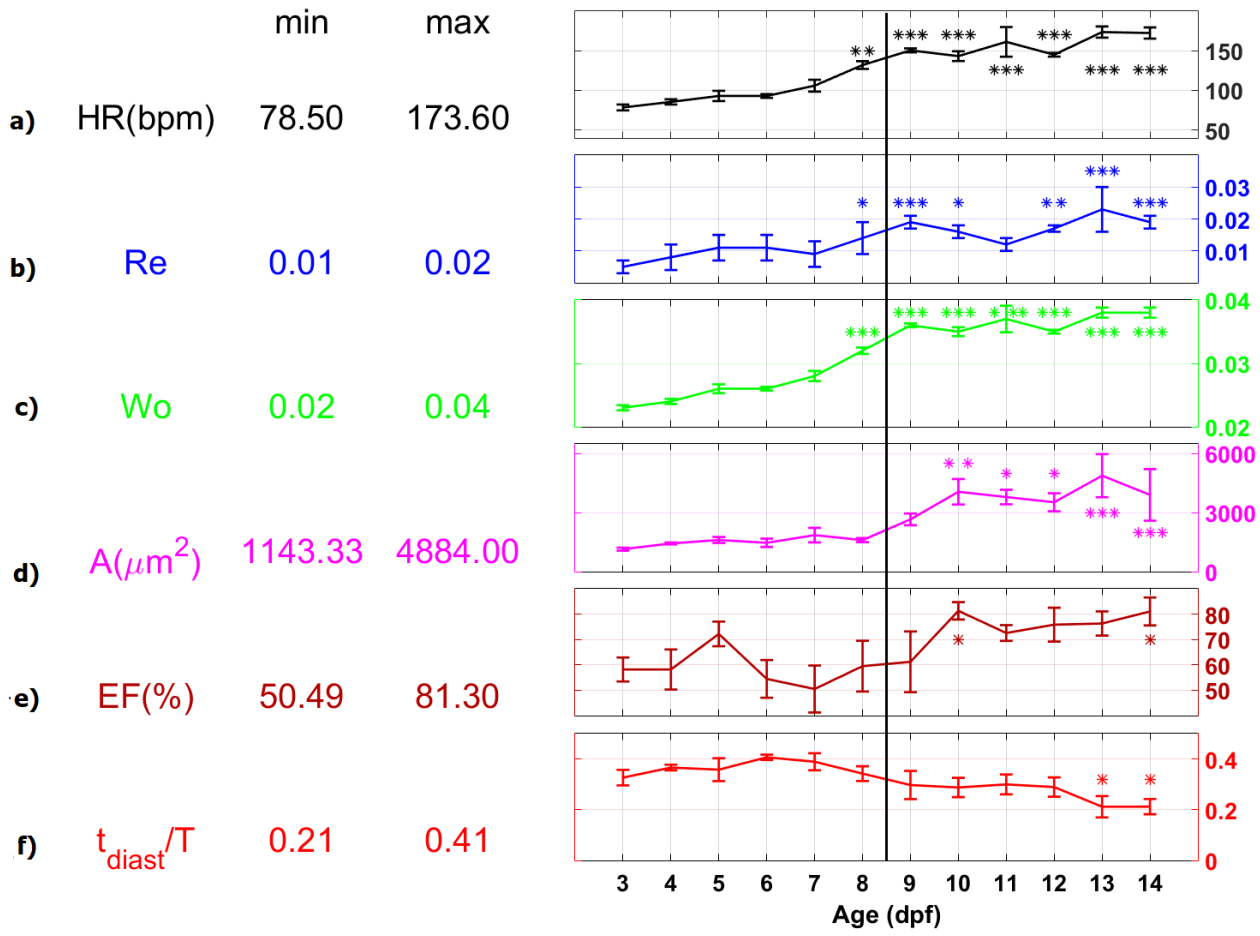

Figure 5.2. Variation of mean **(A)** heart rate (HR), **(B)** Reynolds number (Re) and **(C)** Womersley number (Wo) at atrial inflow, **(D)** end-diastolic ventricle area (A), **(E)** ventricle ejection fraction (EF) and **(F)** fractional ventricle diastolic time (t_{diast}/T) in Japanese medaka over time (dpf). The black vertical line between 8 dpf and 9 dpf denotes hatching. Error bars ± SD. n=5 for each parameter at each dpf. Parameters were compared to 3 dpf values. *** denotes $p < 0.0001$; ** denotes $p < 0.001$; * denotes $p < 0.05$.

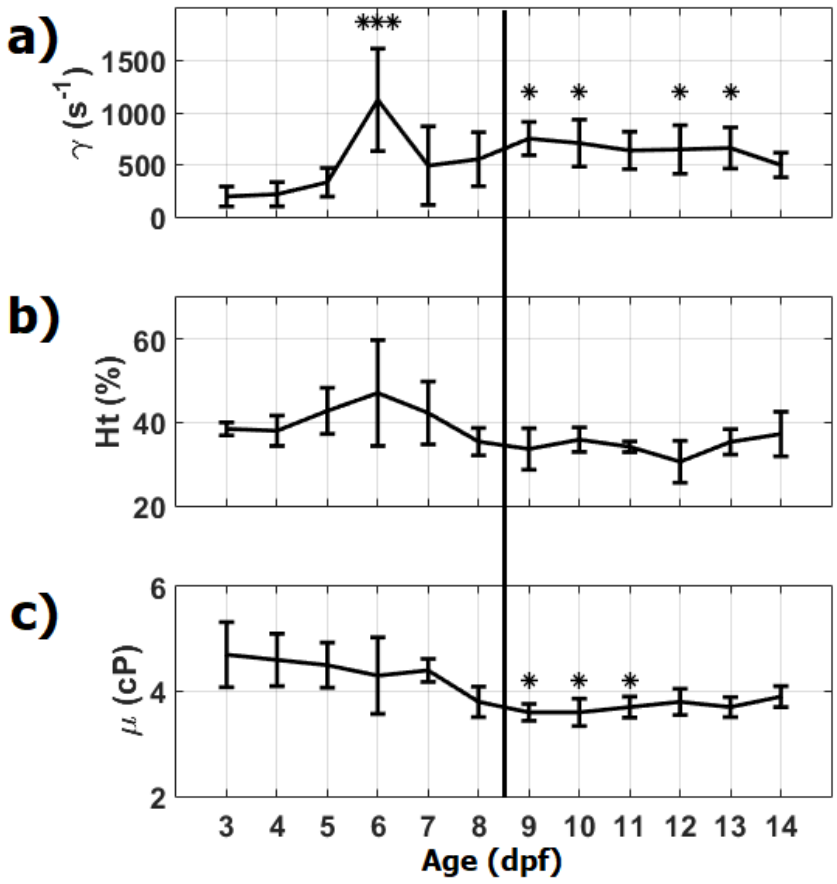

Figure 5.3. Variation of mean **(A)** peak shear rate (γ), **(B)** hematocrit (Ht) and **(C)** blood dynamic viscosity (μ) in ventricle of Japanese medaka over time (dpf). The black vertical line between 8 dpf and 9 dpf denotes hatching. n=5 for each parameter at each dpf. Error bars denote ± SD. Parameters were compared to 3 dpf values. * denotes $p < 0.05$.

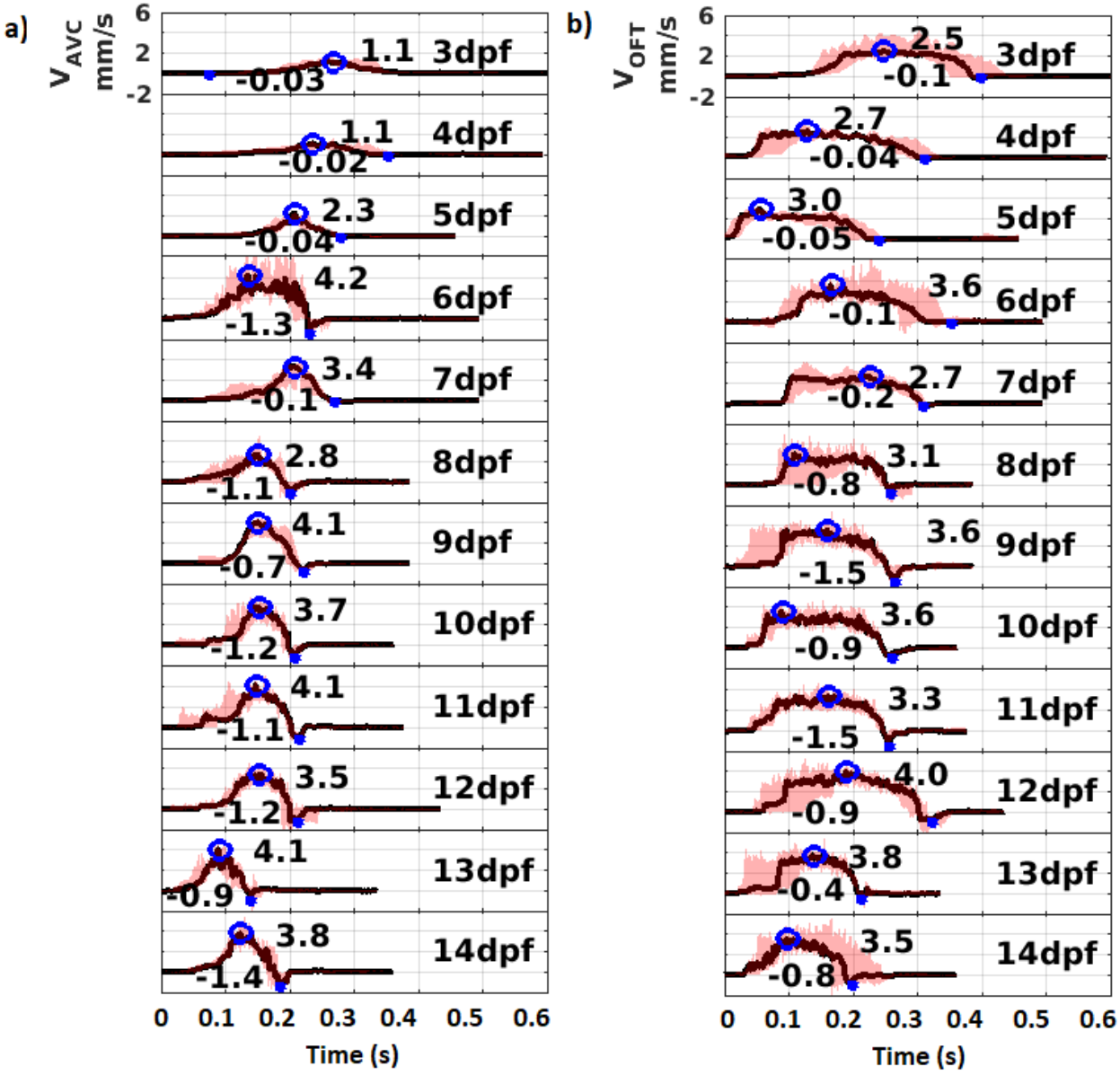

Figure 5.4. Time variation of velocity profiles in the **(A)** atrioventricular canal (AVC) and **(B)** ventricle outflow tract (OFT) of Japanese medaka. Black lines denote the median profiles while the pink shade denotes the region between maximum and minimum profiles. The peak values of the median profile are marked on each plot by a blue circle and the minimum values on the median profile are marked by a blue star. n=5 for each dpf.

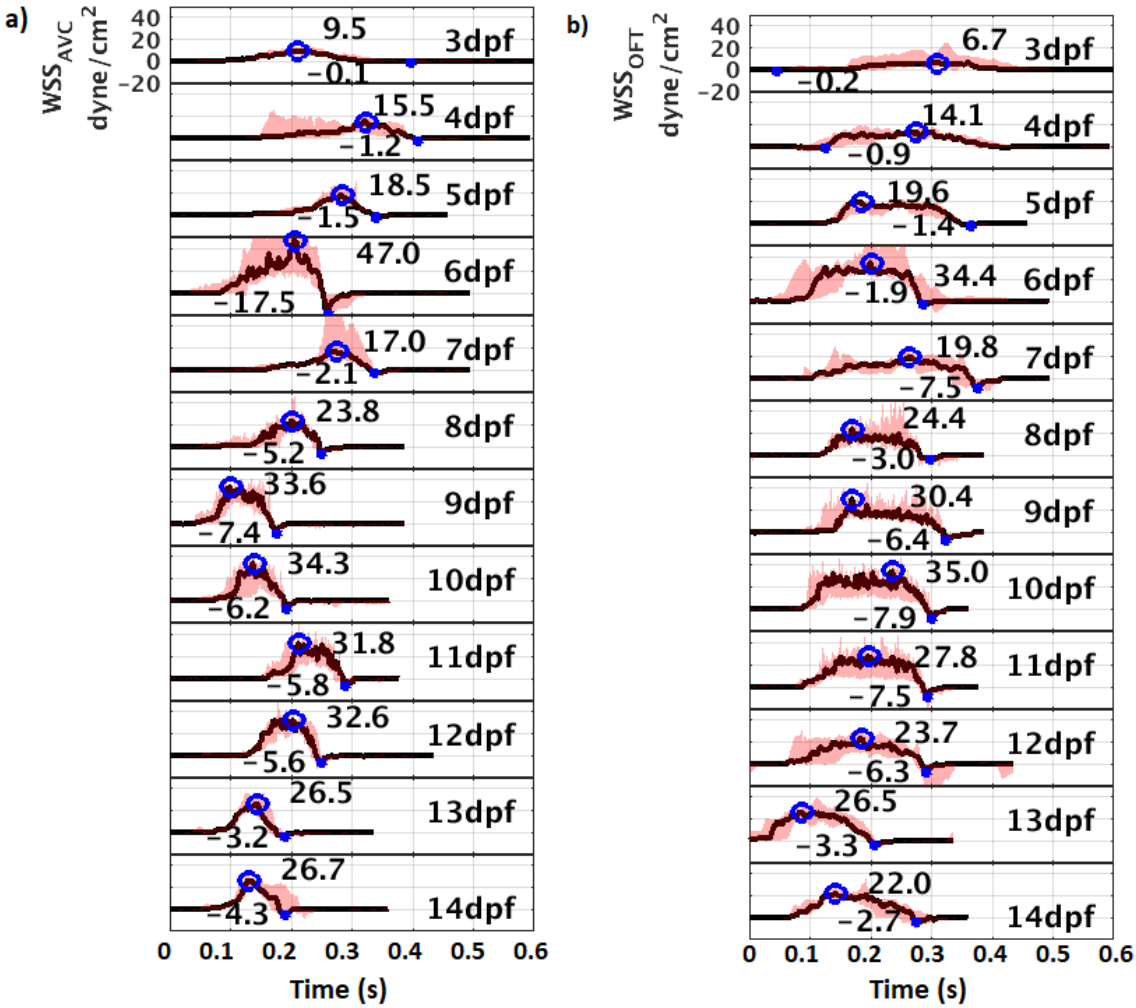

Figure 5.5. Time variation of WSS profiles in the **(A)** atrioventricular canal (AVC) and **(B)** ventricle outflow tract (OFT) of Japanese medaka. Black lines denote the median profiles while the pink shade denotes region between maximum and minimum profiles. The peak values of the median profile are marked on each plot by a blue circle and the minimum values on the median profile are marked by a blue star. n=5 for each dpf.

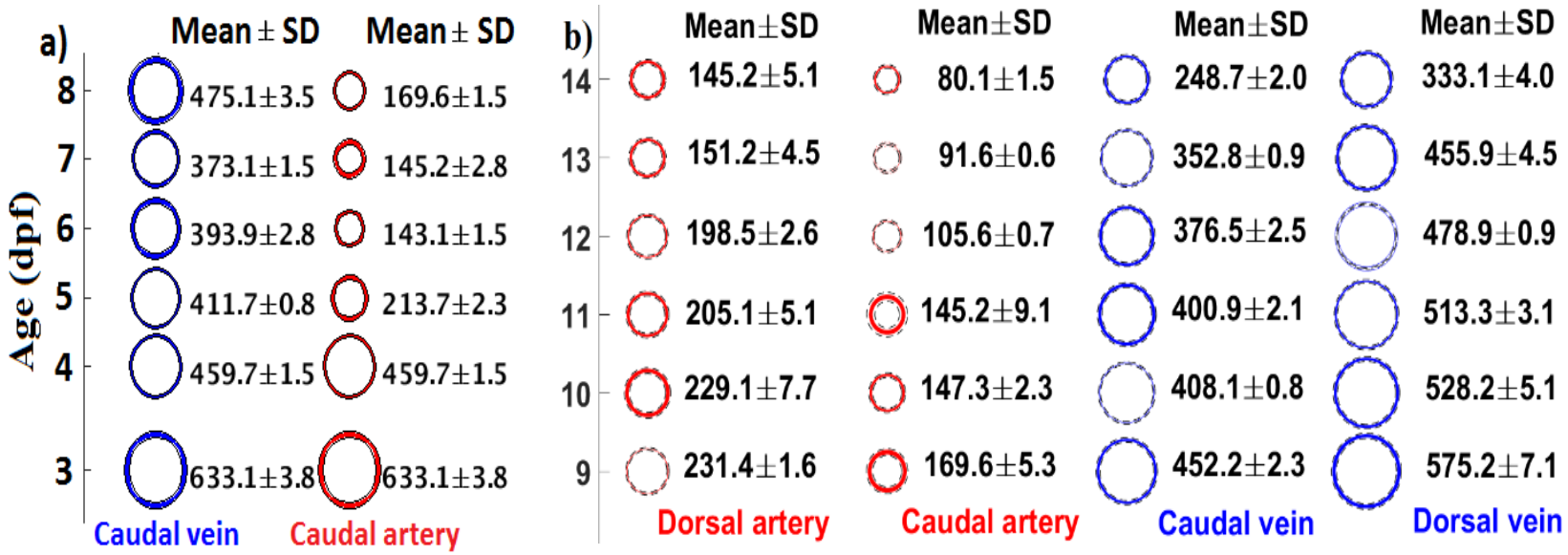

Figure 5.6. Variation of tail vessel cross-sectional area (µm2) over time (dpf) in Japanese medaka. **(A)** Caudal vein and caudal artery variation is captured from 3 dpf to 8 dpf. **(B)** Dorsal artery (DA), caudal artery (CA), caudal vein (CV), and dorsal vein (DV) area variation is captured from 9 dpf to 14 dpf. n=5 for each dpf.

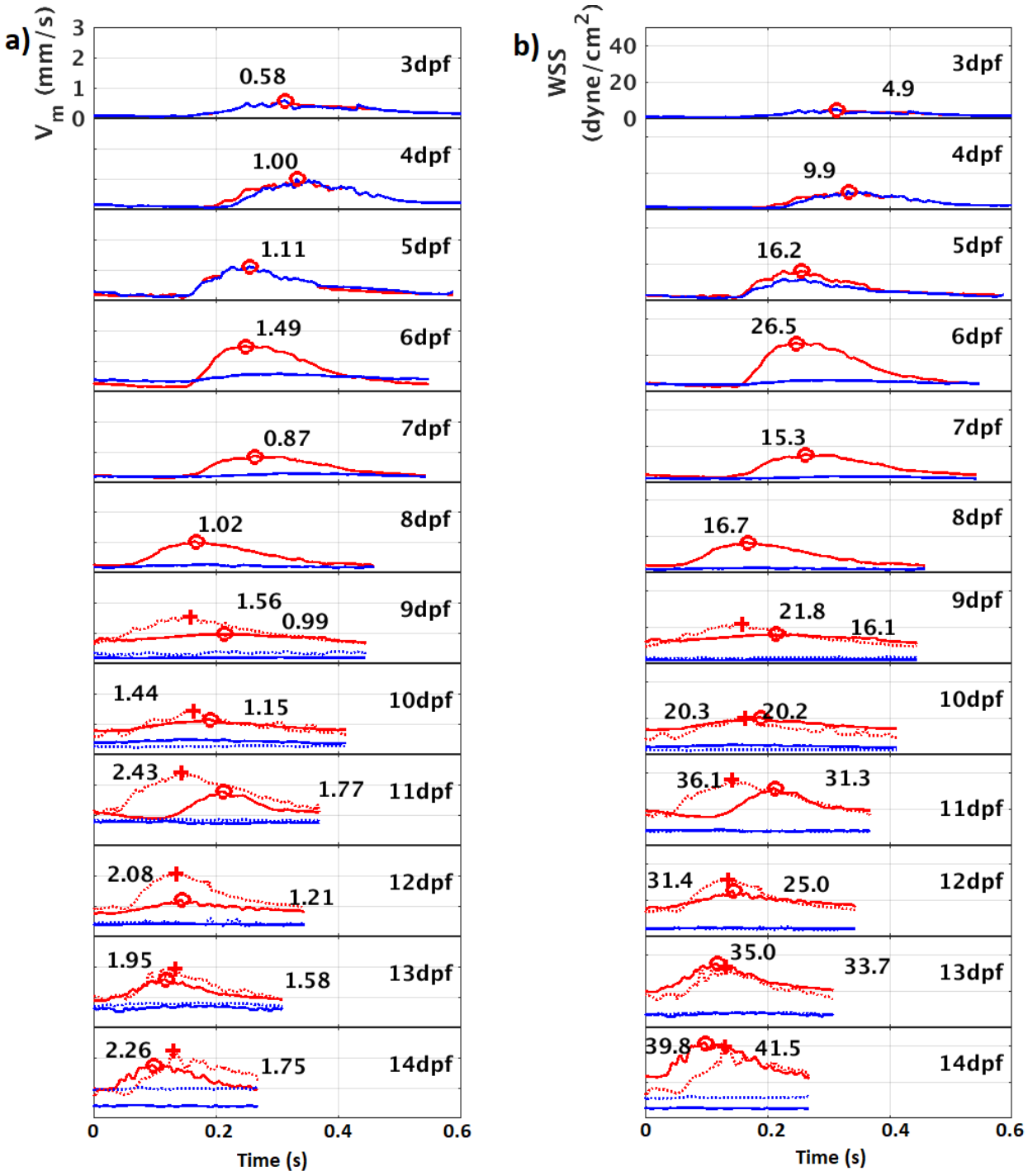

Figure 5.7. Time variation of **(A)** velocity and **(B)** WSS profiles in the tail vessels of Japanese medaka. Red lines denote arterial profiles while the blue lines denote venous profiles. Dotted curves correspond to dorsal vessels and solid curves correspond to caudal vessels. From 9 dpf to 14 dpf the red '+' markers correspond to the peak magnitude in dorsal artery while the red 'o' markers correspond to the peak magnitude in caudal artery. n=5 for each dpf.

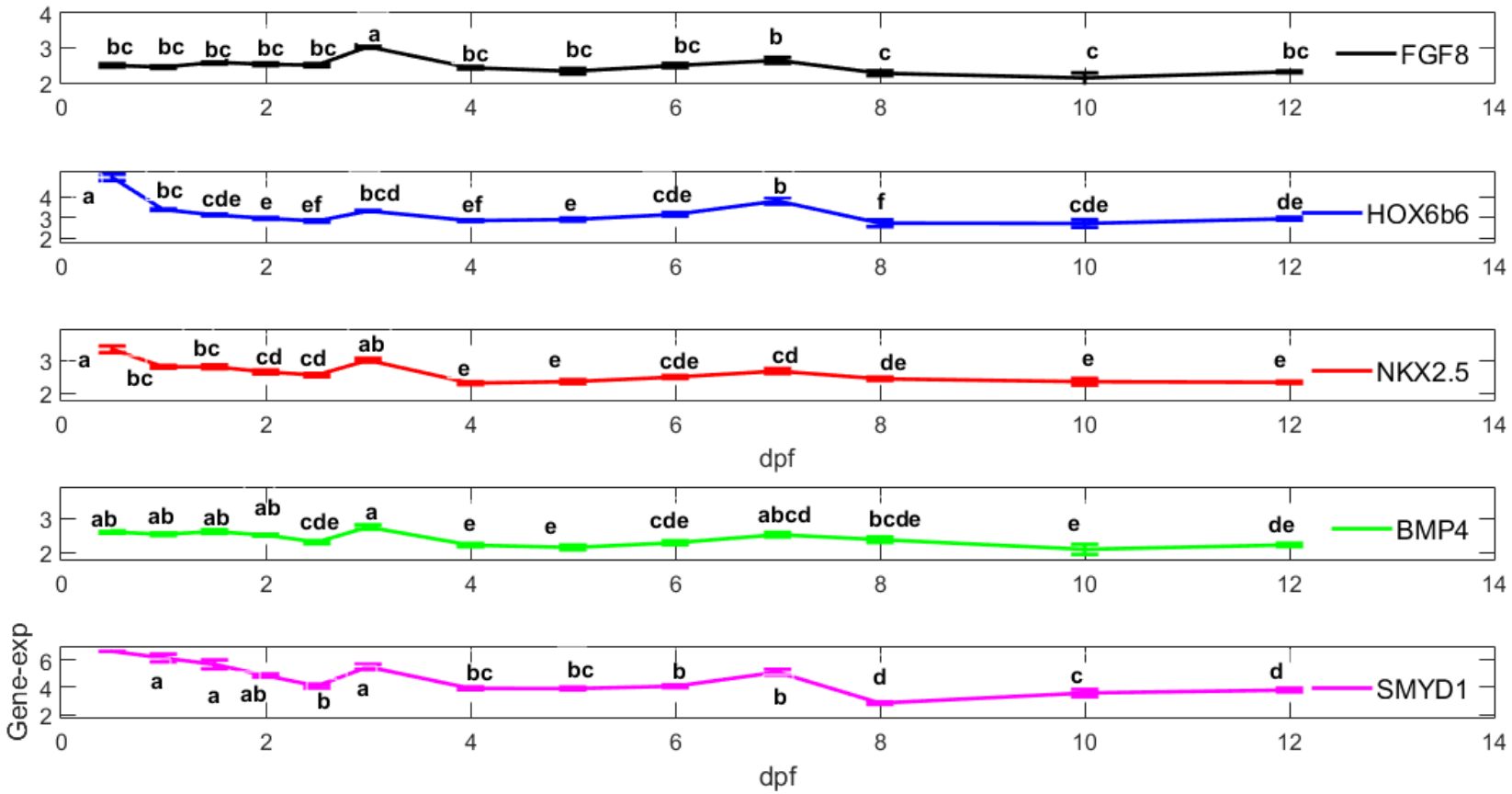

Figure 5.8. Variation in relative gene expression of five cardiac genes throughout cardiac development in Japanese medaka. Time points that are not connected by the same letter display gene expressions that are statistically significantly different. n=8-10 at each dpf. Exception: smyd1 has one sample at 0.5 dpf. $p<0.05$.

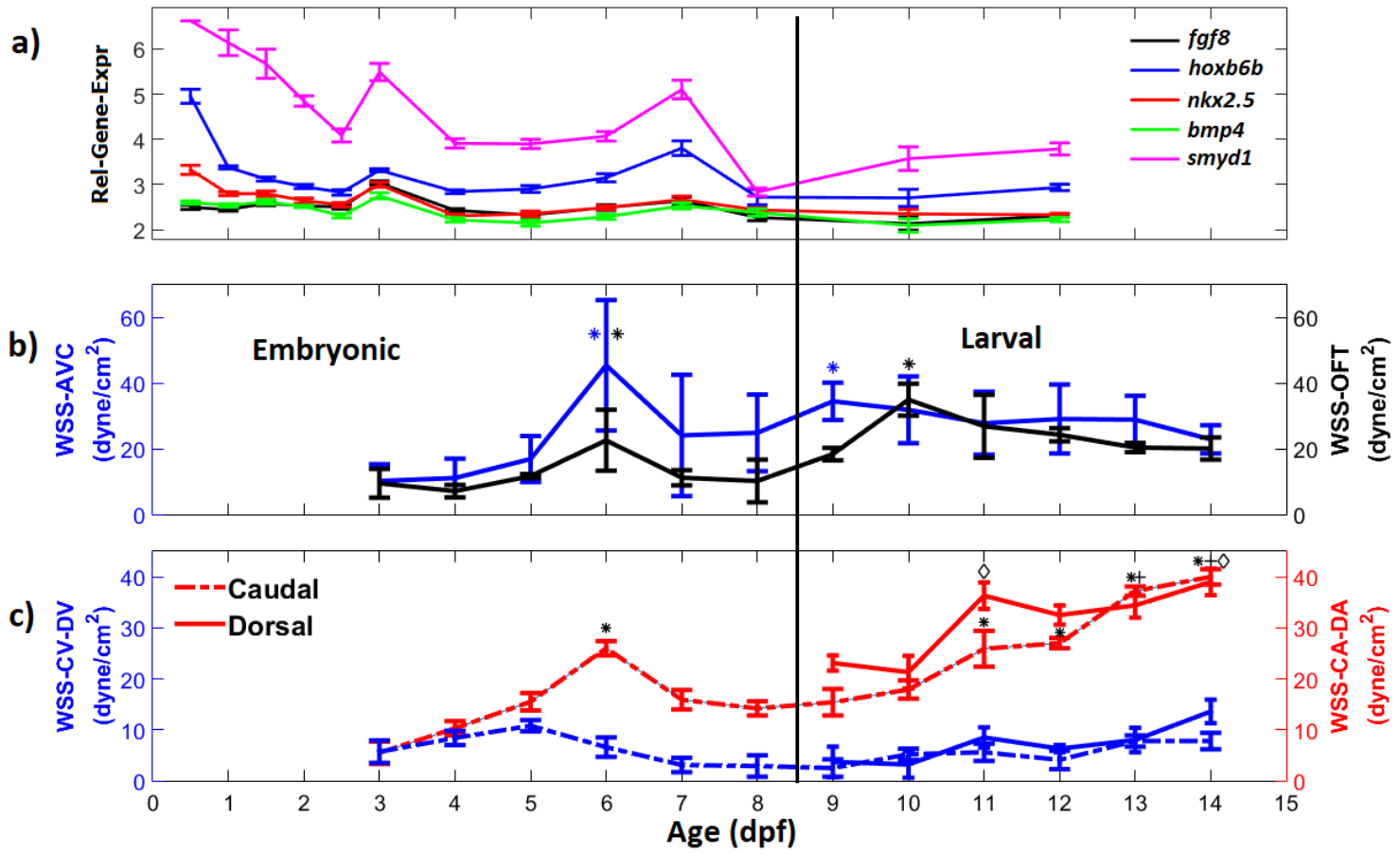

Figure 5.9. Correlation of **(A)** relative gene expressions and peak WSS variation in **(B)** heart and **(C)** tail vessels of Japanese medaka over time (dpf). Asterisks (*) in **(B)** and **(C)** denote statistical significance compared to the control values at 3 dpf. Diamonds (◊) in **(C)** denote statistical significance compared to control values in 9 dpf for Dorsal Aorta (DA) and crosses (+) denote statistical significance compared to control values in 9 dpf for Caudal Aorta (CA). $p<0.05$.

CHAPTER 6. CONCLUSIONS AND FUTURE RESEARCH

6.1 Cardiac transcriptomics

Data presented in Chapters 2 and 3 of this dissertation highlights the importance of environmental influences on cardiac transcriptomes in early life stages of estuarine teleosts. Hypoxia was shown to induce distinct differences in differential gene expression between two species inhabiting the same ecological niche. Although there were differences in gene expression, predicted downstream canonical pathways and toxicological functions appear to be conserved between the species. Overall, exposure to hypoxia in early development resulted in reduced cardiac hypertrophy, modulation of blood pressure, and cardiac apoptosis. While the predicted downstream pathways and functions appear to be conserved, the magnitude of impact appears to be universally greater in sheepshead minnow (*Cyprinodon variegatus*) than the Gulf killifish (*Fundulus grandis*).

Combined exposures to polycyclic aromatic hydrocarbons (PAHs) from Deepwater Horizon oil and environmental abiotic stressors (hypoxia, increased salinity, and elevated temperature) during early life stages impacted signaling pathways involved in cardiac function in post-hatch *F. grandis* larvae. Cardiac transcriptomic responses following exposure to both PAHs and suboptimal abiotic conditions appear to be driven by complex interactions and are not the additive results of responses to two single exposures. Co-exposure to PAHs and adverse environmental factors appear to reduce development of systemic vasculature and impact development of cardiac musculature through cardiomyocyte proliferation which results in cardiac hypertrophy, inhibited cardiac contractility, and modulated blood pressure maintenance.

6.2 Cardiac development & function

To more fully elucidate the effects of PAHs on the developing cardiac system in estuarine fish, *C. variegatus* embryos were exposed to two doses of weathered oil (150 µg/L and 300 µg/L total PAH) from the surface slick of the Deepwater Horizon oil spill throughout their embryonic period. Embryos exposed to both doses of oil showed significant increases in the cardiotoxic phenotype, pericardial edema, and had significantly reduced cardiac output resulting from reduced ventricular stroke volume. Interestingly, there were no differences in the heart rates of control embryos and those exposed to either dose of oil. This is an important finding as many studies rely on heart rate as the primary indicator of impaired cardiac performance. By relying solely on heart rate without accounting for changes in stroke volume, studies may overlook important alterations in cardiac output and overall cardiac performance.

6.3 Mechano-genetics

The mechano-genetic framework that defines the morphogenesis of the teleost cardiovascular system relies on feedback between cardiac gene expression and wall shear stress (WSS) within the heart and major vessels. The WSS and flow dynamics within the cardiovascular system were concomitantly traced with developmental cardiac gene expression throughout the embryonic and post-hatch larval period of Japanese medaka (*Oryzias latipes*). A bimodal pattern of increased cardiac gene expression followed by increased WSS was measured throughout the developmental period. Increases in gene expression at 3 and 7 days post fertilization (dpf) were followed by increased WSS at 6 and 10-11 dpf, respectively. These inflection points align with cardiac remodeling events involved in the development of cardiac cushions and later valvulogenesis within the developing medaka heart.

6.4 Future research needs

Assessment of transcriptomic changes through differential gene expression can be a powerful tool in predicting functional responses to environmental and cardiotoxic stressors. However, transcriptomic alterations do not necessarily result in physiological changes. Therefore, further phenotypic anchoring studies are needed to verify the downstream responses predicted by the differential gene expression analysis presented here. Additionally, further studies into the combined effects of abiotic stressors and PAH exposure are warranted. Estuaries are biogeochemically dynamic ecosystems that regularly undergo fluctuations in dissolved oxygen levels, salinity, and temperatures simultaneously. Therefore, assessment beyond the binary combinations of PAHs and a single environmental stressor as presented in this work are warranted for a more holistic assessment of environmentally relevant cardiac transcriptomic changes.

While the presence of pericardial edema and reduced cardiac output are evidence of cardiac impairment resulting from PAH exposure in *C. variegatus* embryos, the long-term physiological effects of exposure to oil during embryonic development remain to be seen. Follow-up studies are needed to examine the impacts of reduced cardiac performance at the organismal level and should include relevant endpoints such as measurements of aerobic scope and swimming performance.

Finally, the mechano-genetic framework underlying cardiovascular development detailed here corresponds with the initiation of several important morphological transitions within the vertebrate heart including cushion and valve formation, trabeculation, chamber looping, and concentric chamber growth. These developmental landmarks should be further validated through morphological measurements and their responses to environmental perturbations (such as exposure to cardiotoxic substances) should be evaluated. Once the mechano-genetic correlations

have been fully established in the face of cardiotoxic challenges, this framework could be applied to higher vertebrate models and eventually used to improve sensitivity and diagnostic capabilities of cardiac tissue damage.

VITA

EDUCATION

PhD – Aquatic Toxicology 2021

Purdue University; Department of Forestry and Natural Resources, Ecological Sciences and Engineering Interdisciplinary Graduate Program; West Lafayette, Indiana

M.S. – Marine Science 2015

The University of Texas at Austin; Marine Science Institute; Austin, Texas

B.S. – Biology, Ecological Sciences 2012

Shepherd University; Shepherdstown, West Virginia

RESEARCH EXPERIENCE

Graduate Research Assistant 2017-2021

Purdue University; Department of Forestry and Natural Resources

Research advisor: Dr. Maria S. Sepúlveda

Laboratory Manager/ Research Technician 2015-2017

The University of Texas at Austin; Marine Science Institute

Principle Investigator: Dr. Andrew Esbaugh

Graduate Research Assistant 2013-2015

The University of Texas at Austin; Marine Science Institute

Research advisor: Dr. Andrew Esbaugh

Undergraduate Research Assistant 2012

Shepherd University; Department of Environmental and Physical Sciences

Research advisor: Dr. Peter Vila

TEACHING EXPERIENCE

Graduate Teaching Assistant

Purdue University; Department of Forestry and Natural Resources

Ecology and Systematics of Fishes 2020

Instructor of record: Cortney Mycroft

Alternative FNR Practicum 2020

Instructor of record: Dr. Maria S. Sepúlveda

Marine Biology Practicum 2019

Instructor of record: Dr. Reuben Goforth

FNR Summer Practicum 2019

Instructor of record: Dr. Maria S. Sepúlveda

Wildlife Forensics 2018

Instructor of record: Dr. Maria S. Sepúlveda

Graduate Teaching Assistant

The University of Texas at Austin; Marine Science Institute

Fish Physiology Laboratory 2014

Instructor of record: Dr. Andrew Esbaugh

Marine Ecology Field Laboratory 2013

Instructors of record: Dr. Chris Shank & Dr. Dong Ha Min

PUBLICATIONS

Allmon, E., Walker, G., Griffitt, R., Sepúlveda, M.S. (2021) Oil induced cardiac effects in embryonic sheepshead minnows, *Cyprinodon variegatus*. *Manuscript submitted for publication.*

Chakraborty, S., **Allmon, E**., Sepúlveda, M.S., Vlachos, P. (2021). Hemodynamic dependence of mechano-genetic evolution of the cardiovascular system in Japanese Medaka. *Manuscript submitted for publication.*

Allmon, E., Serafin, J., Chen, S., Simning, D., Griffitt, R., Bosker, T., De Guise, S., Sepúlveda, M.S. (2021). The influence of hypoxia on the cardiac transcriptomes of two estuarine species – *C. variegatus* and *F. grandis*. *Comparative Biochemistry and Physiology Part D: Genomics and Proteomics*, 39, 100837. https://doi.org/10.1016/j.cbd.2021.100837

Allmon, E., Serafin, J., Chen, S., Rodgers, M.L., Griffitt, R., Bosker, T., De Guise, S., Sepúlveda, M.S. (2021). Effects of polycyclic aromatic hydrocarbons and abiotic stressors on *Fundulus grandis* cardiac transcriptomics. *Science of the Total Environment*, 752, 142156. doi: 10.1016/j.scitotenv.2020.142156

Magnuson, J., Khursigara, A., **Allmon, E.**, Esbaugh, A., & Roberts, A. (2018). Effects of Deepwater Horizon crude oil on ocular development in two estuarine fish species, red drum (*Sciaenops ocellatus*) and sheepshead minnow (*Cyprinodon variegatus*). *Ecotoxicology and Environmental Safety*, 166, 186-191. doi: 10.1016/j.ecoenv.2018.09.087

Allmon, E., & Esbaugh, A. (2017). Carbon dioxide induced plasticity of branchial acid-base pathways in an estuarine teleost. *Scientific Reports*, 7. doi: 10.1038/srep45680

Brown, E. (2015). Defining the metabolic compensation pathways employed during low-level hypercapnia in red drum (*Sciaenops ocellatus*) (Master of Science). The University of Texas at Austin.

PRESENTATIONS

Hemodynamic dependence of mechano-genetic evolution of the cardiovascular system in Japanese medaka

Oral presentation. Purdue University Office of Interdisciplinary Graduate Programs Spring Reception. May 2021. West Lafayette, IN

Oil induced cardiac effects in embryonic sheepshead minnows, *Cyprinodon variegatus*

Poster presentation. Purdue University's Department of Forestry & Natural Resources Poster Session. April 2021. West Lafayette, IN

The influence of hypoxia on the cardiac transcriptomes of two estuarine species

Oral presentation. SETAC North America 41st annual meeting. November 2020. Fort Worth, TX

Effects of polycyclic aromatic hydrocarbons and abiotic stressors on *Fundulus grandis* cardiac transcriptomics

Oral presentation. Gulf of Mexico Oil Spill & Ecosystem Science Conference. February 2020. Tampa, FL

Combined exposure to oil and abiotic stressors increases cardiac impacts in developing Gulf killifish (*F. grandis*)

Poster presentation. SETAC North America 40th Annual Meeting. November 2019. Toronto, Canada

Cardiotoxic effects of phenanthrene in developing Japanese medaka (*Oryzias latipes*)

Poster presentation. 13th International Congress on the Biology of Fish. July 2018. Calgary, Canada

Tolerance of red drum (*Sciaenops ocellatus*) to varying levels of CO_2

Oral presentation. SEB Prague 2015. June- July 2015. Prague, Czech Republic

Tolerance of red drum (*Sciaenops ocellatus*) to varying levels of CO_2

Oral presentation. Texas Bays and Estuaries Meeting. April 2015. Port Aransas, TX

Phenotypic plasticity in response to hypercapnia induced acid-base disturbances in red drum (*Sciaenops ocellatus*)

Poster presentation. APS Intersociety Meeting: Comparative Approaches to Grand Challenges in Physiology. October 2014. San Diego, CA

HONORS & AWARDS

Graduate Student Research – First Place

Department of Forestry & Natural Resources, Purdue University, 2021

Graduate Student Pathmaker Award

College of Agriculture, Purdue University, 2021

Exemplary Graduate Student Service Award

Department of Forestry & Natural Resources, Purdue University, 2020

SETAC Student Travel Award

Society of Environmental Toxicology and Chemistry 40th Annual Meeting, November 2019

Ross Fellowship

Purdue University, 2017

Dean's Excellence Award

College of Natural Sciences, The University of Texas 2014

Abstract-Based Travel Award

American Physiological Society Intersociety Meeting, October 2014

MENTORSHIP ROLES

Undergraduate Research Mentor

Department of Forestry and Natural Resources, Purdue University, 2019- 2021

Graduate Peer Mentor

Department of Forestry and Natural Resources, Purdue University, 2018-2021

Peer Mentor

Ecological Sciences & Engineering Interdisciplinary Program, Purdue University, 2018-2020

REEU Graduate Student Mentor

"Diversity in Faces, Spaces, & Places", Purdue University, 2019

Graduate Mentor

Mentoring at Purdue Summer Scholars Program, Purdue University, 2018

Semester by The Sea Graduate Student Mentor

University of Texas Marine Science Institute, 2015, 2016, 2017

REU Graduate Student Mentor

University of Texas Marine Science Institute, 2014

LEADERSHIP ROLES

Vice President

Department of Forestry and Natural Resources Graduate Student Council, Purdue University; 2019-2021

Treasurer

Ecological Sciences and Engineering Interdisciplinary Program Graduate Student Organization, Purdue University; 2017-2020

Co-Chair

"In Data We Trust" 12th Annual Ese Symposium; Purdue University; March 2019

Treasurer

Department of Forestry and Natural Resources Graduate Student Council, Purdue University; 2018-2019

EDUCATIONAL OUTREACH

Lafayette Regional Science and Engineering Fair Judge

Purdue University, 2018, 2020, 2021

Science in Schools Session Instructor

Purdue University Interdisciplinary Graduate Programs/ Tippecanoe School Corporation (Wea Ridge Middle School), 2018, 2019

Science Fair Judge & Panelist

Port Aransas Independent School District (Olsen Elementary School, Brundrett Middle School)/ University of Texas Marine Science Institute, 2016, 2017

University of Texas Summer Science Instructor

University of Texas Marine Science Institute, 2016, 2017

National Ocean Sciences Bowl Volunteer

University of Texas Marine Science Institute/ Texas Sea Grant, 2016, 2017

Women in Marine Science Session Instructor

University of Texas Marine Science Institute, 2016, 2017